Development and exploitation of optical diagnostic techniques for simultaneous 2D temperature and equivalence ratio measurements for the understanding of combustion phenomena in reciprocating engine

Von der Fakultät für Ingenieurwissenschaften, Abteilung Maschinenbau und Verfahrenstechnik

der

Universität Duisburg-Essen

zur Erlangung des akademischen Grades

einer

Doktorin der Ingenieurwissenschaften

Dr.-Ing.

genehmigte Dissertation

von

Gabrielle Tea
aus
Abidjan, Elfenbeinküste

Gutachter: Univ.-Prof. Dr. rer. nat. Christof Schulz

Dr. Gilles Bruneaux

Tag der mündlichen Prüfung: 14.10.2014

Summary

A non-intrusive laser diagnostic technique for simultaneous measurements of fuel concentration, temperature, and O_2 concentration has been investigated in conditions representative for internal combustion (IC) engines. The technique is based on two-tracer LIF with single-wavelength laser excitation. One tracer (naphthalene) with high sensitivity to temperature is used to measure temperature based on the redshift of the tracer-LIF signal with increasing temperature. The method requires the determination of the ratio of LIF intensities collected in two distinct spectral ranges. A second tracer (toluene) with a different O_2-sensitivity compared to the first tracer is used to measure the O_2 partial pressure. The ratio of the LIF signals of the two tracers is used to determine O_2 partial pressures. The low level of photophysical interaction between toluene and naphthalene was verified by investigating the photophysical properties of a mixture of toluene and naphthalene for various temperatures, pressures, and O_2 partial pressures. In the present study, the LIF technique was investigated in a high-pressure, high-temperature cell providing well-controlled injection and bath-gas conditions that are representative for in-cylinder IC engine conditions. Furthermore, this cell enables single-parameter variations for temperature and O_2 partial pressure. The investigation of a single-tracer LIF technique (using toluene) enabled the development of a quantitative methodology to evaluate and optimize measurement uncertainty of tracer-LIF technique requiring LIF-ratio calculation. The methodology first developed on single-tracer LIF temperature measurements applied to a vaporized Diesel jet configuration in IC engine conditions allowed to determine a 1-σ precision of 20–40 K. The methodology was then used to evaluate the potential of the two-tracer LIF technique for simultaneous measurements of temperature and O_2 partial pressure at conditions representative for IC engines (high temperatures, high pressures, and high inhomogeneities in temperature and species concentrations). The two-tracer LIF technique has potential for measuring low O_2 partial pressures (up to 0.3 bar) but is limited at higher O_2 partial pressures that are typical for IC engine conditions (2–10 bar).

Zusammenfassung

Eine laser-diagnostische Methode zur gleichzeitigen berührungsfreien Messung von Kraftstoffkonzentration, Sauerstoffkonzentration und Temperatur wurde unter motorischen Bedingungen untersucht. Das Verfahren basiert auf der zwei Tracer-LIF (Laser-Induzierte Fluoreszenz) mit Einzel-Wellenlängen-Laseranregung. Der erste, temperaturempfindliche Tracer (Naphthalin) wird verwendet, um mit zunehmender Rotverschiebung des LIF-Signals die Temperatur zu bestimmen. Dazu wird das Verhältnis der LIF-Intensitäten in zwei verschiedenen Spektralbereichen gemessen. Der zweite Tracer (Toluol) weist eine andere Sauerstoff-Empfindlichkeit auf, so dass auf dem Quotient der LIF-Signalstärke beider Tracer der Sauerstoff-Partialdruck bestimmt werden kann. Das niedrige Niveau der photophysikalischen Interaktion zwischen Toluol und Naphthalin wurde durch die Untersuchung von deren Gemischen bei verschiedenen Temperaturen, Drücken und Sauerstoff-Partialdrücken geprüft. Die entwickelte LIF Technik wurde in einer Hochdruck- und Hochtemperatur-Zelle untersucht, welche reproduzierbare Einspritzung und Gaszustände unter motorähnlichen Bedingungen gewährte. Darüber hinaus ermöglicht diese Messzelle unabhängige Parametervariationen für Temperatur- und Sauerstoff-Partialdruck. Durch Untersuchung der Toluol-LIF konnte weiterhin der Messfehler jener LIF-Verfahren bestimmt werden, die auf dem Intensitätsverhältnis zweier Spektralbänder basieren. Im Fall verdampfenden Diesel-Jets (motorische Bedingungen) konnte so eine 1-σ Präzision von 20-40K bestimmt werden. Anschließend wurde das Potential der Zwei-Tracer-LIF-Technik zur gleichzeitigen Messung von Temperatur und Sauerstoff-Partialdruck unter motorischen Bedingungen bewertet (bei hoher Temperatur, hohem Druck und starker Inhomogenität von Temperatur und Spezieskonzentration). Die Zwei-Tracer-LIF-Technik konnte ihre Eignung zur Messung niedriger Sauerstoff-Partialdrücke (bis 0,3 bar) nachweisen, zur Messung von motortypisch hohen Partialdrücken eignet sie sich aber noch kaum.

Acknowledgement

The completion of this thesis would not have been possible without the support of many – of which I can only mention a few.

Foremost, my gratitude is to my academic advisor Prof. Schulz, whose knowledge and support enabled me to complete the work. I am also indebted to my supervisors at IFPEN, Drs. Bruneaux and Kashdan, who guided me on a daily basis through my research. During the long time this project has taken, they have also become trusted advisors and friends. I am particularly grateful for their trust in my ability to succeed in this work after an initial placement in their group. At the University of Duisburg-Essen, a special thanks is due to Prof. Dreier who helped with guidance and his almost infinite knowledge about laser diagnostics.

This work would have never been finished and much less enjoyable without the support of the friends that I have made at IFPEN and University of Duisburg-Essen. In particular, I wish to thank my long term office colleague Hubert Baya Toda who did not only share good advice but also banter, and my lab-colleague Stefan Faust with whom I closely worked at the University of Duisburg-Essen. I also wish to mention the good ideas, helpful conversations and friendly coffee rounds that I enjoyed with Emre, Khadijeh, Robin, Maria, Jérôme, Vincent, David, Louis-Marie, Matthieu, Sabre, Julien, Haifa, Sulyvan, Cyprien, Betty, Martin, Ralf and many others that I will fondly remember.

Credit is also due to the highly skilled technicians I had the pleasure to work with, at both the University of Duisburg-Essen and IFPEN. Laurent Hermant and Clement Bramoullé deserve a special mention.

I am also indebted to my family, who supported me through my studies, advised me in my choices, and were always there when I needed them most. My brother Loïc, my sister Illa who showed me what to strive for, my sister Irika, my courageous mother and in particular my very supportive father, who always inspired me to struggle, achieve more, and not to be satisfied with the low hanging fruits.

Last, but definitely not least, many thanks to my boyfriend Andreas Kempf for his continual patience, encouragement and support.

Table of Contents

1 Introduction

The development of clean and efficient internal combustion (IC) engines requires a detailed understanding of the physical processes occurring in the combustion chamber. An improved understanding of the processes related to mixture preparation, combustion, and pollutant formation is crucial not only as it can provide guidelines for improving combustion chamber design but also help to improve the predictivity of computational fluid dynamics (CFD) simulations. In order to achieve these objectives, quantitative experimental measurements of the key parameters of interest are required. Optical diagnostic techniques have become a powerful tool over the last twenty years as they enable non-intrusive, in-situ quantitative measurements of numerous parameters within the combustion chambers of IC engines. Two of the most critical parameters for combustion in IC engines are the gas temperature and the equivalence ratio, since they have a significant influence on combustion (e.g., auto-ignition, spark-ignition, flame propagation,…) and pollutant formation. In particular, the oxidation reactions of the fuel/air mixture which occur prior to ignition and the combustion process are particularly sensitive to unburned gas temperature, local fuel/air ratio and charge dilution (i.e., concentration of exhaust gas residuals and/or external exhaust gas recirculation: EGR). There is therefore a significant interest in performing quantitative, in-situ measurements of unburned gas temperature, fuel, and oxygen (O_2) concentration. However, the measurement of these parameters in the harsh conditions which are typically encountered in IC engine combustion chambers represents a major challenge. In-cylinder flows are unsteady, highly turbulent, and subjected to a wide range of pressure and temperature variations. Furthermore, the presence of liquid droplets and soot particles further complicates the application of quantitative, non-intrusive optical diagnostic techniques.

The objective of this PhD is to develop a laser diagnostic technique capable of performing quantitative, planar (2D), simultaneous measurements of unburned gas temperature, fuel concentration, and O_2 partial pressure which would provide a level of measurement accuracy and precision sufficient for the validation of CFD simulations. The present work is based on tracer laser-induced fluorescence (LIF) imaging which enables 2D distributions of temperature, fuel and O_2 concentration to be acquired. Planar imaging is important for example in order to obtain a detailed understanding of turbulent mixing phenomena (e.g., degree of spatial stratification of temperature/equivalence ratio) in the gas mixture prior to ignition. A novel approach is developed in the present work with the objective of performing simultaneous measurements of multiple parameters (temperature, fuel concentration, and O_2 partial pressure) using a two-tracer LIF technique.

The PhD thesis is structured in the following manner. Firstly, a literature review is presented in Chapter 2 with the objective of evaluating the existing non-intrusive optical diagnostic techniques that are capable of measuring temperature, fuel concentration (or fuel/air ratio) in gaseous mixtures. An important consideration was to take into account the suitability of the existing techniques in terms of

their potential to perform measurements in IC engine representative conditions. A summary of the literature review lists the various criteria that were considered and provides the reasoning behind the decision to pursue the development of a LIF technique based on the simultaneous use of two tracers. The literature survey also includes a review of the photophysical properties of a wide range of tracers. The objective was to identify a pair of tracers with the most suitable properties to enable simultaneous, multi-parameter measurements of gas temperature and O_2 partial pressure in engine-like conditions.

Chapter 3 discusses the results of an experimental study in which the photophysical properties of the two selected tracers were characterized in detail. In particular, the two-tracer LIF method developed in this study required fundamental experiments to verify whether photophysical interactions occurred between the two tracers.

The development of the two-tracer LIF technique was performed in two phases. The initial phase focused on the development of the experimental methodology based on single-tracer LIF measurements of unburned gas temperature (Chapter 4). This single-tracer LIF-thermometry technique was used to perform measurements on a Diesel jet in a high-pressure high-temperature constant volume chamber in which the thermodynamic conditions are well controlled and fully representative for IC engine conditions. Single-line tracer LIF was used to develop a measurement methodology that enabled the determination and the subsequent optimization of the measurement uncertainties. The second phase, described in Chapter 5 focused on the development of the two-tracer LIF method. Measurements were performed in the same experimental configuration as in Chapter 4. The results acquired were used to determine the measurement sensitivity and the precision of the two-tracer LIF technique and ultimately evaluate the potential of this experimental methodology for performing multi-parameter measurements in engine-like conditions.

2 Optical diagnostics for multi-parameter measurements

2.1 Laser diagnostics for temperature and species concentration measurements

Several optical diagnostics techniques offer the capability of performing non-intrusive measurements of temperature and species concentration. A brief literature review below presents a number of these laser diagnostics techniques.

2.1.1 Diode laser absorption diagnostics

Diode laser absorption spectroscopy is based on the absorption of the incident laser light as the beam from tunable diode lasers propagates across the probe volume [1]. The Beer-Lambert law, which gives the relation between the transmitted light (I) and the incident light intensity (I_0) through an absorbing gas media with an absorbing species number density (n), describes the absorption process:

$$I = I_0 \exp(-\sigma n l) \tag{2.1}$$

where (σ) is the spectral absorption coefficient and (l) the absorption path length. The spectral absorption coefficient is a function of temperature, pressure and gas species concentration, which enables these parameters to be quantitatively measured. Fundamental spectroscopy properties such as the absorption coefficient of the absorbing species are well known for a number of molecules of interest. For temperature measurements, two different absorption transitions with different ground-state energies of molecular species, such as H_2O and CO_2 [2] are typically probed. The ratio of the integrated absorbance of each transition is a function of temperature, which allows the determination of (line-of-sight integrated) gas temperature measurement. The species concentration is then obtained from the measured absorbance at a selected wavelength, using the known line strengths at the measured temperature.

Different strategies have been demonstrated [3]. Multiplexed-wavelengths sensors, which combine several diode lasers, can simultaneously probe multiple absorption transitions [4]. Tunable diode lasers (TDL) are also used for scanning wavelengths over multiple absorption transitions [5]. Laser-based absorption techniques have been developed for applications in IC engines. For example, in-cylinder gas-temperature measurements were performed in HCCI engines [6,7]. The temperature measurement uncertainty was estimated in motored engine operation to be less than approximately 3% in the temperature range of 400–750 K (i.e., ±22 K at 750 K). A novel strategy was also developed for simultaneous measurement of temperature and fuel concentration [8]. The results showed good sensitivity in the range of temperature from 298 to 1300 K with a claimed accuracy of 4.5% for temperature data

(i.e., ±58 K at 1300 K) and of 1.7% for concentration data. This two-wavelength mid-IR absorption technique was applied for crank-angle-resolved measurements of fuel and in-cylinder temperature [9].

Diode-laser absorption techniques can provide simultaneous temperature and fuel concentration information with reasonable accuracy in IC engines; however, the measurements are integrated along the line-of-sight which prevents the determination of local concentration and can distort the line-of-sight averaged data once the distribution of temperature and concentration is not well correlated. This is a major limitation within the context of the present study since one of the requirements was to obtain two-dimensional distributions of temperature and species concentration data, in order to be able to characterize spatial in-cylinder fluctuations.

2.1.2 Rayleigh scattering

Rayleigh scattering is the elastic interaction between photons emitted from a light source and molecules or particles whose effective diameter is much less than the wavelength of the incident (laser) light. After interaction with the incident photons, the molecules return to the same state they were in previously. Therefore, the scattered light is not shifted from its initial incident wavelength [10]. The absolute Rayleigh signal is directly proportional to the laser intensity, the total number density, and a differential scattering cross section depending on the gas that is being probed. Rayleigh scattering cross sections are known for a range of combustion relevant molecules and are independent of temperature in a first approximation. Rayleigh scattering can therefore be employed for gas density and temperature measurements using the ideal gas law, in case the gas pressure is known.

Due to the simple linear dependence of the Rayleigh scattering signal on the molecular number density, this diagnostics technique is attractive. The signal interpretation for obtaining quantitative measurement is straightforward, the determination of absolute concentration, however, requires calibration. Rayleigh diagnostics can suffer from interference from Mie scattering and spuriously scattered laser light from the surrounding surfaces. Therefore, additional care in the optical setup is required to perform gas fuel distribution and temperature measurements in practical engine conditions [11]. Filtered Rayleigh scattering (FRS) [12] is an evolution of the Rayleigh technique. The pressure and temperature broadening properties of the scattered signal can be exploited to spectrally separate the Rayleigh signal (from the gas) from the laser line and from the scattering signal of surfaces and interfaces. Essentially, in a gas-phase sample, elastically scattered light from molecules is spectrally shifted from the laser wavelength due to translational molecular motion. This Doppler shift leads to temperature broadening whilst collisional shifts result in pressure broadening of the Rayleigh line. These broadening effects are exploited to spectrally discriminate the signal due to gas-phase scattering from other elastic scattering contributions (e.g., from surfaces or particles within the flow). This approach allows temperature measurements in more complicated combustion systems. The temperature and pressure broadening is a result of a spectral shift in the elastically scattered light from molecules in a gas-phase

sample, due to translational motion of the molecules. By an appropriate narrow band pass cut-off optical filter, it is possible to spectrally separate the laser line signal from the broadened Rayleigh line, which is detected by a CCD camera. However, this depends on the use of a narrow band optical filter in addition to a narrow band laser source, which must be stable in frequency.

Quantitative imaging of the fuel-vapor concentration in an evaporating Diesel jet at realistic engine operating conditions was performed using the Rayleigh scattering technique. Equivalence ratio and temperature distributions were obtained from fuel-vapor concentration images by using an adiabatic mixing assumption to model the local temperature of the evaporating Diesel jet [13]. This methodology of applying the Rayleigh scattering technique was implemented for quantitative mixing analysis in a vaporizing Diesel spray under engine conditions. Experimental methods were also optimized to minimize interferences from unwanted elastic scattering sources [11]. Equivalence ratio distributions in the jet were measured for different exhaust-gas recirculation (EGR) levels [14]. The improvements made to the Rayleigh-scatter imaging diagnostics allowed the application of this technique to provide experimental data for model validation [15].

The Rayleigh scattering diagnostics technique has successfully been applied in a constant-volume combustion vessel that simulates engine conditions. However, fuel pyrolysis occurring at high temperatures (above 1000 K) may affect the accuracy of the fuel concentration measurements because the combined Rayleigh cross section of pyrolysis products tends to be smaller of that of the original molecules. In this case, the extent of fuel pyrolysis needs to be characterized to determine the correct fuel concentrations from the Rayleigh scattering measurement technique [16]. Temperature and residence-time limits for this technique can be estimated on the basis of kinetics modeling of the pyrolysis process. Besides measuring the fuel concentration in the vapor phase of a spray using Rayleigh scattering, a combined Mie and Rayleigh scattering techniques that takes advantage of the different combination of polarization of excitation and emission allows a more detailed study of the distribution of liquid (from Mie scattering signal) and evaporated fuel (from Rayleigh scattering signal) [16] than possible from the integral signal that is conventionally used and that assumes that the presence of liquid contributes to a strong enough additional signal that can be clearly distinguished from gas-phase signal.

To a large extent, it remains difficult to apply the Rayleigh scattering technique in an optical engine due to strong elastic scattering of particles (i.e., soot, liquid droplets) or surfaces. Moreover, the Rayleigh technique provides field measurements of fuel concentration from which are deduced equivalence ratio and temperature fields. Direct measurements of temperature and O_2 concentration fields are not possible using this technique, which is the main drawback.

2.1.3 Coherent Anti-Stokes Raman Scattering (CARS)

Coherent Anti-Stokes Raman Scattering (CARS) is a non-linear laser diagnostics technique that allows temperature and species concentration measurements with high temporal and spatial resolution. Three laser beams with frequencies ω_1 and ω'_1 and the Strokes frequency ω_2 are focused into the probe volume, and a fourth beam is generated at the so-called anti-Stokes frequency $\omega_3 = \omega_1 + \omega'_1 - \omega_2$. The generated CARS spectrum is acquired by a spectrometer and the temperature and the species concentration are derived from the spectrum shape after calibration.

The CARS technique has been applied in many practical combustion systems for the measurement of temperature (in burned and unburned gas) and species concentration. The CARS technique is an accurate technique for applications in IC engines [17–24]. However, this technique in general provides point wise measurements only and often integrates over comparably large probe volumes of a few mm^3. This is the major drawback since the objective here is to develop a technique capable of 2D measurements.

Diode-laser absorption, CARS and Rayleigh scattering techniques provide accurate measurements of temperature and species concentration. However, diode-laser absorption and CARS techniques are not easily capable of providing 2D measurements. Furthermore, the Rayleigh scattering technique is not capable of direct measurements of temperature and O_2 concentration, as an estimation of both parameters relies on an assumption of a direct relation between the parameters. Therefore, Rayleigh scattering does not fulfill one of the requirements of the present study, which is to directly measure temperature, fuel and O_2 concentration simultaneously.

2.2 Laser-induced fluorescence (LIF) diagnostics

Laser-induced fluorescence (LIF) techniques can provide two-dimensional temperature and species concentration distributions data with the potential for high precision and accuracy. For these reasons, LIF techniques were considered more suitable for the present work than the techniques discussed before. This section presents a more detailed review of the tracer-LIF techniques that are applicable for temperature, fuel concentration and O_2-concentration measurements in IC engine.

2.2.1 Tracer LIF

Tracer-LIF techniques are frequently used for quantitative studies of fuel concentration, temperature, and fuel/air ratio in practical combustion systems. LIF is the emission of light from an atom or molecule following excitation into an excited state by the absorption of photons, typically in the ultraviolet and visible spectral wavelength range [10].

Commercial fuels are mixtures of numerous organic species. Several of them fluoresce upon excitation in the UV. Quantitative interpretation of the LIF signals generated in commercial fuels is difficult since the source of the LIF emissions is not known precisely. Therefore, well-characterized fluorescent tracer molecules are usually added to a non-fluorescing surrogate fuel. A fluorescent tracer should behave as much as possible like the non-fluorescing fuel to which it is added in terms of droplet formation, evaporation, convection, diffusion, reactivity, and reaction rate [25]. Under these conditions, the tracer-LIF signal intensity that is representative of the local tracer concentration provides quantitative fuel concentrations information. Ideally, the tracer should yield LIF signal intensities that are directly proportional to the desired quantity and should not be influenced by the ambient conditions. However, signals from the majority of well-known fluorescent tracers show at least some dependence on local temperature, pressure, and bath gas composition. Therefore, for quantitative measurements of fuel concentration, the tracer signal intensities must be characterized in terms of their dependence on the surrounding conditions (e.g., temperature, pressure, gas composition). However, these dependences can also be exploited directly as a means of determining temperature and residual gas concentration such as O_2 [25].

LIF techniques that provide two-dimensional information use a laser light sheet as incident excitation from a commercially available laser source (e.g., KrF-excimer laser at 248 nm, frequency-quadrupled Nd:YAG laser at 266 nm). Intensified CCD cameras are generally used to detect the LIF signals that are then converted into temperature, fuel concentration and equivalence ratio images after appropriate corrections and calibrations (as further described in Chapter 4 and 5).

Two types of molecules, ketones and aromatic compounds, are most frequently used as fuel fluorescent tracers for the measurement of fuel concentration, equivalence ratio and temperature to characterize the unburned gas mixture in IC engine. There are a large number of tracers that can be used for LIF measurements as reported in [26], but only a few are discussed here. The priority was given to the tracers that are sensitive to temperature and/or O_2 concentration.

2.2.2 Aliphatic ketone tracers

Basic physical and thermodynamic properties of a selection of aliphatic ketones and commonly used surrogate fuels are presented in Table 2-1 and the fluorescence properties in Table 2-2. Aliphatic ketones are frequently used as fluorescence tracers in surrogate gasoline fuel such as iso-octane, since their evaporation properties are similar. For quantitative measurements of fuel concentration and temperature, acetone, 3-pentanone and biacetyl are among the most frequently used tracers. Ketones (e.g., acetone, 3-pentanone) and di-ketones (e.g., biacetyl) were studied with respect to their photophysical behavior, and were applied in various practical engine conditions.

The influence of collisional quenching by molecular O_2 on ketones is much lower compared to that on aromatic compounds (see below). Therefore, fuel concentration and temperature measurements have the advantage of being mostly independent on the O_2 concentration. To determine the fuel concentration the tracer-LIF signal is corrected for temperature (also measured by tracer LIF). For the determination of equivalence ratio, the air concentration can be calculated from pressure measurements using the ideal gas law, taking into account the fuel concentration, the total pressure and temperature. This calculation is based on the assumption that the sum of the fuel and the air partial pressures is equal to the (constant) total pressure.

Acetone

Acetone shows broadband absorption features (225–320 nm) which are accessible with commercial lasers such as krypton fluoride (KrF) excimer lasers (248 nm), the fourth harmonic of Nd:YAG lasers (266 nm) and xenon chloride (XeCl) excimer lasers (308 nm). Temperature, pressure, and excitation wavelength dependences of acetone absorption and fluorescence signals have been investigated extensively [27−33]. The absorption spectrum of acetone is shifted towards longer wavelengths with increasing temperature. The subsequent fluorescence spectrum between 350 and 550 nm is relatively insensitive to the excitation wavelength.

Besides being a suitable tracer for quantitative imaging of fuel concentration [27,34], acetone allows quantitative imaging of temperature based on the temperature dependence of its fluorescence properties [29,35]. Single- and dual-wavelength LIF strategies for temperature imaging have been demonstrated [35]. The single-wavelength LIF approach was restricted to experimental flows with homogeneous acetone concentrations. However, the dual-wavelength LIF approach allows temperature imaging in inhomogeneously mixed or reacting flows using a temperature-dependent spectral shift in the acetone absorption spectrum. Dual-wavelength measurements strategies are based on calculating the ratio of two fluorescence images taken with laser excitation at two different wavelengths (e.g., 308/248 nm or 308/266 nm), which depend on temperature. Thurber et al. [36] demonstrated that the 308/248 nm ratio is more temperature sensitive than the 308/266 nm ratio.

For simultaneous measurements of fuel concentration and temperature, images of temperature derived from dual-wavelength strategies allow corrections for temperature in images of fuel concentration derived from one of the two fluorescence images [36,37]. Simultaneous quantitative measurements of temperature and fuel concentration fields have been applied in many different practical situations [38–42].

Concerning fuel measurements, the precision was estimated to be within 5% for single-shot images obtained in an engine operated in skip-firing mode [34]. Thurber et al. [35] first compared the single- and dual-wavelength LIF strategies for measuring temperature and gave an estimation of temperature

uncertainties. No detailed information was given about the methodology used to estimate these temperature uncertainties, which were claimed to be between 0.3 and 1.9% in the temperature range of 300–1000 K, depending on the diagnostics strategy used. However, more details were given when applying the dual-wavelength acetone-LIF strategy in a heated turbulent jet [36] for simultaneous measurement of temperature and acetone mole fraction. In this experimental case, a calibration was performed at room temperature with a uniform acetone concentration. The results demonstrated single-shot root mean square (rms) fluctuations in the mixture fraction of 1.3% (in the free stream) and 2.2% (at the nozzle) and in temperature of 6 K (in the free stream) and 8 K (at the nozzle). Averaged images of mixture fraction and temperature were compared only in a qualitative way.

3-pentanone

Similar to acetone, 3-pentanone shows broadband absorption in the UV (220–320 nm) which is accessible with commercial lasers such as krypton fluoride (KrF) excimer lasers (248 nm), the fourth harmonic of Nd:YAG lasers (266 nm) and xenon chloride (XeCl) excimer lasers (308 nm). Temperature, pressure, and excitation wavelength dependences of the 3-pentanone absorption and fluorescence signal were thoroughly investigated [28,31,34,43–45]. Within these studies, LIF imaging techniques were applied to measure temperature and fuel concentration. The absorption spectra of 3-pentanone are red-shifted with increasing temperature. The fluorescence emission between 330 and 600 nm is relatively insensitive to the excitation wavelength.

Initially 3-pentanone was used as a tracer primarily for quantitative imaging of fuel concentration [34,46]. Richter et al. [34] used Raman scattering for in-situ calibration for fuel/air ratio measurements using 3-pentanone-LIF in a heated cell. 3-pentanone-LIF imaging provided relative fuel concentration distributions while the Raman scattering technique enabled point measurements of absolute fuel and O_2 concentration. The 3-pentanone-LIF images were calibrated in order to obtain absolute fuel/air ratio distributions. The precision and accuracy of this method was investigated in a stoichiometric methane/air mixture at fixed pressure. A precision of 12% was determined from the standard deviation of the measured single-shot oxygen/methane ratio. Although the authors mentioned that the accuracy was determined by comparing the measured oxygen/methane ratio with the ratio calculated from the oxygen and methane partial pressure in the cell, no quantitative data was given. A tracer-LIF technique using 3-pentanone was also developed in [46] to measure fuel concentration distributions in a spark-ignition engine. Fuel/air ratios were obtained after in-situ calibration by measuring homogeneous fuel distributions and by determining the corresponding fuel/air ratio of the gas mixture with an analysis of the exhaust gas. An underestimation of 3% for spatially averaged data was determined as measurement accuracy of the equivalence ratio.

The temperature dependence of the fluorescence signal in addition allows quantitative imaging of temperature. The spectral shift of the absorption spectra with temperature is used for measuring temperature. After excitation at two separated wavelengths, the ratio of the fluorescence signal intensities is proportional to local temperature and is independent of the local tracer concentration. Simultaneous quantitative measurements of temperature and fuel concentration fields have been applied in a variety of practical situations [43,47−51] and enabled, e.g., the investigation of temperature stratification [52−54]. The 3-pentanone-LIF method was also adapted for simultaneous imaging of temperature and EGR in engines [50,53,55]. Other qualitative studies were carried out using 3-pentanone to investigate fuel vaporization in IC engines [56,57].

In Ref. [48], temperature, fuel concentration and equivalence ratio fields were measured in the unburned gas region of an IC engine. Using a two-line technique (quasi-simultaneous excitation at 248 and 308 nm), 3-pentanone-LIF images were first converted into temperature fields after calibration at a known reference temperature. A precision of ±17 K in the motored and ±25 K in the fired engine (i.e., relative error of approximately 4%) was determined for single-shot temperature imaging between 300 and 650 K. The precision was evaluated by calculating the standard deviation of 100 single-shot temperature measurements in a region of the image where the LIF signal was typically uniform. The temperature results from the LIF technique were also compared to adiabatic calculations showing good agreement, however no estimation of measurement accuracy was given. Based on the temperature results, fuel concentration distributions were obtained from a single-wavelength measurement after correction for temperature effects on a per-pixel basis. Finally, the local fuel/air equivalence ratio was determined by measuring the air intake flown and the amount of fuel consumed. The precision was not evaluated for the measured fuel concentration and equivalence ratio in this case.

The selection of excitation wavelengths for 3-pentanone-LIF thermometry was first investigated by Koch et al. [43]. They demonstrated that the fluorescence signal ratio of 3-pentanone has an improved sensitivity with temperature using the excitation wavelengths pair 308/266 nm rather than 308/248 nm. Temperature and mixture fraction were measured in a heated air turbulent jet using 308/266 nm excitation. By evaluating the rms variation of temperature and mole fraction in a relatively small and homogeneous area in the jet, temperature and mole fraction measurement precision was determined as ±15 K between 300 and 650 K and as 0.15% for the 3-pentanone concentration at 650 K for single-shot images.

A methodology for estimating the relative precision of single-shot measurements of simultaneous mole fraction and temperature under engine relevant conditions was developed by Rothamer et al. [49,50,55]. This methodology was used to investigate the optimal wavelength combination (277 and 308 nm) for simultaneous temperature and mole-fraction measurements using the 3-pentanone-LIF technique with two-line excitation. 3-pentanone-LIF measurements of a uniform mixture during the

compression stroke in a motored engine were used to determine the measurement uncertainty. The standard deviation calculated from single-shot images in a uniform area revealed a temperature measurement precision below ±12 K (i.e., 2.1% for 600 K). For the determination of accuracy, the measured ensemble-averaged temperatures were compared to temperature data calculated based on the assumption of isentropic compression. The absolute accuracy was evaluated to be below ±30 K (i.e., 5% for 600 K).

Biacetyl

Biacetyl has broadband absorption features in the 340–470 nm range. The absorption cross-section σ_{abs} at 266 nm decreases with temperature (at 300–650 K). However, the absorption cross-section at 355 nm is lower than at 266 nm and is independent of temperature [31]. Temperature, pressure, O_2 and tracer concentration effects on biacetyl fluorescence have been extensively investigated [58] in conditions close to those encountered in IC engines, in order to convert measured LIF signals into quantitative concentration measurements. The biacetyl fluorescence signal with excitation at 355 nm excitation does not have a monotonous dependence on temperature. The fluorescence signal increases from 373 to 423 K and then decreases until 523 K at atmospheric pressure. This behavior demonstrates the limitations of biacetyl LIF for thermometry.

Laser-induced fluorescence of biacetyl with excitation at 355 nm was applied in an optical engine for fuel concentration distribution measurements with high spatial and temporal resolution [59,60]. The pressure and temperature effects on the LIF signal were quantified for corrections on biacetyl-LIF images in order to obtain fuel concentration information after calibration.

2.2.3 Aromatics tracers

Basic physical and thermodynamic properties of a selection of aromatics and commonly used surrogate fuels are presented in Table 2-1 and their fluorescence properties are given in Table 2-2. Aromatic molecules are frequently used as fluorescence tracers in surrogate Diesel fuel such as *n*-dodecane or *n*-heptane due to their similar evaporation properties. Aromatics typically have high fluorescence quantum yields compared to ketones. Consequently, fluorescence signals from aromatic tracers are stronger, compared to ketone tracers at similar conditions. However, the fluorescence of aromatic molecules is strongly quenched by molecular oxygen. The sensitivity to O_2 quenching means that aromatics can potentially be used for O_2 concentrations imaging. The aromatics-LIF signal additionally depends on the tracer concentration and on temperature.

Toluene (single-ring aromatic)

Toluene is a tracer often used for fuel mixing studies in IC engines [26]. The dependence of the toluene fluorescence on temperature and O_2 partial pressure was well characterized for temperature and

fuel/air ratio measurements. Toluene photophysics have been thoroughly investigated by Koban et al. [61] at elevated temperatures (300–1000 K) at atmospheric pressure. The absorption spectrum is broadband (240–290 nm with a maximum at around 260 nm) and red-shifts with increasing temperature. Commonly used excitation wavelengths are 248 nm with KrF excimer lasers and 266 nm with frequency quadrupled Nd:YAG lasers. The absorption cross-section at 248 nm is relatively independent of temperature in the 300–950 K range at 1 bar. However, the absorption cross-section at 266 nm increases with temperature in the same range. Fluorescence spectra were studied in nitrogen with excitation at 266 and 248 nm, respectively. The broadband emission spectrum (260–400 nm with a maximum at around 280 nm) red-shifts with increasing temperature by approximately 2 nm/100 K. In the 300–950 K range at 1 bar, the fluorescence signal intensity decreases exponentially by three orders of magnitude for a laser excitation at 266 nm and by more than three orders of magnitude for a laser excitation at 248 nm. The fluorescence spectrum shifts to the red with increasing O_2 partial pressure for laser excitation at 248 nm but this red-shift is limited to low O_2 partial pressures. For laser excitation at 266 nm, the fluorescence spectrum does not change much in terms of spectral shape with O_2 partial pressure.

The well-characterized temperature-dependence of toluene fluorescence [61] was used for the development of single-line and two-line temperature measurement strategies [62,63]. A single-line temperature measurement strategy is usually applied in homogeneously seeded flows. In this case, after single-wavelength laser excitation at 248 or 266 nm, the toluene-LIF signal depends on temperature only. The fluorescence signal intensity, which decreases with increasing temperature, is collected in one spectral band by a camera equipped with the appropriate filter. Temperature information is then obtained after calibration for the temperature-dependence of the toluene-LIF signal and a measurement at a reference temperature. A two-line temperature measurement strategy is usually applied in spatially inhomogeneous flows. In this case, the toluene-LIF signal after single-wavelength laser excitation at 248 or 266 nm depends on temperature and on the local variation in tracer concentration. The redshift of the fluorescence signal with increasing temperature is exploited for determining temperature. The fluorescence signal is captured in two distinct spectral bands by two cameras equipped with the appropriate (different) filters. The resulting ratio of the fluorescence signal from the two different spectral bands depends on temperature and is independent of the local tracer concentration. Again, the signal ratio must be calibrated with its typical temperature dependence and a reference measurement.

After validation of the two-line temperature measurement strategy using toluene as a tracer in heated gas flows [62], this technique was applied in a motored optically accessible spark-ignition direct-injection (SIDI) engine [64]. For single-pulse measurements, the authors claimed a 1σ temperature precision of ±34 K below 625 K (i.e., 5.5% at 600 K). The precision was evaluated by averaging temperature in a spatially homogeneous zone with toluene-LIF thermometry and calculating the standard deviation for single-shot images. These results were based on the assumption that the pressure effect

was negligible. The results obtained by LIF thermometry were compared to temperatures derived from a thermodynamic analysis of measured in-cylinder pressures. The discrepancy between the two sets of data increased with increasing temperature. However, the absolute accuracy was not assessed from those comparisons since the assumptions made for the thermodynamic analysis were questionable.

Further studies on toluene fluorescence signal at higher pressures and higher temperatures were performed [65]. Toluene emission spectra after laser excitation at 248 nm were acquired in an optical engine during the compression phase without ignition. Measured toluene fluorescence spectra are available at simultaneous high temperature and high pressure from 293 K, 1 bar to 773 K, 23.6 bar. The influence of pressure variations on toluene fluorescence was quantified and an evaluation of the additional error on temperature measurements by neglecting the pressure effects was given (i.e., an error of 1.7% in N_2). The toluene-LIF technique was applied for several practical engine conditions. Thermal stratification was investigated in an HCCI engine using single-line toluene-LIF imaging with laser excitation at 266 nm [66,67]. The measurement uncertainty in [67] was associated with the camera shot-noise and was determined as 7 K. The same technique was also applied in an optically accessible rapid compression machine at high pressures and temperatures in order to characterize the thermal distribution of internal flows generated by aerodynamic processes encountered in HCCI engines [68].

Once temperature is known, toluene LIF can also be exploited for measuring the tracer (i.e., fuel) concentration after corrections for temperature, as long as the O_2 partial pressure is not varying spatially (or even better: in N_2 only). In the presence of O_2, the fluorescence signal and thus the sensitivity of the toluene-LIF thermometry technique is reduced significantly. However, previous studies [69,70] tried to exploit the toluene fluorescence dependence on O_2 to measure the fuel/air ratio via the FARLIF (i.e., Fuel-Air Ratio by Laser-Induced Fluorescence) technique. The toluene fluorescence signal was assumed to be directly proportional to the fuel/air ratio at constant temperature as long as O_2 quenching is the dominant de-excitation channel. An accuracy of 2% and a precision of 10% for the equivalence ratio measurement were claimed by the authors [69]. This technique was then applied in an IC engine to provide quantitative fuel/air ratio measurements in homogeneous mixtures [70]. Measurements were performed during the compression stroke for different equivalence ratios and the results were correlated with results from an analysis of engine exhaust gas emissions. Nevertheless, studies on toluene fluorescence signals under engine-related pressures, temperatures and O_2 mole fractions [44,71–74] showed that the FARLIF assumption is not valid at elevated temperatures. In reality, O_2 quenching is not dominant at elevated temperatures and therefore the toluene fluorescence signal is no longer inversely proportional to O_2 partial pressure under all the pressure and temperature conditions encountered in the compression stroke of IC engines. The FARLIF technique seems to be applicable only for laser excitation at 266 nm and for temperatures below 500 K. For other conditions, the exploitation of the toluene-LIF signal for obtaining quantitative fuel/air ratio information requires the

evaluation of additional quantities such as temperature. A way to simultaneously measure temperature and fuel/air ratio is to use an additional tracer to toluene such as 3-pentanone, allowing for temperature measurements. This strategy is described in detail in Section 2.2.4.

1,2,4-Trimethylbenzene (TMB, single-ring aromatic)

Fluorescence signal of 1,2,4-trimethylbenzene (TMB) with laser excitation at 266 nm was investigated for temperatures in the 350–900 K range, for pressures in the 1−30 bar range and for O_2 partial pressure in the 0–0.21 bar range [75]. The absorption cross-section reduces by about 20% from 350 to 900 K. The fluorescence signal intensity decreases by about three orders of magnitude as temperature increases from 350 to 900 K. The fluorescence spectrum is broadband between 260 and 360 nm, with a peak at approximately 290 nm. The fluorescence spectrum is red-shifted with increasing temperature by approximately 2 nm/100 K (at the point of 310 nm). This value is similar to the one obtained for toluene [61]. The fluorescence spectrum is slightly red-shifted with increasing O_2 partial pressure. At 450 K and 1 bar, the red-shift is determined at approximately 1 nm as the O_2 partial pressure increases from 0 to 0.21 bar. The effect of O_2 quenching on TMB-LIF results in fluorescence signal intensities that strongly decrease by a factor of 20 with increasing O_2 partial pressure in the range of 0 to 0.21 bar.

Tracer-LIF thermometry using TMB was applied in a preheated jet [75]. The fluorescence signal for a laser excitation at 266 nm was collected in two different spectral bands. The corresponding signal ratio acquired depends on temperature. The authors claimed a precision of ±50 K at 650 K (i.e., 7.7% at 650 K) for single-shot measurements in air, although information about the accuracy was not provided.

Naphthalene and 1-methylnaphthalene (two-ring aromatics)

Naphthalene is also a good candidate as an aromatic tracer for tracer-based LIF imaging to visualize fuel concentration, temperature and O_2 concentration. Naphthalene LIF was used in a lab-scale burner to visualize fuel distributions [76]. Naphthalene was also used for simultaneous quantitative measurements of temperature and equivalence ratio [77]. Naphthalene and 1-methylnaphthalene showed similar fluorescence behavior with laser excitation at 266 nm. At 500 K and 1 bar, the naphthalene fluorescence spectrum is slightly red-shifted with increasing O_2 partial pressure up to approximately 0.1 bar. A further increase of the O_2 partial pressure does not further red-shift the emission. At 1 bar, in the 400–928 K range, the fluorescence spectrum of 1-methylnaphthalene is red-shifted with increasing temperature and the red-shift at half maximum is approximately 16 nm, while in nitrogen it is approximately 21 nm. The red-shift of the spectrum with increasing temperature is exploited to determine temperature. The ratio of the fluorescence signals from two different spectral bands depends on temperature. The calibration curves giving the evolution of the LIF ratio with the temperature was inde-

pendent of the equivalence ratio (when varied from 0.2 to 5), indicating that naphthalene is a good candidate to measure temperature independently of the O_2 partial pressure in the 350–900 K temperature range and at 1 bar. The equivalence ratio was obtained from the naphthalene fluorescence signal after calibration on a heated jet. The results from the imaging experiment were used to confirm the observations made in the spectral measurements. In addition, the application of naphthalene LIF in a heated jet allowed the determination of the temperature measurement uncertainty of approximately 10% in the 348–700 K range (i.e., ±70 K). The corrections applied during the post-processing for obtaining the temperature and weak signal-to-noise ratio of LIF images were considered to be responsible for the limited accuracy of the temperature measurement.

The dependence of the naphthalene fluorescence signal on temperature, pressure and O_2 partial pressure was investigated for laser excitation at 266 nm [78]. The fluorescence signal strongly decreases with increasing temperature and O_2 partial pressure at 1 bar but the effect of pressure in nitrogen is limited. The fluorescence signal of naphthalene decreases by roughly an order of magnitude with increasing temperature in the 350–900 K range at 1 bar. However, the fluorescence signal of toluene decreases by three orders of magnitude for laser excitation at 266 nm and by more than three orders of magnitude for laser excitation at 248 nm (in the 350–900 K temperature range at 1 bar). The fluorescence signal of naphthalene strongly decreases by nearly two orders of magnitude when increasing the O_2 partial pressure at 1 bar. In addition, naphthalene spectra are red-shifted with increasing temperature by 5 nm/100 K between 340 and 400 nm. However, toluene has a red-shift of 2 nm/100 K between 260 and 400 nm. It was concluded that temperature has a stronger influence in terms of the red-shift for di-aromatics (e.g., naphthalene) than for single-ring aromatics (e.g., toluene).

Fluoranthene (multi-ring aromatic)

Fluoranthene fluorescence was investigated for laser excitation at 266 and 355 nm under varying conditions of temperature (473–873 K) and pressure (1–40 bar) [79]. The aim of this study was to provide data that allows to quantitatively measure temperature and fuel concentration based on fluoranthene LIF. The absorption cross-section at 266 and 355 nm increased steadily with temperature in the 473–873 K range. Fluoranthene fluoresces between 380 and 600 nm with a peak at 450 nm and the emission spectrum does not depend on the excitation wavelength (266 or 355 nm). The signal intensity decreases significantly with increasing temperature for both excitation wavelengths. The fluorescence signal ratio between the signal obtained for laser excitation at 266 and 355 nm shows a dependence on temperature in nitrogen at 30 bar in the 473–873 K temperature range, which demonstrated the potential of the technique for measuring temperature. No error estimate is available for the application of fluoranthene LIF. In addition, the use of fluoranthene as a tracer is limited to Diesel fuel due to its high boiling temperature (648 K).

2.2.4 Multi-tracer LIF measurements

Tracer-LIF techniques allow multi-parameter measurements, such as temperature, fuel concentration and fuel/air ratio. Ketone tracers are less sensitive to the quenching of O_2. Consequently, ketones are good tracer candidates to perform simultaneous measurements of fuel concentration and temperature, independently of the presence of O_2. However, aromatic tracers have the advantage of providing higher signal levels and their dependence on O_2 can be exploited to measure fuel/air ratio. Therefore, aromatic tracers are good candidates to perform measurements of temperature with high sensitivity particularly in an O_2-free environment and measurements of fuel/air ratio after corrections for temperature.

A direct measurement of the absolute O_2 concentration is feasible by combining two different tracers that respond differently to O_2 quenching and that can be detected separately upon excitation with a single laser wavelength. This technique was previously demonstrated [25,80–82] using a suitable tracer pair, one aromatic (e.g., toluene) and one ketone (e.g., 3-pentanone). O_2 fluorescence quenching on the ketones (e.g., 3-pentanone) is negligible compared that on the aromatics (e.g., toluene). After UV excitation, fluorescence signals of 3-pentanone centered at 420 nm and of toluene centered at 280 nm are spectrally separated.

This technique was first applied and validated in turbulent mixing processes of interacting air nitrogen flows [80] seeded with the respective tracers, for room-temperature and ambient-pressure conditions. The O_2 partial pressure was measured in the 0–0.21 bar range and the accuracy was determined at ±10% for 0.06 bar and at ±7% for 0.13–0.21 bar. Measurements were not accurate for O_2 partial pressure below 0.014 bar due to errors resulting from tracer interactions (energy transfer). The application of this two-tracer LIF technique was further extended to high-temperature and high-pressure conditions in an engine [81]. The results of absolute fuel and O_2 concentrations were in agreement with the metered fuel and air flows, as well as exhaust gas measurements but no measurement error was reported in this case. The two-tracer LIF technique using toluene and 3-pentanone was also applied in an optical engine in order to investigate the effect of skip-firing on the available in-cylinder O_2 concentration [82]. In this study, temperature was assumed to be homogeneous and the spatial variation was evaluated by calculating the standard deviation. However, in this study the authors reported no measurement precision.

In the case of spatial temperature gradients, a simultaneous imaging measurement of temperature is required to correct the fluorescence signals of toluene and 3-pentanone (that depend on temperature). For this purpose, an additional excitation wavelength and detector would be required to obtain temperature from 3-pentanone-LIF thermometry (described earlier). It would be then possible to measure simultaneously fuel concentration, O_2 concentration and temperature, which could fulfill the initial

objectives of this work. However, the use of two lasers for two-line excitation is increasing experimental cost and complexity compared to single-line excitation. Furthermore, a ketone/aromatics mixture shows photophysical interaction between the two components [83]. Ledier et al. [83] compared the fluorescence spectrum of the 3-pentanone/toluene mixture to the one rebuilt from the fluorescence spectra of 3-pentanone and toluene respectively weighted by their respective concentration. In the two-tracer mixture, a decrease of the fluorescence peak intensity of toluene and an increase of the fluorescence peak intensity of 3-pentanone were observed compared to the case where the two tracers were pure. This analysis showed a photophysical interaction between toluene and 3-pentanone, a possible energy transfer between the two molecules. This energy transfer depends on the partial pressure of the tracers into the mixture. The fuel concentration in this case, either from toluene or 3-pentanone fluorescence signal intensities would be measured with high uncertainties. The same analysis was followed with the mixture of two aromatics (e.g., 1,2,4-trimethylbenzene/naphthalene and naphthalene/fluoranthene). For each mixture, the fluorescence spectrum of the fluorescence mixture matched very well with the one rebuilt from the fluorescence spectra of each component weighted by their respective concentration. This observation has demonstrated negligible energy transfer between the tracers.

A ketone/aromatics mixture shows more photophysical interaction compared to an aromatics/aromatics mixture. When a mixture of two tracers is required for measuring several parameters (i.e., fuel concentration, O_2 concentration and temperature), an aromatics/aromatics mixture is preferred. However, this aspect needs to be verified for each specific mixture, since there is only limited data available on two-tracer mixtures and on the effects of tracer-tracer photophysical interactions.

2.2.5 Consideration about measurement uncertainty

The tracer-LIF techniques discussed above have limited precision and accuracy. The random error (precision) of tracer-LIF measurement techniques is usually evaluated *a posteriori* by calculating the standard deviation in a small region in a spatially homogeneous LIF image. For reducing the random error, the LIF images are averaged and filtered. However, this method for determining the precision does not include all of the potential error sources that can affect the measurement and are not carried out in conditions that are identical to the measurements. Errors related to image superposition (in case of calculating LIF-signal ratio images) for instance are not taken into account since only spatially homogeneous images are considered. In addition, since the error determination is carried out under homogeneous conditions, this approach does not take into account the high-temperature gradients that exist under real measurement conditions, which could cause additional errors. As a result, such *a posteriori* error evaluations can potentially underestimate the actual random error of the measurement technique. In addition, they do not provide information on how the random error could subsequently be optimized.

In the present work, an *a priori* random error determination methodology was developed to allow for a better determination of the actual random error directly related to the measurement configuration. This methodology is carried out in the same configuration as the actual measurement and therefore takes into account in particular uncertainties of the image superposition and the effects of high-temperature gradients. In addition, determining this *a priori* error also allows an improved identification of the different error sources and enables these error sources to be minimized in terms of their influence on the total error. In addition, the accuracy (systematic error) was assessed using an in-situ determination based on the comparison of the measurement with another technique (thermocouple) in an equivalent configuration. Again, this comparison is performed in the same configuration as the actual measurements in order to ensure that the comparison is representative, which is not usually the case when examining the approaches reported in the literature (e.g., lower temperature, homogeneous conditions, etc.).

2.3 Two-tracer LIF diagnostics

In the present work a two-tracer LIF technique using two aromatic tracers to measure simultaneously three parameters, fuel concentration, O_2 concentration and temperature was developed.

2.3.1 Tracer fluorescence signal interpretation

The following expression gives the detected fluorescence signal intensity S_{fl} in the linear excitation limit [1]:

$$S_{\mathrm{fl}} = \left(\frac{E}{hc/\lambda}\right) V n_{\mathrm{tr}} \sigma_{\mathrm{abs}} \phi_{\mathrm{fl}} \frac{\Omega}{4\Pi} \eta_{\mathrm{opt}} \tag{2.2}$$

S_{fl} is the number of photons per pixel incident on the detector or the photocathode of an intensified camera (in photons/pixel). E is the local laser fluence (in J/cm²), hc/λ is the energy of a single absorbed photon (in J) with the excitation wavelength λ of the laser source, consequently the term in brackets represents the photon flux. n_{tr} is the number density of the fluorescence tracer in the observed volume V that has the absorption-cross section σ_{abs} (in cm²). ϕ_{fl} is the fluorescence quantum yield which represents the fraction of excited molecules that actually fluoresce. $\Omega/4\pi$ is the collection solid angle of the optics used for imaging the fluorescence, and η_{opt} is the optical transmission efficiency of optics and filters within the detection system.

As a consequence, for a given laser energy and detection system, the fluorescence signal intensity S_{fl} is proportional to the number density of the fluorescing tracer molecules n_{tr}, the absorption cross-section σ_{abs} and the fluorescence quantum yield ϕ_{fl}:

$$S_{\mathrm{fl}} \propto n_{\mathrm{tr}} \sigma_{\mathrm{abs}} \phi_{\mathrm{fl}} \tag{2.3}$$

The absorption cross-section σ_{abs} and the fluorescence quantum yield depend ϕ_{fl} on the excitation wavelength λ_{exc}, temperature T and pressure p. The fluorescence quantum yield ϕ_{fl} depends additionally on the O_2 partial pressure p_{O_2} since aromatic fluorescence is strongly quenched by O_2 assumed to be the principal quencher. The fluorescence signal intensity from equation (2.3) can be written as:

$$S_{\mathrm{fl}} = \left(\frac{E}{hc/\lambda}\right) V n_{\mathrm{tr}} \sigma_{\mathrm{abs}}(\lambda_{\mathrm{exc}}, T, p) \phi_{\mathrm{fl}}(\lambda_{\mathrm{exc}}, T, p, p_{O_2}) \frac{\Omega}{4\Pi} \eta_{\mathrm{opt}} \tag{2.4}$$

For tracer mole fraction imaging (i.e., fuel mole fraction imaging), the number density of the tracer n_{tr} can be written in terms of mole fraction x_{tr} of the tracer:

$$n_{\mathrm{tr}} = \frac{x_{\mathrm{tr}} p}{kT} \tag{2.5}$$

where p is the total pressure, T the temperature and k the Boltzmann constant.

Using equation (2.5), the fluorescence signal intensity S_{fl} from equation (2.4) becomes:

$$S_{\mathrm{fl}} = \left(\frac{E}{hc/\lambda}\right) V x_{\mathrm{tr}} \left(\frac{p}{T}\right) \sigma_{\mathrm{abs}}(\lambda_{\mathrm{exc}}, T, p) \phi_{\mathrm{fl}}(\lambda_{\mathrm{exc}}, T, p, p_{O_2}) \frac{\Omega}{4\Pi} \eta_{\mathrm{opt}} \tag{2.6}$$

2.3.2 Two-tracer LIF measurement strategy

The previous paragraph presents the equations describing the detected fluorescence signal intensity S_{fl} of aromatic tracers after UV excitation. Based on these equations, a measurement strategy using two-tracer LIF was introduced for measuring simultaneously three parameters, temperature, O_2 concentration, and fuel concentration.

Temperature measurement (1)

The first step consists of exploiting the fluorescence signal of one aromatic tracer to provide temperature measurements. For many aromatic compounds, the fluorescence emission spectrum after a single wavelength excitation shows a red-shift with increasing temperature. This red-shift can be exploited to provide temperature information as described in Section 2.2.1. The red-shift is quantified by collecting the fluorescence signal in two distinct spectral bands with appropriate filters. More details about the tracer-LIF thermometry are given in Chapter 4.

The ratio of the two collected signals depends on temperature. Using equation (2.6), the fluorescence signal ratio is given by the following equation after simplification:

$$\frac{S_{\mathrm{fl}}^{1}}{S_{\mathrm{fl}}^{2}} = \frac{\eta_{\mathrm{opt}}^{1}\phi_{\mathrm{fl}}^{1}(\lambda_{\mathrm{exc}}, T, p, p_{\mathrm{O_2}})}{\eta_{\mathrm{opt}}^{2}\phi_{\mathrm{fl}}^{2}(\lambda_{\mathrm{exc}}, T, p, p_{\mathrm{O_2}})} = f(T, p, p_{\mathrm{O_2}}) \tag{2.7}$$

By calculating the ratio from equation (2.6), the laser excitation energy E and tracer number density n_{tr} cancel. Consequently, the fluorescence ratio depends only on temperature T, pressure p and O_2 partial pressure $p_{\mathrm{O_2}}$. T and p are correlated and their influence on the absorption cross-section σ_{abs} and the fluorescence quantum yield ϕ_{fl} should be well characterized.

However, at this stage, $p_{\mathrm{O_2}}$ is unknown and should be determined in the following steps. The fluorescence of aromatics is quenched by molecular O_2. For some aromatic compounds, the fluorescence emission spectra shift to the red with increasing $p_{\mathrm{O_2}}$, depending on conditions such as excitation wavelength λ_{exc} and $p_{\mathrm{O_2}}$. This aspect will be analyzed in Section 2.3.3 in more detail. Let us assume at this stage that the molecular O_2 quenching does not change the fluorescence spectra and that the observed red-shift is only caused by the temperature effect. In this case, equation (2.7) changes to:

$$\frac{S_{\mathrm{fl}}^{1}}{S_{\mathrm{fl}}^{2}} = \frac{\eta_{\mathrm{opt}}^{1}\phi_{\mathrm{fl}}^{1}(\lambda_{\mathrm{exc}}, T, p)}{\eta_{\mathrm{opt}}^{2}\phi_{\mathrm{fl}}^{2}(\lambda_{\mathrm{exc}}, T, p)} = R_T(T, p) \tag{2.8}$$

R_T is the fluorescence signal ratio of two distinct spectral bands. The temperature calibration curve for the fluorescence ratio is obtained from known fluorescence spectra at various T and p, and considering the spectral dependence of the detection system.

O_2 concentration measurement (2)

In a second step, $p_{\mathrm{O_2}}$ is measured by exploiting the differences in sensitivity of the fluorescence signals of the two aromatic tracers as a function of $p_{\mathrm{O_2}}$. The interaction of the excited aromatic molecule with molecular oxygen is visible through (a) a redshift of the fluorescence spectrum with increasing $p_{\mathrm{O_2}}$ and (b) a decrease of the fluorescence signal intensity with increasing $p_{\mathrm{O_2}}$.

The first aspect (a) will be analyzed in Section 2.3.3 in more detail. Let us assume at this stage that the O_2 quenching shifts the fluorescence spectra slightly to the red and that the red-shift observed is mainly caused by temperature effects. The second aspect (b) is exploited here. Similarly to the two-tracer LIF technique developed in [80,81], $p_{\mathrm{O_2}}$ can be obtained from the ratio of the fluorescence signals resulting from excitation at the same wavelength:

$$\frac{S_{fl}^{\mathrm{tr1}}}{S_{\mathrm{fl}}^{\mathrm{tr2}}} = \frac{\eta_{\mathrm{opt}}^{\mathrm{tr1}}\sigma_{\mathrm{abs}}^{\mathrm{tr1}}(\lambda_{\mathrm{exc}}, T, p)\phi_{\mathrm{fl}}^{\mathrm{tr1}}(\lambda_{\mathrm{exc}}, T, p, p_{\mathrm{O_2}})}{\eta_{\mathrm{opt}}^{\mathrm{tr2}}\sigma_{\mathrm{abs}}^{\mathrm{tr2}}(\lambda_{\mathrm{exc}}, T, p)\phi_{\mathrm{fl}}^{\mathrm{tr2}}(\lambda_{\mathrm{exc}}, T, p, p_{\mathrm{O_2}})} = R_{\mathrm{O_2}}(T, p, p_{\mathrm{O_2}}) \tag{2.9}$$

In equation (2.9) the laser excitation energy E cancels. The tracer number density n_{tr} also cancels when assuming similar behavior between the tracers and the fuel. Consequently, the ratio depends

only on T, p, and p_{O_2}. R_{O_2} is the fluorescence signal ratio of both tracers. The measurement of p_{O_2} required the determination of calibration curves for the fluorescence signal ratio that can be obtained from the fluorescence signal well characterized at various T, p, and p_{O_2} for the two tracers, and considering the spectral sensitivity of the detection system. The dependence of the signal ratio on p_{O_2} is studied in more detail in Chapter 5. The O_2 concentration (i.e., O_2 mole fraction x_{O_2}) is derived from p_{O_2} by equation (2.10).

$$x_{O_2} = \frac{p_{O_2}}{p} \tag{2.10}$$

Fuel concentration measurement (3)

The third step consists of measuring the tracer mole fraction x_{tr} from the fluorescence signal of one tracer given by equation (2.6). At this stage, knowing T, p, and p_{O_2} allows to determine x_{tr} from the fluorescence signal of a single tracer. The fuel mole fraction x_{fuel} corresponds to the tracer mole fraction x_{tr} by assuming similar transport behavior of tracers and fuel.

2.3.3 Selection of tracers: Toluene and naphthalene

The methodology for measuring simultaneously three parameters (fuel concentration, temperature, and O_2 concentration) using a two-tracer LIF technique has been described above. Two aromatic tracers must be carefully selected taking into account the following the requirements.

Excitation wavelength

The two tracers should have absorption bands that are accessible with commercial lasers available such as a (KrF) excimer laser (248 nm) or a frequency-quadrupled Nd:YAG laser (266 nm). All the tracers presented in Table 2-2 meet this requirement.

Selective fluorescence emission signal detection

The fluorescence signal of each tracer should be spectrally separated to allow unambiguous detection of the LIF signals corresponding to each tracer. The fluorescence emission spectra of the single-ring aromatic tracers (e.g., toluene, 1,2,4-trimethylbenzene) are shifted to the red by 40 to 50 nm compared to the bi- and multi-ring aromatic tracers (e.g., naphthalene, 1-methylnaphthalene, fluoranthene) [84]. Therefore, in the case of selecting two aromatics, one of the tracers should be single-ring aromatic and the other tracer bi- or multi-ring aromatic in order to enable spectrally independent detection.

O_2 dependence of the fluorescence signal

The fluorescence signals of the two tracers should have different sensitivities on O_2 partial pressure (i.e., one tracer should be more sensitive to O_2 quenching than the other). The Stern-Volmer coefficient (cf. Chapter 3) gives information about the sensitivity of the fluorescence emission with p_{O_2} [26] and usually depends on temperature. Figure 2-1 shows the dependence of the Stern-Volmer coefficient (in the 0–0.21 bar O_2 partial pressure range) on temperature for several tracers. For all tracers, the Stern-Volmer coefficient decreases with increasing temperature, demonstrating that the quenching effect of O_2 is less important at higher temperatures. Therefore, the sensitivity of the fluorescence of aromatic tracers on p_{O_2} decreases with increasing temperature.

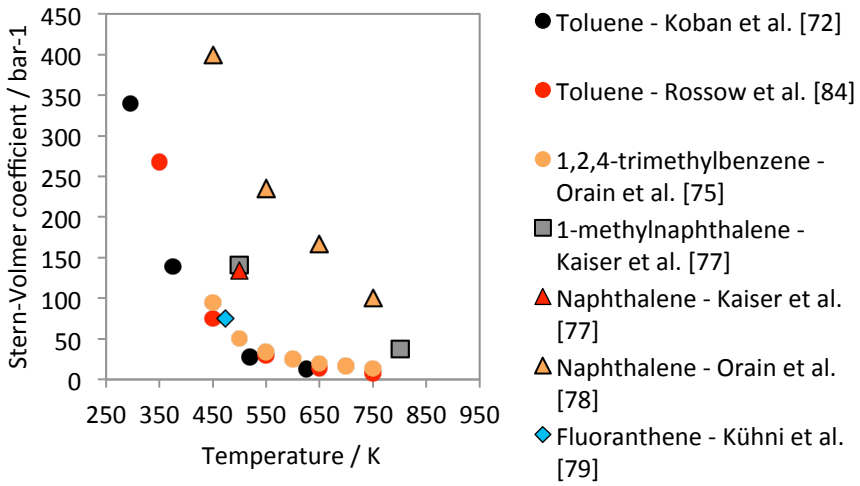

Figure 2-1: Temperature dependence of the Stern-Volmer coefficients for a selection of aromatic tracers. The dots represent the single-ring aromatics and the squares the bi- and multi-ring aromatics. The Stern-Volmer coefficients are derived from photophysical data measured in the 0–0.21 bar O_2 partial pressure range for laser excitation at 266 nm.

The tracers mentioned in Figure 2-1 do not have the same response to O_2 quenching in the 0–0.21 bar O_2 partial pressure range. As a single-ring aromatic tracer, toluene tracer is a good candidate due to its relatively low sensitivity to O_2 quenching. However, O_2 quenching is more pronounced for naphthalene and the dependence of the Stern-Volmer coefficient on temperature is less important. Therefore,

the di-aromatic tracer naphthalene is a good candidate as a tracer with relatively high sensitivity to O_2 quenching. Additionally, naphthalene is a good candidate for temperature measurements using the two-color LIF technique since the O_2 quenching effects are less dependent on temperature. In this case, the temperature measurement results would be less dependent on the presence of O_2.

Photophysical interaction between tracers

The Stern-Volmer coefficient of toluene and naphthalene indicates that these two tracers are good candidates for simultaneously measuring temperature, fuel and O_2 concentration using the two-tracer LIF technique. In addition, the fluorescence signals of the two tracers are spectrally well separated (i.e., fluorescence peaks at around 280 nm and 320 nm for toluene and naphthalene, respectively) which facilitates the selective detection of the two LIF signals. However, it is crucial to study the photophysical interactions between both tracers, which should be either negligible or well characterized. This aspect will be investigated in Chapter 3.

Photophysical data

In order to use toluene and naphthalene for the two-tracer LIF technique, their dependences in terms of LIF signal as a function of temperature, pressure and O_2 partial pressure need to be well characterized. Concerning toluene, LIF emission spectra under conditions of interest (i.e., temperature, O_2 partial pressure) are available in the literature as reported by Koban et al. [61,72] and Rossow et al. [84]. However, in Figure 2-1, the Stern-Volmer coefficients of toluene at various temperatures show a discrepancy for the two sources (Koban et al. [61,72] and Rossow et al. [84]). For naphthalene, LIF emission spectra are available from Kaiser et al. [77] but at a single temperature only (500 K). The naphthalene LIF spectra reported by Orain et al. [78] are available for more conditions. However, the Stern-Volmer coefficients for 500 K from the two sources differ (Figure 2-1).

At the time of this PhD, the naphthalene fluorescence data from Orain et al. [78] were not published yet. Therefore, photophysical measurements were performed on naphthalene for various conditions of temperature, pressure and O_2 partial pressure. Additionally, it was a means to compare naphthalene LIF data in the case of pure naphthalene with the case of a mixture of toluene and naphthalene, in order to investigate possible photophysical interactions between naphthalene and toluene under the conditions of interest.

2.4 Approach of the present work

2.4.1 Objectives

The objective of the present work is to simultaneously measure three parameters (fuel concentration, temperature and O_2 concentration) with an emphasis on high spatial resolution and low measurement uncertainty. The technique should be applicable for in-cylinder measurements in IC engines. A non-

intrusive laser diagnostics technique was selected among the various existing techniques described above.

The tracer-LIF techniques provide temperature and fuel concentration measurements offering potentially high spatial resolution. The use of two tracers is required to measure fuel concentration, temperature, and O_2 concentration. One tracer should ideally have a high sensitivity to temperature and thus enable temperature measurements without being affected by O_2 quenching. A second tracer should possess an O_2-sensitivity that differs from the first tracer to enable direct O_2 concentration measurements based on the different response on O_2 quenching after taking into account temperature dependences.

Various tracers are promising for a two-tracer LIF technique that fulfills the above requirements. As discussed in the previous sections, tracer-tracer photophysical interactions in aromatics/aromatics tracer mixtures are less important compared to aromatics/ketone tracer mixtures. Therefore, a tracer mixture composed of two aromatics is preferred. Toluene/naphthalene mixtures were selected based on their photophysical properties. These fulfill the requirements, in particular:

- both tracers can be excited at the same wavelength
- the LIF emission from both tracers can be spectrally separated
- the sensitivity on O_2 is significantly different for both tracers
- the photophysical interaction between the tracers is low
- photophysical data that is available for both tracers for various temperatures, pressures and bath gas compositions

2.4.2 Development of a multi-parameter measurement strategy

Based on this tracer selection a measurement strategy was developed that provides the capability of multi-parameter measurements with high spatial resolution. A particular focus was on characterizing the sources of measurement uncertainty with the aim to increase precision and accuracy. The technique should ultimately be applied in an environment representative of in-cylinder conditions, characterized by high temperature, high pressure and in-homogeneities in temperature and species concentration.

The spectral properties of the two tracers used in this study were analyzed in detail. Their spectral responses were characterized as a function of temperature, pressure and O_2 partial pressure as well as their intermolecular photophysical interaction. Although some data were available in the literature, a range of additional measurements was required (Chapter 3).

Subsequently, a quantitative measurement methodology was developed that allows an evaluation and optimization of measurement uncertainties. This analysis was performed with a single-tracer LIF technique using toluene but with the objective to apply the same approach in general to tracer-LIF techniques requiring LIF-ratio calculations and to multi-parameter measurements (Chapter 4).

Finally, the two-tracer LIF technique using toluene and naphthalene was investigated under high-temperature and high-pressure conditions. An optimized experimental strategy was developed to validate the technique for future applications in optical engines (Chapter 5).

Table 2-1: Physical, thermodynamic properties of some ketone tracers, aromatic tracers and surrogate fuels.

KETONE TRACERS			
	Molecular weight [g/mol]	Density at 25°C [g/cm^3]	Boiling point [K]
Acetone	58.1	0.79	329
3-Pentanone	86.1	0.81	375
Biacetyl	86.1	0.98	361
AROMATIC TRACERS			
	Molecular weight [g/mol]	Density at 25°C [g/cm^3]	Boiling point [K]
Toluene	92.1	0.87	384
1,2,4-Trimethylbenzene	120.2	0.88	444
Naphthalene	128.2	1.14	491
1-Methylnaphthalene	142.2	1	251
Fluoranthene	202.3	1.25	648
SURROGATE FUELS			
	Molecular weight [g/mol]	Density at 25°C [g/cm^3]	Boiling point [K]
iso-Octane	114.2	0.69	372
n-Dodecane	170.3	0.75	489
n-Heptane	100.2	0.68	371

Table 2-2: Fluorescence properties of some ketone tracers and aromatic tracers.

KETONE TRACERS				
	Absorption band [nm]	σ_{abs} [cm²]	Emission band [nm]	Φ_{fl}
Acetone	225–320	$\sim 10^{-20}$	350–550 Peak: 430	$\sim 10^{-3}$
3-Pentanone	220–320	–	330–600Peak: 420	$\sim 10^{-3}$
Biacetyl	340–470	$\sim 10^{-19}$	400–600 Peak: 480	$\sim 10^{-3}$
AROMATIC TRACERS				
	Absorption band [nm]	σ_{abs} [cm²]	Emission band [nm]	Φ_{fl}
Toluene	240–290	$\sim 10^{-19}$	225–320	$\sim 10^{-1}$
1,2,4-Trimethylbenzene	(266)	$\sim 10^{-18}$	225–320	–
Naphthalene	240–280	$\sim 10^{-17}$	225–320	$\sim 10^{-1}$
1-Methyl-naphthalene	(266)	–	225–320	$\sim 10^{-1}$
Fluoranthene	240–360	$\sim 10^{-17}$	225–320	$\sim 10^{-1}$

3 Photophysical measurements on toluene and naphthalene

Based on photophysical data available in the literature, a mixture of toluene and naphthalene appears to be a good combination for simultaneously measuring three parameters, temperature, O_2 partial pressure and fuel concentration, using the two-tracer LIF technique with excitation at 266 nm. This chapter aims at describing the photophysics of aromatic molecules before presenting photophysics measurements on naphthalene and on a mixture of naphthalene and toluene. The results provide additional understanding and characterization of the respective tracers' fluorescence signals under various conditions (i.e., temperatures, total pressures, and O_2 partial pressures).

3.1 Photophysics of aromatic tracers

Schulz et al. [26] described in detail the photophysics of popular organic tracer species such as aromatics. A brief overview of the fundamental photophysics of aromatic tracers is given below to allow an interpretation of its fluorescence emission signal after UV excitation.

3.1.1 Absorption and deactivation of excited molecules

Organic molecules can absorb photons in the UV leading to the population of excited electronic levels. The ability of a molecule to absorb a photon is given by the absorption cross-section $\sigma_{abs}(\lambda,T)$, which depends on the excitation wavelength and the temperature.

After absorbing photons, the excited molecule can lose its excess energy through photo-physical processes:

- Radiative processes when the excess energy (or part of it) is emitted by spontaneous emission such as fluorescence or phosphorescence
- Non-radiative processes when the excess energy is thermalized by vibrational and rotational energy transfer
- Collisional quenching consisting of electronic de-excitation of colliding molecules (i.e., electronic energy transfer)

The Jablonski diagram presented in Figure 3-1 shows the photophysical processes during energy redistribution through radiative (straight lines) and non-radiative (wavy lines) channels.

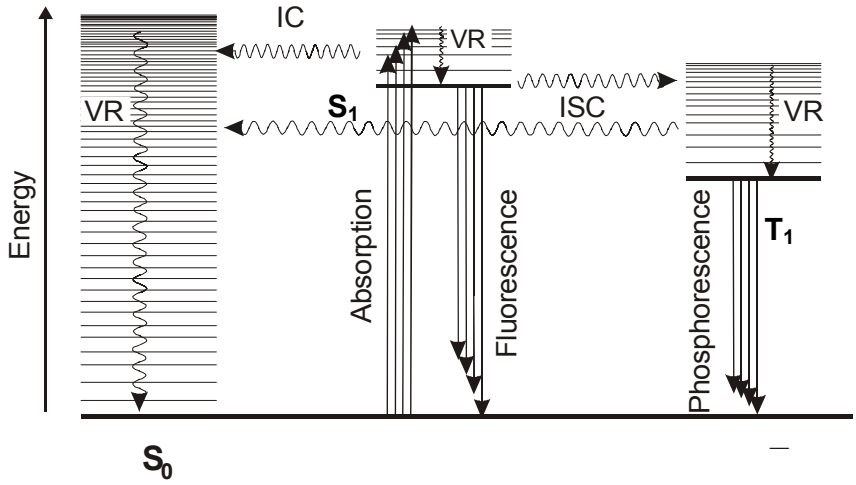

Figure 3-1: Jablonski diagram showing the photophysical processes during electronic excitation and deactivation of organic molecules. Straight and wavy lines indicate radiative and non-radiative processes, respectively [26].

Radiative processes

The excited molecule can lose energy by spontaneous emission of light through the transition from the S_1 to the S_0 state. This phenomenon, called fluorescence, can be observed during a short interval of 1–100 ns. The molecule in the excited state S_1 can also be transferred to the T_1 state through intersystem crossing (ISC). ISC is a non-radiative process and the molecule can subsequently emit light through the spontaneous transition T_1–S_0. This phenomenon is called phosphorescence and – because it is spin-forbidden – has a typical lifetime of milliseconds to seconds, much longer than the fluorescence life-time (nanoseconds).

Non-radiative intra-molecular processes

Non-radiative intra-molecular electronic transitions occur "horizontally" without changing the total energy. The non-radiative transition between states of different spin multiplicity (S_1–T_1 transition) and between states of the same spin multiplicity (S_1–S_0 transition) are called intersystem crossing (ISC) and internal conversion (IC) respectively. Vibrational relaxation (VR) occurs through collisions with bath-gas molecules. In this way the excess vibrational energy can be lost either in the ground state (S_0) or in the excited states (S_1 and T_1).

3.1.2 Kinetics of photophysical processes

Schulz et al. [26] explained in detail the kinetics of photophysical processes in order to characterize the relaxation process of the excited molecules. Only a brief overview of the characteristic parameters of photophysical processes is given below.

Radiative and effective lifetimes

The temporal variation of the concentration of excited molecules is given by a first-order differential equation, leading to an exponential decay with the rate *k* for the relevant deactivation process and the initial concentration. All the equations are detailed in [26]. The lifetime τ of a deactivation process is related to the rate *k* with the following equation:

$$\tau = 1/k \tag{3.1}$$

The radiative lifetime ($\tau_{\mathrm{rad}} = 1/k_{\mathrm{rad}}$) corresponds to the lifetime if the fluorescence emission was the only pathway of relaxation of the excited molecules. The radiative lifetime τ_{rad} is an intrinsic property of the molecule and assumed to be constant.

The effective fluorescence lifetime ($\tau_{\mathrm{eff}} = 1/k_{\mathrm{tot}}$) accounts for the total rate of depopulation of the excited state, including all individual radiative (such as fluorescence) and non-radiative (such as ISC, IC) depopulation processes respectively. As a consequence, the effective lifetime τ_{eff} is shorter than the radiative lifetime τ_{rad}. The effective lifetime τ_{eff} is the fluorescence lifetime time that is directly accessible in an experiment.

Fluorescence quantum yield

The fluorescence quantum yield, Φ_{fl}, is the fraction of excited molecules that actually emit fluorescence. The other fraction corresponds to the relaxation of the molecules through non-radiative processes. The fluorescence quantum yield Φ_{fl} can be interpreted as the ratio of rate coefficients of fluorescence k_{fl} and total depopulation k_{tot} or the ratio of the effective fluorescence lifetime τ_{eff} and the radiative lifetime τ_{rad}:

$$\Phi_{\mathrm{fl}} = \frac{k_{\mathrm{fl}}}{k_{\mathrm{tot}}} = \frac{\tau_{\mathrm{eff}}}{\tau_{\mathrm{rad}}} \tag{3.2}$$

By assuming the radiative lifetime being constant for a molecule, the fluorescence quantum yield is proportional to the effective fluorescence lifetime. As a consequence, relative fluorescence quantum yields can be determined from effective fluorescence lifetime measurements.

3.1.3 Collisional quenching

Only intra-molecular processes were mentioned so far as non-radiative deactivation pathways. Non-radiative relaxation can also occur through intermolecular collisional energy transfer. The excited molecule loses energy by quenching collisions with specific colliding molecules. In the case of aromatic tracers, quenching collisions occur predominantly with O_2 molecules.

Quenching collisions are a possible additional non-radiative deactivation pathway leading to the decrease of the fluorescence quantum yield Φ_{fl}. An additional term is added to the denominator of the equation of Φ_{fl} stated in (3.2):

$$\Phi_{\mathrm{fl}} = \frac{k_{\mathrm{fl}}}{k_{\mathrm{tot}} + \tilde{k}_{\mathrm{q}}\, n_{\mathrm{q}}} \tag{3.3}$$

k_{fl} is the fluorescence rate, k_{tot} the sum of fluorescence rate and non-radiative intra-molecular deactivation rates, $\tilde{k}_{\mathrm{q}}$ the quenching rate coefficient and n_{q} the number density of the quenching species.

The ratio of the fluorescence signal intensity in the absence of quenching S_{fl}^{0} and the fluorescence signal intensity with quenching effect S_{fl} represents the efficiency of the quenching effect:

$$\frac{S_{\mathrm{fl}}^{0}}{S_{\mathrm{fl}}} = \frac{k_{\mathrm{fl}}}{k_{\mathrm{tot}}} \frac{k_{\mathrm{tot}} + \tilde{k}_{\mathrm{q}}\, n_{\mathrm{q}}}{k_{\mathrm{fl}}} = 1 + \frac{\tilde{k}_{\mathrm{q}}}{k_{\mathrm{tot}}} n_{\mathrm{q}} = 1 + k_{\mathrm{SV}} n_{\mathrm{q}} \tag{3.4}$$

The factor k_{SV}, called the Stern-Volmer coefficient, can be obtained experimentally by measuring the fluorescence signal intensity with varying quencher number density under similar conditions. Therefore, the impact of O_2 quenching relative to the total intra-molecular de-excitation rate k_{tot} is experimentally indicated by the Stern-Volmer coefficient k_{SV}.

3.2 Experimental investigation of tracer fluorescence

Spectral and temporal fluorescence properties of naphthalene and a mixture of naphthalene and toluene were investigated for laser excitation at 266 nm to obtain experimental data of fluorescence spectra and lifetimes in specified conditions relevant for applications in IC engines (i.e., at various temperatures, pressures and O_2 partial pressures). Fluorescence spectra and lifetimes were acquired in the temperature range of 370–830 K, in the pressure range of 1–10 bar in N_2 and air bath gas, respectively. For investigating O_2 quenching, fluorescence spectra and lifetimes were acquired in N_2/O_2 bath-gas mixtures at 1 bar total pressure, by varying the O_2 partial pressure from 0 to 0.21 bar in the temperature range of 370–830 K.

3.2.1 Experiment

The experiment was performed in a high-temperature high-pressure flow cell with optical access, allowing study of spectral and temporal fluorescence properties of vaporized tracer molecules, under well-defined conditions of temperature, pressure, and bath-gas composition [85].

Flow cell design

Figure 3-2 shows the schematics of the high-temperature high-pressure flow cell at the University of Duisburg-Essen for investigating fluorescence properties of vaporized tracers under well-controlled conditions. The flow cell consists of two concentric ceramic tubes with four circular openings at 90° for optical access to the probe volume in the center of the inner tube. The inner flow chamber with a diameter of 55 mm and the outer flow chamber with a diameter of 90 mm are placed inside a stainless-steel vessel of 400 mm diameter. Electric heaters are located around the outer flow chamber and are thermally insulated against the vessel walls. The gas mixture of interest enters the stainless-steel vessel

through its bottom via a concentric tube-in-tube feed through. The path of the gas flow is shown in Figure 3-2. The gas mixture reaches the lower chamber and is preheated. Then the gas flows upwards through the outer flow chamber consisting of eight ceramic tubes. As the heated gas flow reaches the upper chamber, the flow direction is reversed downwards into the inner chamber (i.e., the probe volume) through seven holes. Finally, the gas exits through the inner stainless-steel tube and the feed-through in the bottom plate of the vessel.

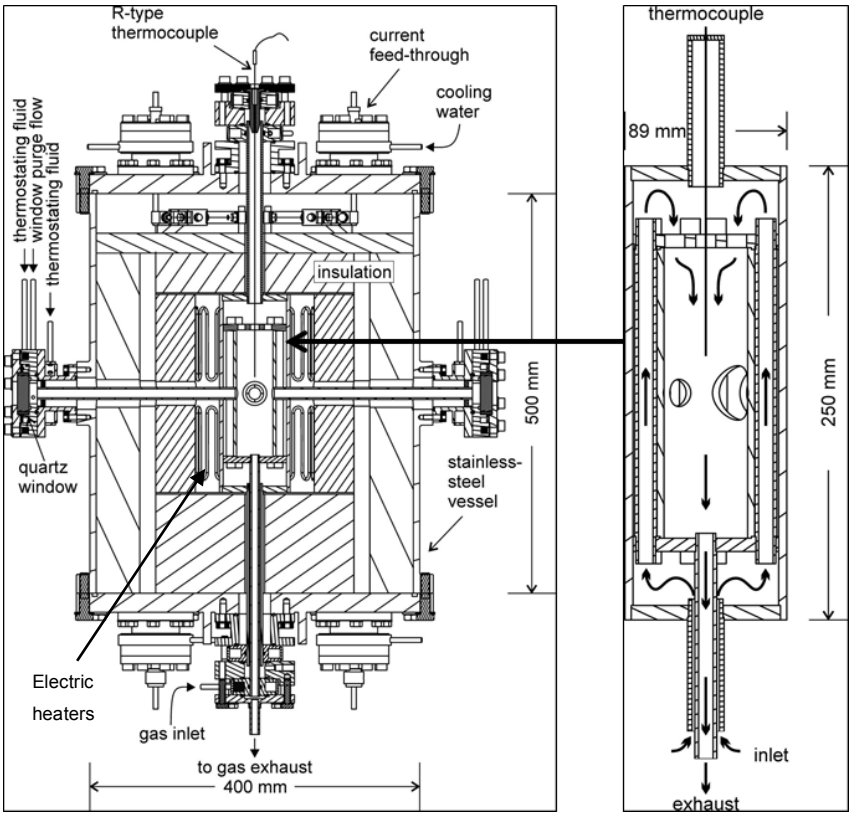

Figure 3-2: Schematics of the high-temperature high-pressure flow cell at the University of Duisburg-Essen for investigating fluorescence properties of vaporized tracers under well-controlled conditions. Left: Overview of the entire flow cell. Right: Path of the inner gas flow (i.e., the flow from the outer cell towards the inner flow chamber and measurement location).

The stainless-steel vessel is equipped with four optical ports (quartz windows of 30 mm clear aperture) in line with the opening of the outer and inner chambers. The windows are equipped with purge flows to keep the volume between the windows and the outer chamber free of absorbing species. The purge flow rate is negligible compared to the main flow.

Tracer and gas flow control

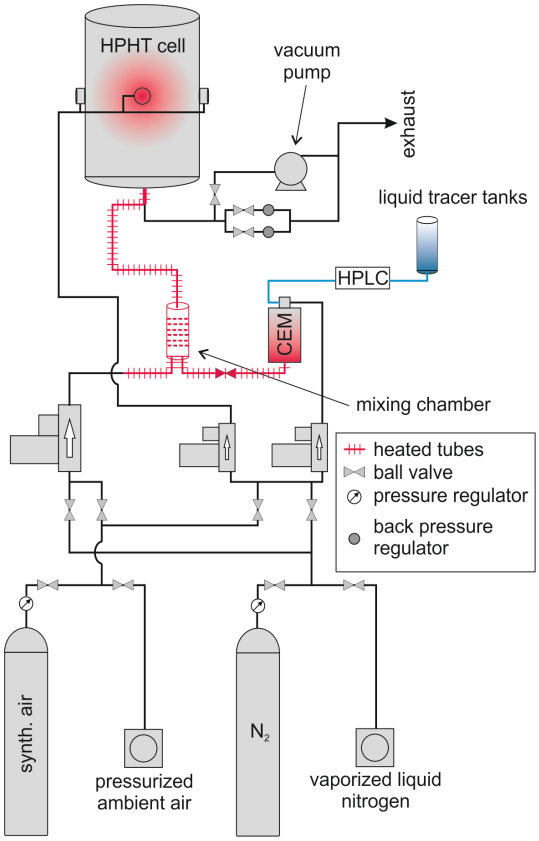

Figure 3-3: Schematics of the tracer evaporation, gas supply, and mixing.

Figure 3-3 shows the scheme describing the delivery of tracer(s) mixture and gas flows to the cell. The tracer can either be liquid (e.g., toluene) or solid (e.g., naphthalene) at ambient conditions. Solid tracers must be provided in solution in a non-fluorescing solvent. The liquid tracer or the tracer solution is stored in a tank connected to a HPLC (High Performance Liquid Chromatography) pump (Compact Pump 2250, Bischoff-Chrom). The liquid flow is metered by the HPLC pump before entering a CEM (controlled evaporator mixer, Bronkhorst) system where it is completely evaporated and mixed with the carrier gas. A mass-flow controller (Bronkhorst) with the range of 1–4 slm (standard liter per minute) controls the carrier gas. The mixture of the evaporated tracer and the carrier gas enters the gas-mixing chamber, which is additionally connected to another supply line equipped with a mass-flow controller (Bronkhorst). This line provides gas flow (air or N_2) to the gas-mixing chamber in the 1–20 slm range to optionally further dilute the tracer concentration or to modify the bath-gas composition by admixture of additional gases. After the gas-mixing chamber, the gaseous mixture enters the cell. The bath-gas composition is controlled by the carrier gas flow set in the CEM and the gas flow fed into the gas-mixing chamber, which allow a study of the tracer in a bath gas of N_2, air and a mixture of N_2 and air with various O_2 partial pressures in the range of 0–0.21 bar.

Temperature and pressure control

The heating temperature of the outer flow chamber of the high-temperature high-pressure cell is controlled by a thermocouple (R-type). The gas temperature inside the cell is measured with another thermocouple (R-type) located at the vertical central axis of the inner flow chamber, shortly above the probe region. The flow cell is designed for a maximum temperature of 1400 K.

Pressures between 1 and 10 bar can be obtained by varying the total flow rate in the range of 2–20 slm and by using a back-pressure regulator (Hoke) placed between the exit of the cell and the exhaust (cf. Figure 3-3). The needle valve position of the back-pressure regulator is controlled manually.

Optical arrangement

The optical arrangement is the one used by Faust et al. [85] for investigating temperature and bath-gas composition effects on effective lifetimes of toluene fluorescence. Figure 3-4 shows the arrangement for UV-laser excitation, the optics and the fluorescence detection system for measuring spectrally- and temporally-resolved fluorescence signals of tracers (naphthalene and a mixture of naphthalene and toluene in this work).

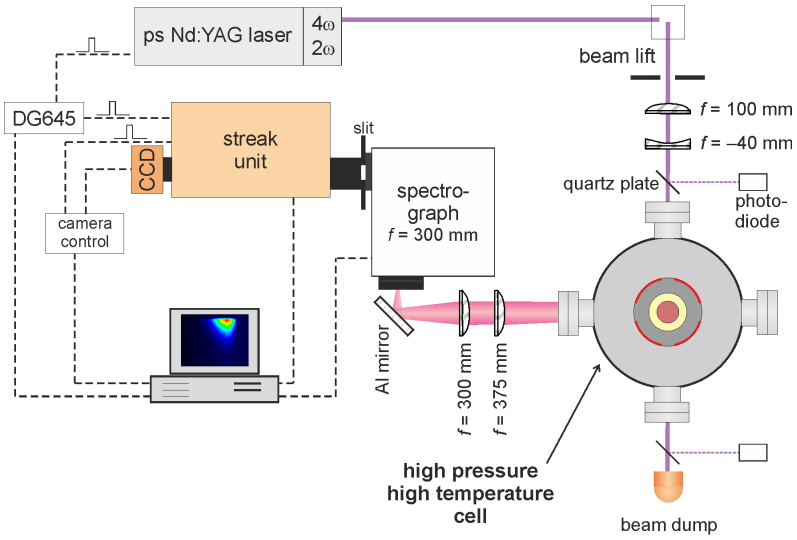

Figure 3-4: Optical arrangement for measuring spectrally- and temporally-resolved tracer fluorescence. M1: aluminum mirror, L1-L4: quartz lenses, CCD: CCD camera, DG465: pulse delay generator [85].

A flashlamp-pumped frequency-quadrupled Nd:YAG laser (PL2143B Ekspla, 26 ps pluse length, 10 Hz repetition rate) was used for laser excitation at 266 nm. A Galilei telescope (f_1 = 100 mm and f_2 = −40 mm) reduced the diameter of the circular laser beam cross section (Gaussian intensity profile) to a size of 3 mm before entering the cell. The fluorescence signal was collected perpendicular to the laser beam through a quartz window. The fluorescence signal was focused on the entrance slit of a spectrograph (f = 300 mm, Acton SP2300, Princeton Instruments with a 150 grooves/mm grating) with two quartz lenses (f_3 = 375 mm and f_4 = 300 mm) via an UV-enhanced aluminum mirror. The spectrally-resolved fluorescence signal was then projected onto the entrance slit of a streak camera (C5680-

24C, Hamamatsu Photonics) composed of a streak module (M5677-01) and a CCD camera (Orca R2, 640×512 pixels). The system delivers two-dimensional images representing the fluorescence wavelength on the *x*-axis and the time on the *y*-axis. Laser and camera were synchronized with trigger pulses from the laser via a pulse delay generator (DG645, Stanford Research Systems).

3.2.2 Fluorescence signal evaluation

The streak-camera system provides two-dimensional images that represent the fluorescence wavelength on the *x*-axis and the time on the *y*-axis. 300 single-shot images were acquired and then averaged for improving the signal-to-noise ratio.

Image post-processing

Single-shot images were averaged after correction for laser jitter by applying a jitter correction function provided by the streak-camera software. Background images were obtained by averaging over 200 single-shot images acquired without firing the laser and with N_2 flowing through the cell. A background image was subtracted from the averaged fluorescence image. A resulting sample image is shown in Figure 3-5.

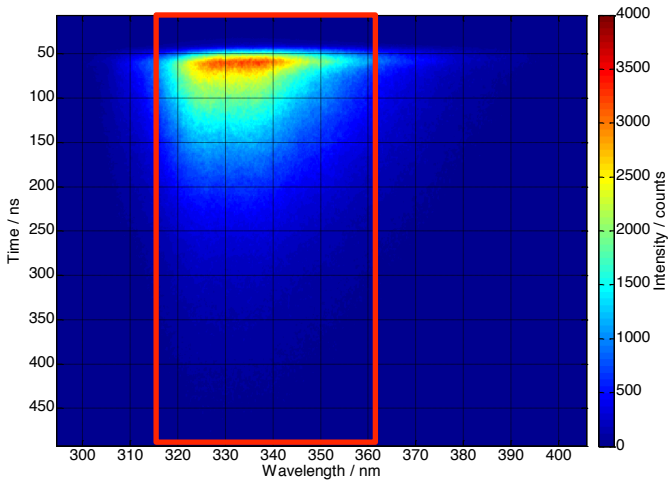

Figure 3-5: Sample image after correction (average over 300 single-shot images) of temporally- and spatially-resolved naphthalene fluorescence (423 K, 1 bar, N_2 bath gas). The red rectangle corresponds to the vertical binning range for extracting the temporally-resolved naphthalene fluorescence decay profiles, where the signal-to-noise ratio is maximized.

Spectrally-resolved fluorescence (fluorescence spectra)

Fluorescence spectra were obtained by summing the signal from horizontal pixels rows along the entire height of the image shown in Figure 3-5. In order to reach acceptable signal-to-noise levels during the measurements, the gain of the camera was adjusted to the changing signal intensity levels encountered for the various conditions investigated (i.e., various temperatures, pressures, and bath-gas compositions). Thus, the acquired fluorescence signal was corrected for the variation in gain. For that pur-

pose, the response intensity of the camera with various gain settings (cf. Figure 3-6) was evaluated by measuring the fluorescence signal for a fixed tracer concentration.

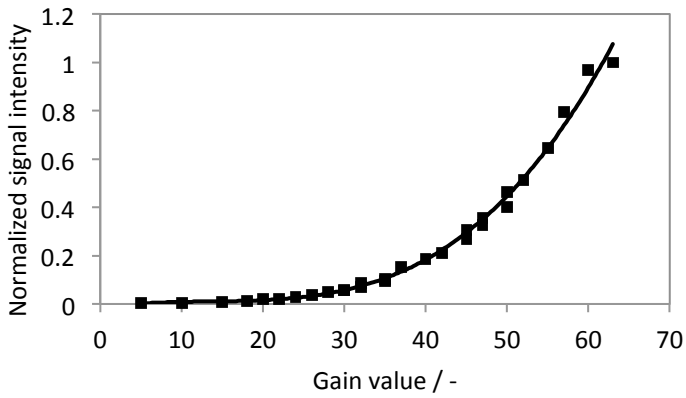

Figure 3-6: Intensity response of the camera with various gain settings.

In addition, the fluorescence spectra were corrected for the spectral response of the entire detection system. The detection system was calibrated by measuring the intensity spectrum of a well-known light source producing a broadband spectrum, a calibrated deuterium lamp in the spectral range of interest (290–410 nm). Figure 3-7 shows fluorescence spectra of naphthalene before and after correction for the spectral sensitivity of the detection system. The corrected spectra are smoothed using a mean average filter with a span of 5.4 nm.

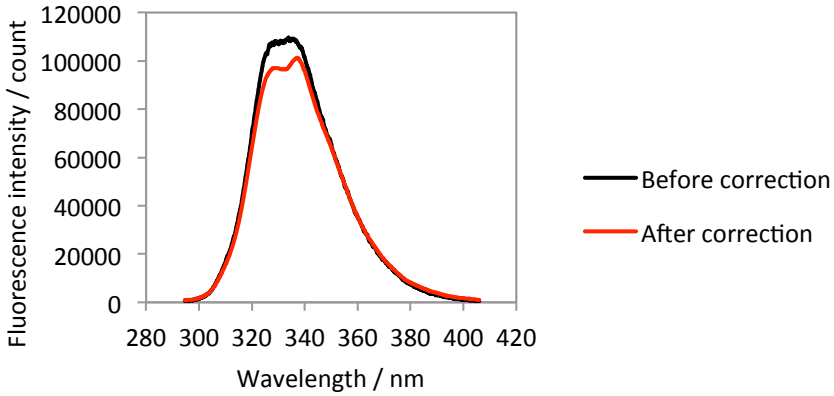

Figure 3-7: Naphthalene fluorescence spectrum (477 K, 1 bar, N_2 bath gas). The corrected spectrum (red line) accounts for the spectral response of the entire detection system and is smoothed with a mean average filter with a span of 5.4 nm.

Determination of effective fluorescence lifetimes via temporally-resolved fluorescence measurements

Effective fluorescence lifetimes τ_{eff} were evaluated from the fluorescence decay. As shown in Figure 3-5, the fluorescence decay profiles were calculated by binning a certain number of columns delimited by the red rectangle, where the signal-to-noise ratio is best. Figure 3-8 shows two examples of temporally-resolved fluorescence decay curves obtained in N_2 bath gas at 1 bar for 374 and 477 K. Because fluorescence lifetimes are significantly affected by variations in environmental conditions (i.e., temperature, pressure, O_2 partial pressure), the acquisition time span was adjusted for optimizing the temporal resolution of the streak-camera.

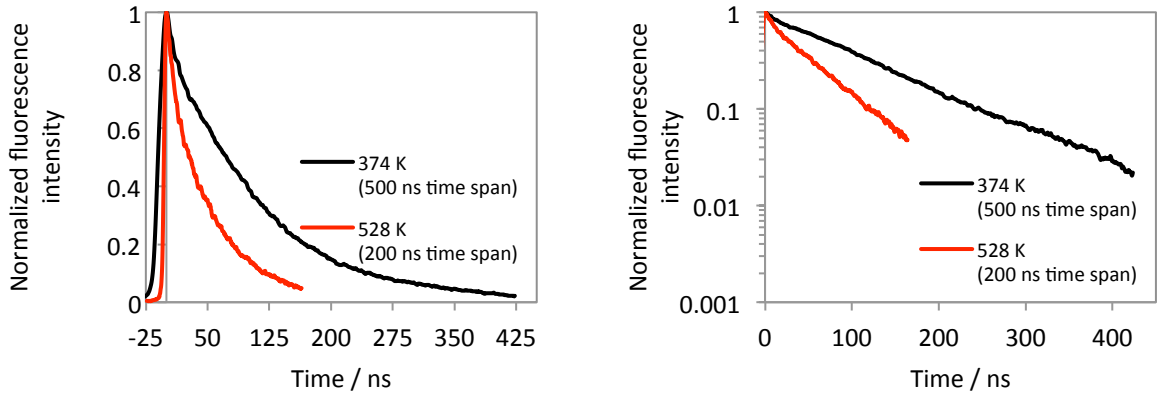

Figure 3-8: Naphthalene fluorescence decay curves obtained in N_2 bath gas at 1 bar for 374 K (blue, acquired with a time span of 500 ns) and 528 K (red, acquired for 200 ns). Left: Linear scale. Right: Logarithmic scale.

Naphthalene has two lifetime components at 266 nm laser excitation as shown by Ossler et al. [86] and Faust et al. [85] and the decay curve can be fitted by a bi-exponential function. In our measurements, the streak-camera had limitations in its dynamic range on the time axis and one needs to measure the fast and slow decay times separately, using two different time-span settings. A single time-span setting was used to determine the long lifetime component. As a first approximation, the short fluorescence lifetime component was considered negligible compared to the long lifetime for the full signal trace and the naphthalene measured fluorescence lifetimes were approximated by a single-exponential decay. Figure 3-8 shows an example of temporally-resolved fluorescence decay curves with effective lifetimes of 110 and 45 ns at 1 bar in N_2 bath gas for 374 and 528 K, respectively.

3.2.3 Investigation of dissolved solid tracers

Naphthalene is a solid tracer at ambient conditions. One option to investigate it is evaporation from a solution in a non-fluorescing solvent (Figure 3-2 and Figure 3-3). Providing constant and well-controlled naphthalene concentrations in the gas phase was not simple and depending on the solvent used, strong temporal fluctuations in the resulting naphthalene-LIF signal (hence tracer concentration) were observed. To investigate the reason for these fluctuations, fluorescence measurements

were carried out for naphthalene diluted in three different solvents, iso-octane, *n*-dodecane, and decane. The boiling points of the two tracers (naphthalene and toluene) and the non-fluorescing solvents (iso-octane, decane, and *n*-dodecane) are given in Table1-1. The fluorescence was detected simultaneously with a measurement of the laser intensity at the entrance and exit of the cell using two photodiodes (Figure 3-4) in order to evaluate the relative laser attenuation in the cell. The pulse-integrated photodiode signals from the entrance of the cell is proportional to the incident laser pulse energy and the measure of the photodiode located at the exit of the cell is proportional to the transmitted laser energy, which was attenuated within the optical path in the cell. The flow cell is not suitable for quantitative measurements of absorption properties because the beam path outside the fluorescence probe volume contains an undefined gas composition. Therefore, the attenuation measurements only represent the fluctuations in tracer concentrations in a qualitative way. The photodiode voltage signals were gated, time-integrated and recorded by a boxcar integrator and a PC-based data-acquisition system using a LabView program. The evaluated relative laser attenuation S_{att} (transmittance) is given by the following expression:

$$S_{\mathrm{att}} = -\log\left(S_{\mathrm{output}}/S_{\mathrm{input}}\right) \tag{2.1}$$

S_{output} and S_{input} are the signals collected by the photodiodes at the entrance and at the exit of the cell respectively.

Figure 3-9 shows the temporal variation of the instantaneous fluorescence signal (in black) and the relative laser attenuation (in red). The fluorescence signal was evaluated by integrating signal from the entire image of the streak-camera (single-shot fluorescence images). The total duration of this experiment was selected longer than the acquisition time required for 300 single-shot images (i.e., longer than 30 s) to observe the temporal variation of the naphthalene fluorescence signal. When naphthalene was diluted in iso-octane the signal showed strong variations of time. The correlation with the temporal variation in the laser attenuation signal showed that the variation is due to concentration fluctuations attributed to preferential evaporation of the solvent iso-octane due to its significantly lower boiling point (372 K compared to 491 K for naphthalene). Using a solvent with a boiling point close enough to the tracer such as decane (447 K) and *n*-dodecane (489 K) prevented this complication.

In the following work, *n*-dodecane was used as non-fluorescing solvent for naphthalene and later to dissolve a mixture of naphthalene and toluene. However, the concern about temporally varying evaporation of the different components causing a variation in tracer concentration and subsequently strong fluctuation in fluorescence signal intensities was still present for the solution of a mixture of naphthalene and toluene tracers diluted in *n*-dodecane, because the boiling point of naphthalene (491 K) is much higher than that of toluene (384 K). The variation in tracer concentration affects the fluorescence signal intensity but not the fluorescence lifetime. Therefore, the remaining small variation in the

LIF-signal intensity was considered irrelevant and only the shape of the spectra was analyzed to derive effective fluorescence lifetimes (cf. Section 3.1.2).

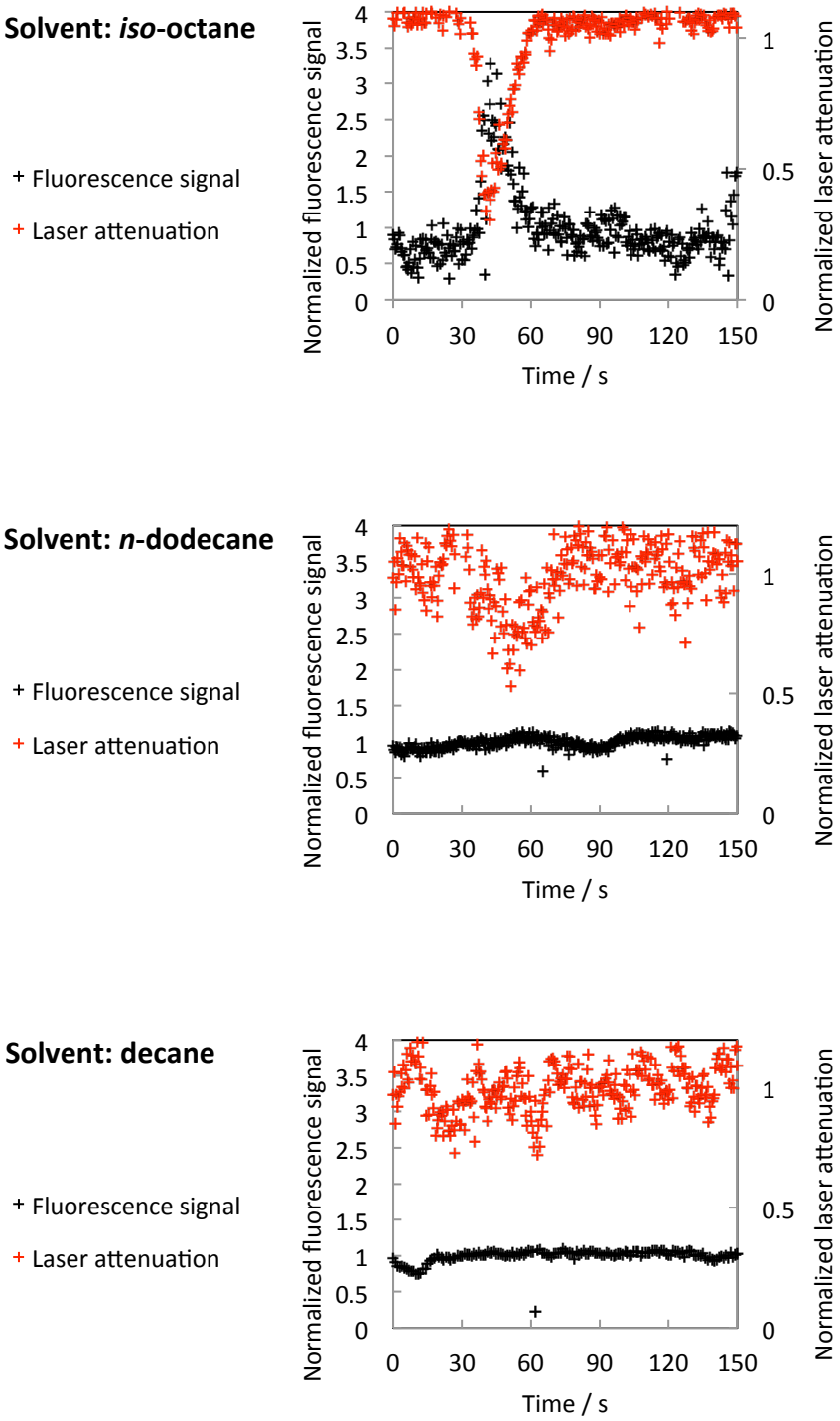

Figure 3-9: Fluorescence signal (black) and relative laser attenuation (red) as a function of time for naphthalene diluted in three non-fluorescing solvents, respectively. The signals were acquired at 374 K at 1 bar in N_2. Similar behavior was found for other temperatures and pressures investigated.

3.3 Results for naphthalene

Naphthalene LIF after laser excitation at 266 nm was investigated over a wide range of temperatures, pressures, and O_2 partial pressures.

3.3.1 Preliminary tests

Tracer-LIF techniques for measuring temperature, fuel concentration, and O_2 partial pressure rely on operating in the linear fluorescence regime, i.e., the generated signal intensity varies linearly with laser energy. Linearity tests were performed to determine the highest laser fluence that can be used to optimize signal-to-noise ratio while remaining in the linear regime. Tracer-LIF saturation is usually affected by temperature, pressure, and O_2 partial pressure and the saturation is reached at lower fluences in N_2 bath gas compared to air and for lower temperatures [92]. Linearity tests were performed in N_2 at 1 bar and 374 K. The fluorescence signal and the laser beam energy were acquired simultaneously when varying the laser beam energy via modification of Q-switch timing. Laser pulse energies were measured with a laser power/energy meter (FieldMaxII-TOP, Coherent). Figure 3-10 shows the naphthalene-LIF signal intensity versus the laser fluence. The LIF intensity is obtained by integrating all signal recorded by the steak camera. The laser fluence is calculated from the measured laser pulse energy divided by the laser beam cross-section of 7.1×10^{-2} cm². In Figure 3-10, the linear signal response is represented as a red line extrapolated from the signal dependence on low fluences. The maximum acceptable excitation laser fluence value in the linear regime was 16 mJ/cm^2 which was subsequently used for the naphthalene-LIF measurements. When operating the laser with a nominally constant laser pulse energy, the signal collected by the photodiode showed a fluctuation of 5%.

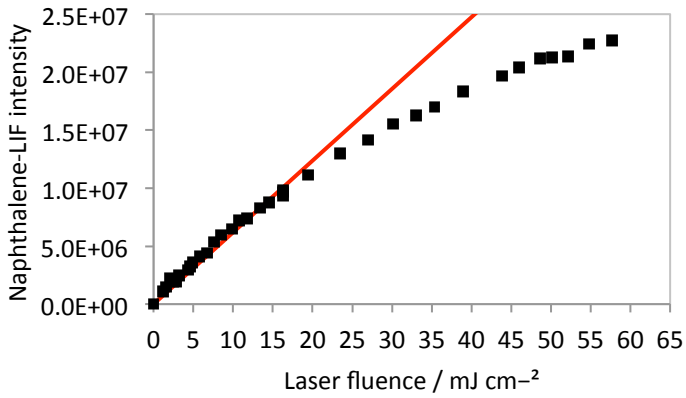

Figure 3-10: Dependence of the naphthalene-LIF signal on the laser fluence at 1 bar and 374 K in N_2.

It must be noted, that in these experiments the total signal intensity showed a strong variability because of the difficulties of evaporating the naphthalene solution as discussed in Section 3.2.3. The temporal variability of the naphthalene-LIF intensity was investigated for a supposedly fixed tracer concentration to verify the reliability of the tracer concentration control. Figure 3-11 shows the naphthalene-LIF intensity at various times after switching on the HPLC pump that feeds naphthalene dis-

solved in *n*-dodecane into the evaporator and mixing chamber. A certain time span (40 minutes) was required to reach stable signal intensities. However, after approx. 140 minutes, the naphthalene-LIF intensity increases making the measurements not reliable anymore. Because the total mass flow of tracer and carrier air was maintained through the cell over the entire time, it is unlikely that naphthalene was trapped inside the cell. The variations are attributed to naphthalene being trapped inside the evaporator or a dysfunction of the HPLC pump. Due to time limitations at that time of experiments, these aspects were not further investigated.

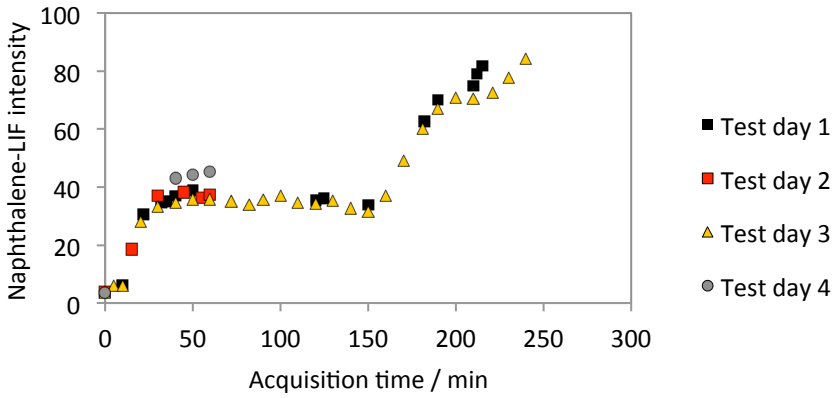

Figure 3-11: Temporal variation of the LIF signal intensity acquired in N_2 at 1 bar for 374 K after initiating the naphthalene mass flow for a naphthalene mole fraction of 0.016%. Solvent: *n*-dodecane. Four test series were acquired at different days.

The effect of the apparent concentration variations on the determination of lifetimes was checked (Figure 3-12). Variations of O_2 partial pressure in the 0.004–0.016 bar range leads to constant lifetimes, ruling out self-quenching and ensuring the linearity of the LIF signal intensity with the tracer concentration.

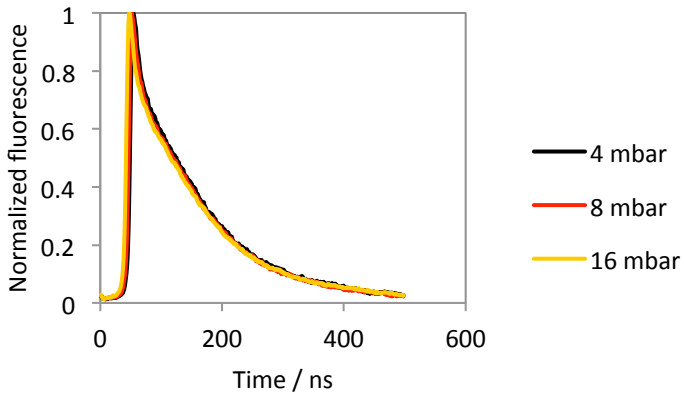

Figure 3-12: Naphthalene fluorescence decay curves for various partial pressures of naphthalene in N_2 at 1 bar and 374 K.

All the measurements presented below were performed following a specific experimental procedure to ensure as reproducible conditions as possible. The measurements were started with evacuating the cell for 2 h at 374 K to remove residual naphthalene left over from previous experiments. The data acquisition is then started only when the tracer-LIF signal intensity has stabilized (after typically 40 min). With all these precautions, the LIF signal intensity still varied with a relative standard deviation of 9% but the shape of the fluorescence spectra (i.e., normalized spectra) and the decay curves were repeatable under constant conditions. The reliable spectral shape and fluorescence lifetime (derived from the decay curves) measurements allows to characterize the photophysical behavior of naphthalene-LIF under the conditions investigated in this study.

3.3.2 Fluorescence spectra of naphthalene

The measured naphthalene LIF emission spectra were normalized relative to their maximum intensity to investigate the dependence of the spectral shape on temperature, pressure, and O_2 partial pressure.

Spectrally-resolved LIF of naphthalene in a N_2

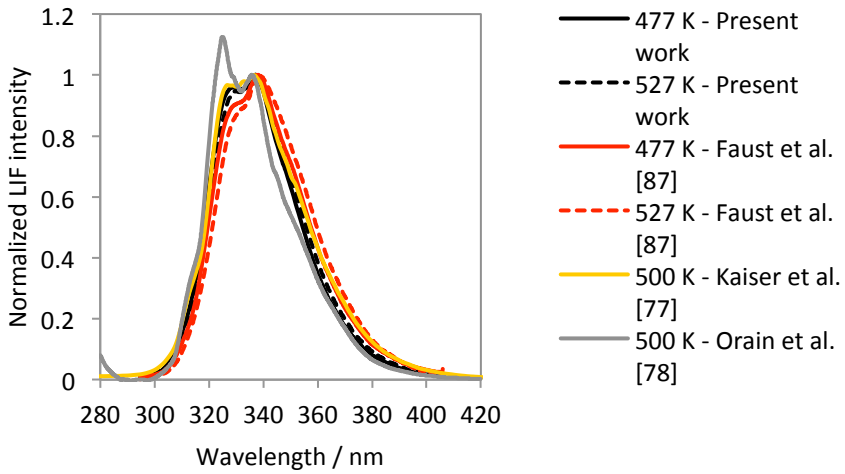

Figure 3-13: Peak-normalized LIF spectra of naphthalene obtained in the present work and from Faust et al. [87] using the same experimental set-up (colored lines) compared to data from Kaiser et al. [77] (dashed black line) and from Orain et al. [78] (solid black line).

Figure 3-13 shows naphthalene-LIF emission spectra normalized to the peak intensity obtained in N_2 at 1 bar, in the 470–530 K temperature range with 266 nm laser excitation. The spectra obtained in the present work and the ones from Kaiser et al. [77] match well, unlike the spectra from Orain et al. [78] and from Faust et al. [87] that differ in terms of spectral shape although all spectra were corrected for spectral and intensity sensitivity of the respective detection systems. The main difference is the peak at ~320 nm, which is strongest for the spectra from Orain et al. [78] and lowest for the spectra from Faust et al. [87]. Additionally, the naphthalene spectra in the presence of O_2 (cf. Figure 3-16) show that the respective signal decreases with increasing O_2 partial pressure. Therefore, the low level of the 320 nm peak observed on our spectra and in the ones from Faust et al. [87] could be the result of some residual

O_2 in the supposedly pure N_2 environment, in spite of the precaution of purging the lines with N_2 before measurements. The spectra shown here and the ones from Faust et al. [87] were acquired with the same experimental configuration. As a consequence, the quality of the N_2 used during these experiments is questionable as well as potential leakages in the cell when operating in pure N_2. In the future, these aspects must be investigated to ensure reliable data.

Temperature dependence of naphthalene-LIF spectra

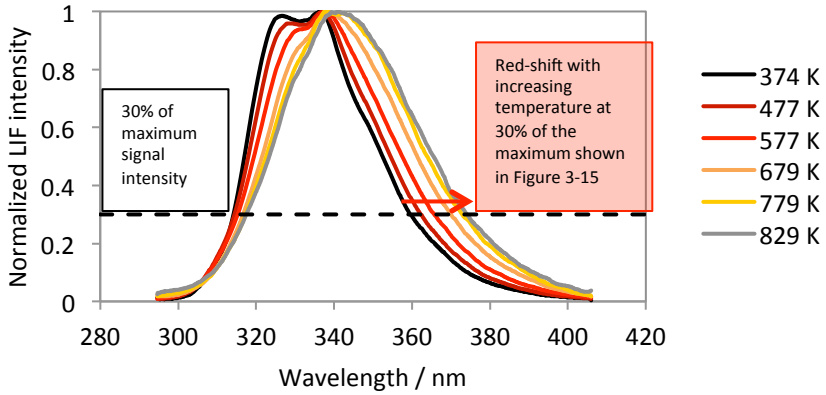

Figure 3-14: Peak-normalized fluorescence spectra of naphthalene obtained in N_2 at 1 bar and 374–829 K, with 266 nm excitation.

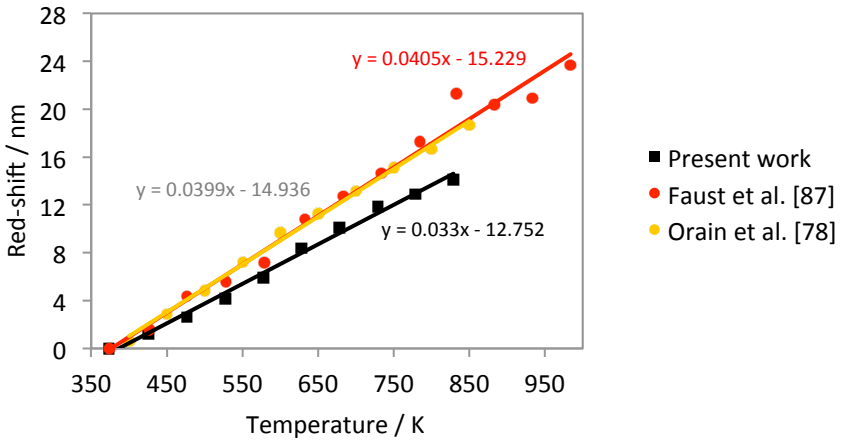

Figure 3-15: Red-shift of the red slope of the naphthalene fluorescence spectrum as a function of temperature at 1 bar in nitrogen. The location in the spectra used for determining the red-shift is shown in Figure 3-14.

The temperature dependence of the naphthalene fluorescence spectra was investigated in N_2 at 1 bar in the 370–830 K temperature range with 266 nm excitation. The peak-normalized LIF spectra are depicted in Figure 3-14. As observed by Orain et al. [78], the FWHM (full width at half maximum) of the spectra is reduced with increasing temperature. In addition, the long-wavelength slope of the naphthalene-LIF spectrum shifts towards the red with increasing temperature (cf. Figure 3-14). This is quantified by identifying the wavelength where the signal reaches 30% of its maximum value. In Figure 3-15 the red-shift of these values relative to the spectral shape measured at 370 K are plotted ver-

sus temperature for a measurement in 1 bar N_2. The present data are compared with results from the literature [78,87]. As a result, the redshift of the spectra from different sources are similar with a value of around 4 nm per 100 K.

Pressure dependence of naphthalene-LIF spectra

The pressure dependence of naphthalene-LIF spectra was investigated in N_2 at pressures between 1 and 10 bar in the 370–830 K temperature range. The peak-normalized naphthalene-LIF spectra reveal no pressure-induced variation for all temperatures investigated. In N_2, only temperature has an influence on the shape of the naphthalene-LIF spectra as already observed by Orain et al. [78].

Effect of O_2 quenching on naphthalene-LIF spectra

The effect of O_2 quenching on the naphthalene-LIF spectra was investigated at 1 bar total pressure and 374 K for various O_2 partial pressures (Figure 3-16). The naphthalene fluorescence spectrum is red-shifted with increasing O_2 partial pressure but not in a linear way. The maximum O_2 partial pressure investigated in Figure 3-16 is 0.105 bar. According to literature [78,87], the red-shift saturates at about 0.1 bar O_2 partial pressure.

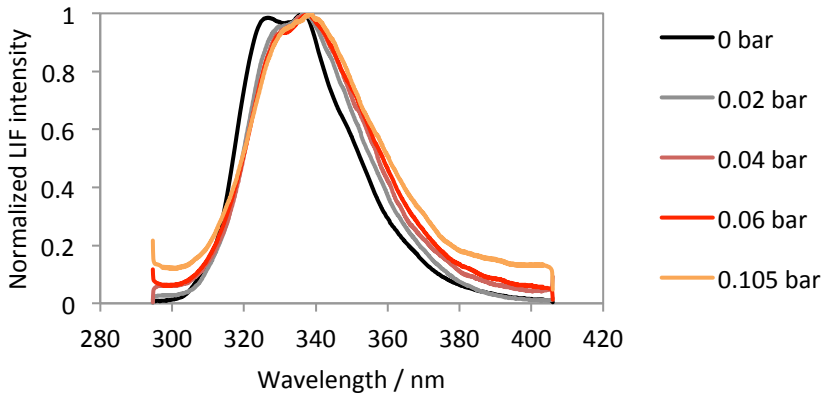

Figure 3-16: Peak-normalized fluorescence spectra of naphthalene at 370 K for various O_2 partial pressures in the range of 0-0.105 bar.

3.3.3 Effective fluorescence lifetimes of naphthalene

Naphthalene effective fluorescence lifetimes were determined from spectrally-integrated time-resolved fluorescence decay curves after short-pulse laser excitation at 266 nm. The dependence of the effective fluorescence lifetime on various parameters such as temperature, pressure and O_2 partial pressure also provides information about the variation of the fluorescence quantum yield on the respective parameters.

Temperature dependence of the naphthalene fluorescence lifetime

The temperature effect on the effective naphthalene fluorescence lifetime with 266 nm excitation was investigated in the 374–829 K temperature range at 1 bar in nitrogen (Figure 3-17). The time spans of

the streak-camera settings were adapted to the temperature-dependent decay times. The fluorescence decay curves show a decrease of the decay time (i.e., the effective fluorescence lifetime) with increasing temperature. These values are shown in Figure 3-18 as a function of temperature, with a comparison to data in [78,84,86-88]. The uncertainty of the determination of the lifetimes is determined as 20%.

As observed in [78, 84,86-88], the effective naphthalene fluorescence lifetimes (which is proportional to the fluorescence quantum yield) strongly decrease with increasing temperature (Figure 3-18). With increasing temperatures, higher vibrational levels are accessed in the excitation process. The rates for ISC and IC generally increase with increasing vibrational energy in the S_1 state and the relative importance of the non-radiative decay increases leading to a corresponding decrease of the fluorescence quantum yield [86].

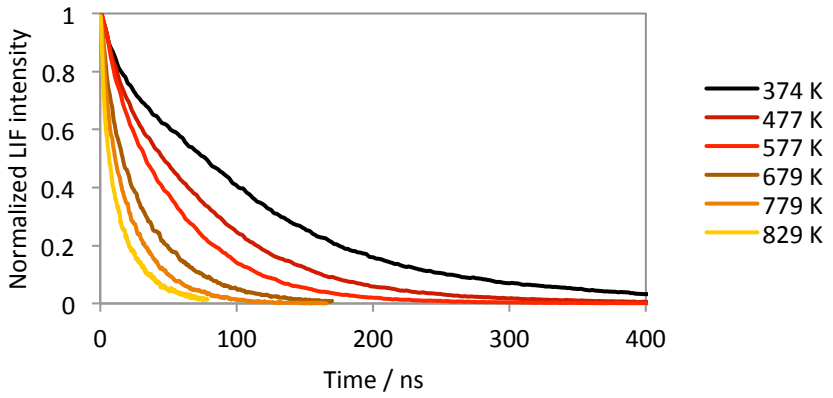

Figure 3-17: Naphthalene fluorescence decay curves for temperatures in the 374–829 K range at 1 bar in N_2.

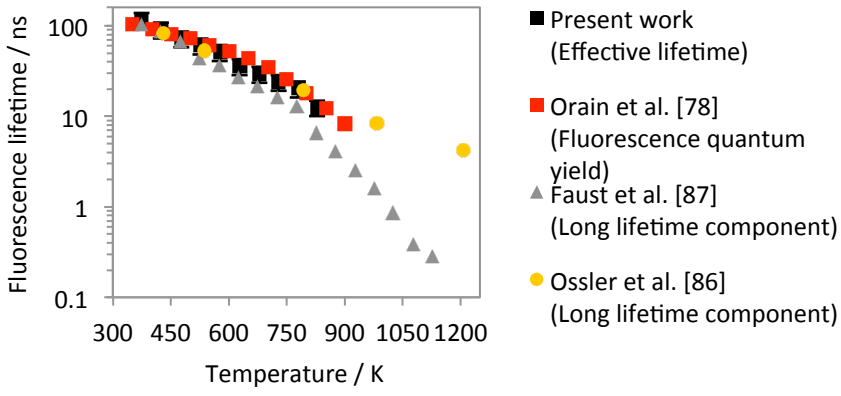

Figure 3-18: Temperature dependence of the effective fluorescence lifetimes of naphthalene at 1 bar in N_2.

The effective naphthalene fluorescence lifetimes obtained in the present work are consistent (within the measurement error) with the fluorescence quantum yield data from Orain et al. [78] under similar conditions, and with the long lifetime component data from Ossler et al. [86] in the 400–800 K temperature range (Figure 3-18). However, the effective lifetimes obtained in the present work (including

the long and short lifetime components) are slightly higher than the long lifetime component measured by Faust et al. [87]. The naphthalene lifetime measurements by Faust et al. [87] were performed by using the same experimental set-up but with a better adapted selection of time spans to differentiate the short and the long lifetime components. In addition, Faust et al. [87] determined the long lifetime component from a double-exponential fitting, unlike in the present case where a single-exponential decay was used (cf. Section 3.2.2). Although the short lifetime component has a small amplitude, its contribution to the effective lifetime is not completely negligible.

Pressure dependence of the naphthalene fluorescence lifetime

The pressure effect on the effective naphthalene fluorescence lifetime with 266 nm excitation was investigated between 1 and 10 bar in the 370–830 K temperature range in N_2. Figure 3-19 shows the pressure dependence for 374 and 424 K. The present results are consistent with the long lifetime component from Faust et al. [87]. The effective naphthalene fluorescence lifetime (and the fluorescence quantum yield) increases with pressure and approaches a limiting value. As the pressure increases, the number of collisions with the bath gas increases [78]. This increases vibrational relaxation in the S_1 state leading to a population of low-lying states with lower rates of non-radiative intersystem crossing, thus increasing the fluorescence lifetime and the fluorescence quantum yield.

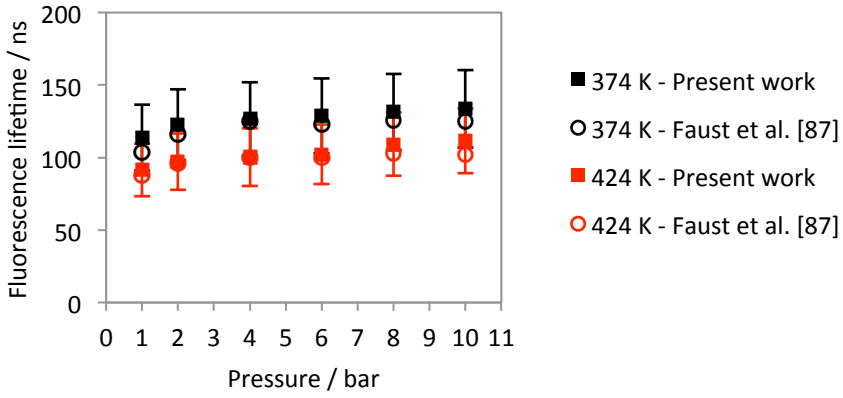

Figure 3-19: Pressure dependence of the effective fluorescence lifetimes of naphthalene for 374 and 424 K.

Effect of O_2 quenching on the naphthalene fluorescence lifetimes

The effect of O_2 quenching on the naphthalene fluorescence lifetime was investigated by varying the O_2 partial pressure at 1 bar total pressure in the 370–880 K temperature range from 0.084 to 0.21 bar (Figure 3-20). The effective fluorescence lifetimes, obtained at 374 K were compared with the long lifetime component values from Faust et al. [87] and the two sets of data are in good agreement. Data from Faust et al. [87] are also presented for a higher temperature of 877 K. The naphthalene effective fluorescence lifetime (and the fluorescence quantum yield) decrease significantly with increasing O_2 partial pressure, but with an attenuation of this O_2 quenching effect with increasing temperature.

The efficiency of collisional quenching is commonly described by the Stern-Volmer factor k_{SV} (cf. Section 3.1.2). The Stern-Volmer factor is the ratio of the quenching rate coefficient $k_q(O_2)$ and the total intra-molecular de-excitation rate k_{tot} (see equation (3.4)). The decrease of the Stern-Volmer factor k_{SV} with increasing temperature is caused by a decrease of the quenching rate coefficient $k_q(O_2)$ and/or an increase of the total intra-molecular de-excitation rate k_{tot}.

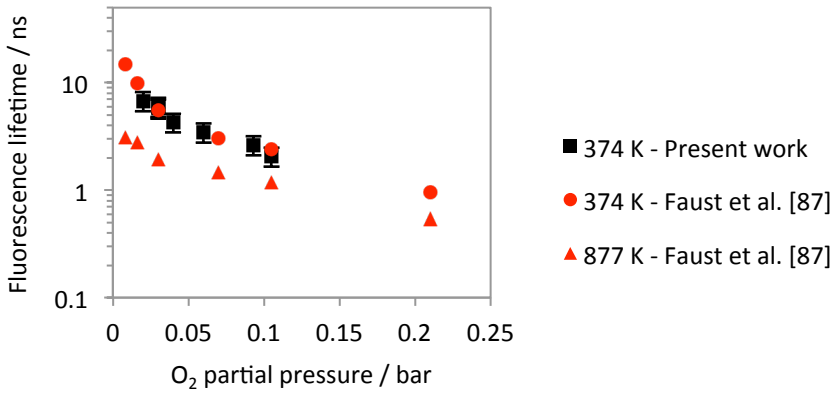

Figure 3-20: Dependence of naphthalene fluorescence lifetimes on the O_2 partial pressure at 1 bar total pressure for 374 and 877 K. Comparison with the long lifetime component values of Faust et al. [87] under similar conditions and for a higher temperature of 877 K.

In this part, the data from Faust et al. [87] were used because the fluorescence lifetime measurements were available for a larger temperature range. By evaluating the fluorescence lifetime as a function of O_2 partial pressure, Stern-Volmer plots can be generated for various temperatures as shown in Figure 3-21.

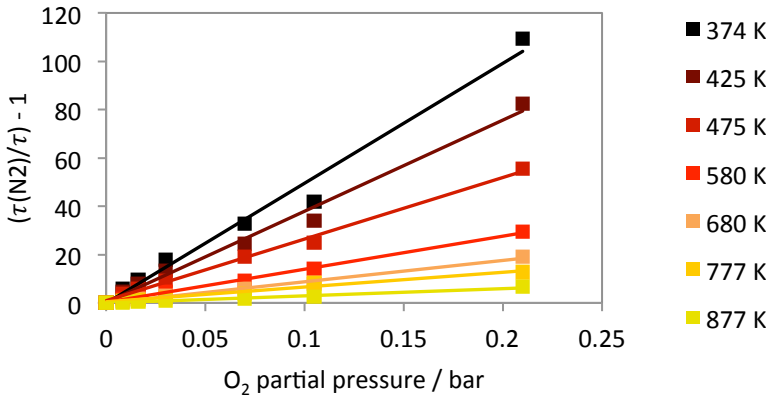

Figure 3-21: Stern-Volmer plots for naphthalene obtained with 266 nm excitation, at 1 bar total pressure and for several temperatures. $\tau(N_2)$ is the fluorescence lifetime in N_2 and τ is the fluorescence lifetime at the specific O_2 partial pressure. The fluorescence lifetimes was measured in [87] for the long lifetime components.

The slope of a Stern-Volmer plot represents the Stern-Volmer factor. In Figure 3-22, Stern-Volmer factors are shown as a function of temperature indicating the temperature dependence of the quenching

effect. The naphthalene Stern-Volmer factors from Faust et al. [87] using the same experimental set-up as in the present work are compared with the ones in [77,78] under similar conditions. The data from Orain et al. [78] show higher Stern-Volmer factors compared to the data from Faust et al. [87] whereas the data from Kaiser et al. [77] are lower at 500 K. However, the same temperature dependence is visible and the Stern-Volmer factor reduces with increasing temperature. With increasing temperature, the intra-molecular non-radiative decay rate k_{nr} increases as the rate for ISC and IC generally increase with increasing vibrational energy. As a consequence, the total intra-molecular de-excitation rate increases with increasing temperature.

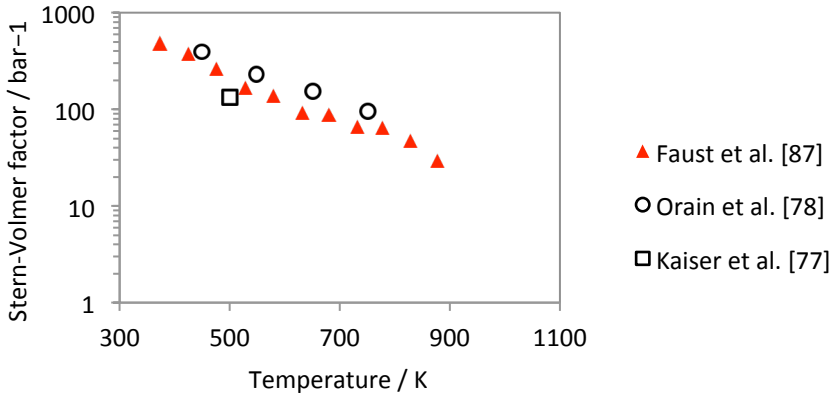

Figure 3-22: Temperature dependence of the Stern-Volmer factors for naphthalene at 1 bar total pressure and in the 0–0.21 bar O_2 partial pressure range. The Stern-Volmer coefficients by Faust et al. [87] calculated from the long lifetime components, the ones by Orain et al. [78] and by Kaiser et al. [77] from fluorescence quantum yield from integrated fluorescence spectra between 300–420 nm.

The dependence of naphthalene LIF on temperature (in the 370–830 K range), pressure (in the 1–10 bar range), and O_2 partial pressure (in the 0–0.21 bar range) was investigated and the data are in good agreement to other data from the literature [77,78,87] that became available in the open literature after our experiments were conducted. Our results for naphthalene validate the experiments for one tracer and thus for an extended application of a mixture of two tracers (naphthalene and toluene). Within the same conditions, the fluorescence of a mixture of naphthalene and toluene can be compared to the fluorescence of naphthalene to investigate photophysical interactions between the two tracers. The experiment presented in this work was further pursued by Faust et al. [87,88]. These advanced measurements were also presented here in comparison to the initial measurements conducted by the author.

3.4 Results for naphthalene and toluene mixtures

It has been demonstrated in the previous chapter that toluene and naphthalene are good tracer candidates for applying the two-tracer three-color LIF technique to simultaneously measure temperature, fuel concentration and O_2 partial pressure. Naphthalene and toluene were well characterized separately

in previous studies at various temperature, pressure and O_2 partial pressure. However, fluorescence signal evaluations of the two-tracer mixture are required to investigate for possible interactions between the two tracers in terms of variations of the emission spectra and the fluorescence lifetimes (which are proportional to the fluorescence quantum yields).

3.4.1 Mixture composition

Toluene and naphthalene were diluted in *n*-dodecane and their partial pressures were kept below 0.16 mbar for naphthalene (cf. Section 3.3.1) and 4 mbar for toluene [87,88] (at 1 bar and 370 K in N_2). The fluorescence quantum yields of naphthalene and toluene have the same order of magnitude. However, the absorption cross-section of toluene at 266 nm is smaller than that of naphthalene by about two orders of magnitude. Therefore, four mixtures (Table 3-1) with various proportions of the tracers (toluene and naphthalene) were investigated to select the concentrations that provide similar LIF signal intensity for toluene and naphthalene. The investigation was performed at 1 bar and 370 K in N_2, at conditions that provide the highest LIF signal in the present work. The peak normalized fluorescence spectra of the different two-tracer mixtures are shown in Figure 3-23. The emission peak of toluene is between 260 and 310 nm and of naphthalene between 320 and 360 nm. Mixture #4 (with a 99:1 ratio of toluene and naphthalene) provided comparable LIF signal for both tracers (at 1 bar and 370 K in N_2) and was used throughout these investigations.

Table 3-1: Conditions of toluene and naphthalene partial pressures and number densities (in gas volume) in the high-temperature high-pressure cell at 370 K and 1 bar N2.

	Ratio in liquid volume	Partial pressure in mbar (in gas volume)			Number density in cm^{-3} (in gas volume)		
	Toluene: Naphthalene	Naphthalene	Toluene	Combined tracers	Naphthalene	Toluene	Combined tracers
Mixture #1	5:1	0.013	0.071	0.84	2.57×10^{20}	1.38×10^{21}	1.63×10^{21}
Mixture #2	19:1	0.007	0.131	0.138	1.32×10^{20}	2.54×10^{21}	2.68×10^{21}
Mixture #3	49:1	0.005	0.224	0.229	1.04×10^{20}	4.37×10^{21}	4.47×10^{21}
Mixture #4	99:1	0.009	0.900	0.909	6.95×10^{19}	7.29×10^{21}	7.36×10^{21}

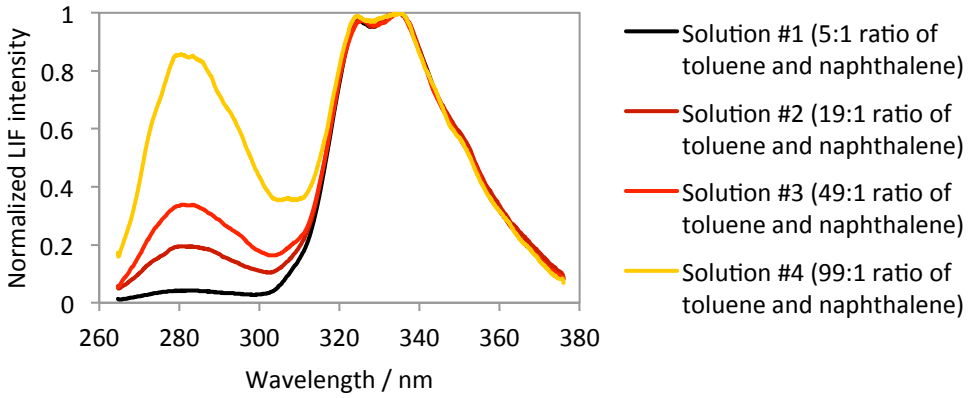

Figure 3-23: Normalized fluorescence spectra of several toluene and naphthalene mixtures (cf. Table 3-1) in 1 bar N_2 at 374K.

3.4.2 Fluorescence spectra of a mixture of toluene and naphthalene

Photophysical interaction between toluene and naphthalene that potentially changes the spectral distribution of signal light was investigated by measuring the fluorescence spectra of a mixture of toluene/naphthalene and of the individual components (naphthalene and toluene), under same conditions of temperature, pressure, and O_2 partial pressure. Comparisons of fluorescence spectra are shown in Figure 3-24 for 830 K at 1 bar in N_2 and in Figure 3-25 for 370 K at 1 bar in air. The fluorescence spectra of the mixture of naphthalene/toluene were normalized to the naphthalene peak at around 340–350 nm in Figure 3-24 and to the toluene peak at around 280–300 nm in Figure 3-25. The fluorescence spectra of the individual components (toluene and naphthalene) were adjusted in terms of intensities at the peak maxima to match the intensities obtained with the mixture of tracers. The superposition of the fluorescence spectra demonstrates that the spectral shape of the LIF signal of the respective tracer is not significantly affected by the presence of the other tracers in the mixture. The LIF signal of naphthalene (around 310–380 nm), however appears at slightly shorter wavelengths in the mixture compared to the pure naphthalene. This wavelength shift is at about 3.5 nm and no additional influence on the fluorescence spectra was observed for lower temperature in the 370–830 K and higher pressure in the 1–10 bar in N_2 (Figure 3-24) and for O_2 partial pressure lower than 0.21 bar (Figure 3-25). These observations on the fluorescence spectra demonstrate a weak interaction between the toluene and naphthalene within the temperatures, pressures, and O_2 partial pressures investigated. This statement is valid only by observing the spectral distribution of the LIF signal. The absolute intensity of the LIF signal is considered in Section 3.4.3 in terms of fluorescence lifetimes instead of fluorescence quantum yield to circumvent the limitations of the experiments (cf. Section 3.2.3 and 3.3.1).

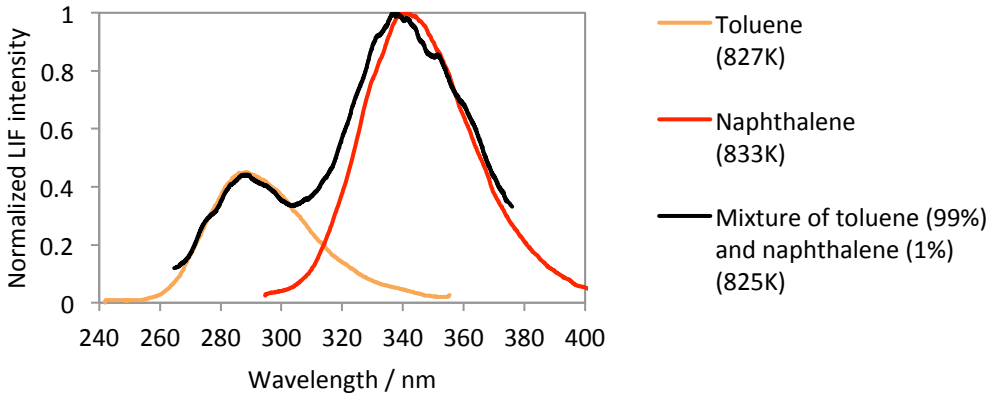

Figure 3-24: Fluorescence spectra of toluene (blue line), of naphthalene (red line) and of the mixture of 0.009 mbar naphthalene and 0.900 mbar toluene at 1 bar in N_2 (black line).

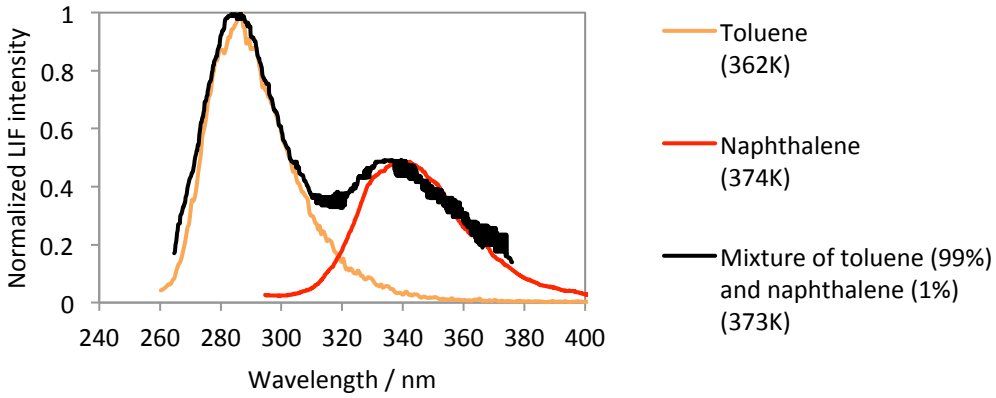

Figure 3-25: Fluorescence spectra of toluene (blue line), of naphthalene (red line) and of the mixture of 0.009 mbar naphthalene and 0.9 mbar toluene at 1 bar in air (black line).

3.4.3 Fluorescence lifetimes of mixtures of toluene and naphthalene

The photophysical interaction between toluene and naphthalene was also investigated by analyzing the fluorescence lifetime. Figure 3-26 shows a comparison (at 1 bar in the 370–925 K temperature range) between the fluorescence lifetimes of toluene as an individual tracer and in a mixture of toluene/naphthalene (partial pressure of 0.9 mbar for toluene and 0.009 mbar for naphthalene in N_2). Figure 3-27 shows the same comparison but for naphthalene. The effective fluorescence lifetimes of the individual tracers (toluene and naphthalene) were given for partial pressures of 4 mbar at 296 K for toluene in [85,88] and of 0.4 mbar at 374 bar in [87,88]. The number densities of the respective tracers (toluene and naphthalene) were low enough to prevent self-quenching and thus to assume that the effective fluorescence lifetime is independent on number density. The effective fluorescence lifetime (proportional to the fluorescence quantum yield) of toluene and naphthalene are comparable for measurements with individual tracers and with a mixture of toluene/naphthalene within the precision of the measurements. However, the fluorescence lifetime of naphthalene stays lower for the individual naph-

thalene compared to the mixture of toluene/naphthalene, especially at higher temperatures between 875 and 975 K. In addition, the effective fluorescence lifetimes of the individual tracers (toluene and naphthalene) and those of the tracer mixture (0.9 mbar toluene and 0.009 mbar naphthalene in N_2) were identical for various O_2 partial pressures in the range of 0–0.21 bar (Figure 3-28 and Figure 3-29).

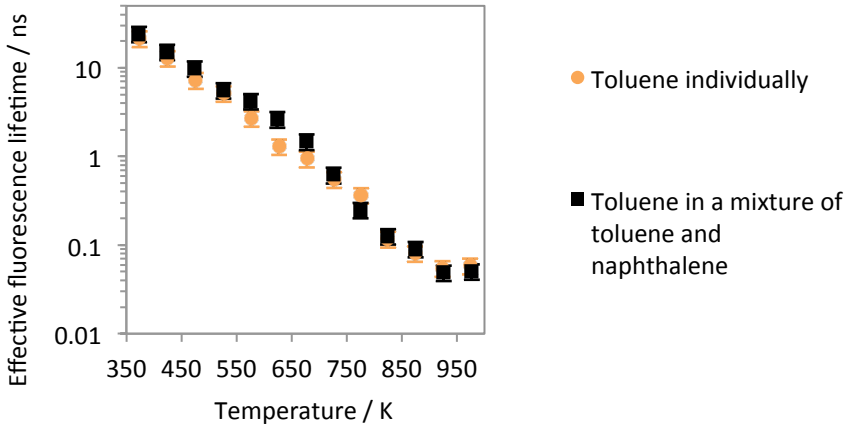

Figure 3-26: Effective fluorescence lifetimes of toluene individually (partial pressure of 4 mbar) and in a mixture of 0.9 mbar toluene and 0.009 mbar naphthalene at 1 bar in N_2 as a function of temperature in the 370–980 K range.

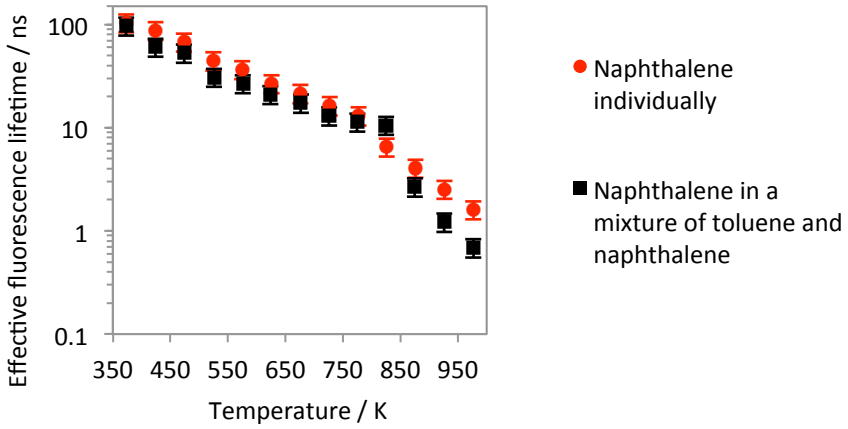

Figure 3-27: Effective fluorescence lifetimes of naphthalene individually (partial pressure of 0.4 mbar) and in a mixture of 0.9 mbar toluene and 0.009 mbar naphthalene at 1 bar in N_2 as a function of temperature in the 370–980 K range.

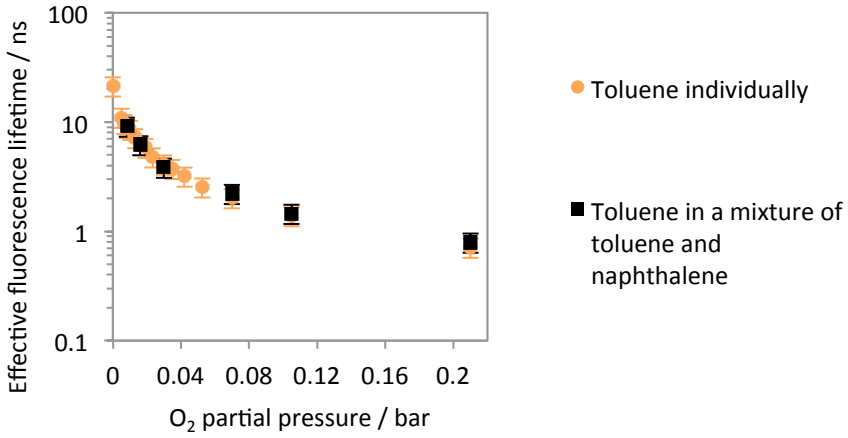

Figure 3-28: Effective fluorescence lifetimes of toluene individually (partial pressure of 4 mbar) and in a mixture of 0.9 mbar toluene and 0.009 mbar naphthalene in N_2/O_2 mixtures as a function of O_2 partial pressure in the range of 0–0.21 bar at 1 bar and 373 K.

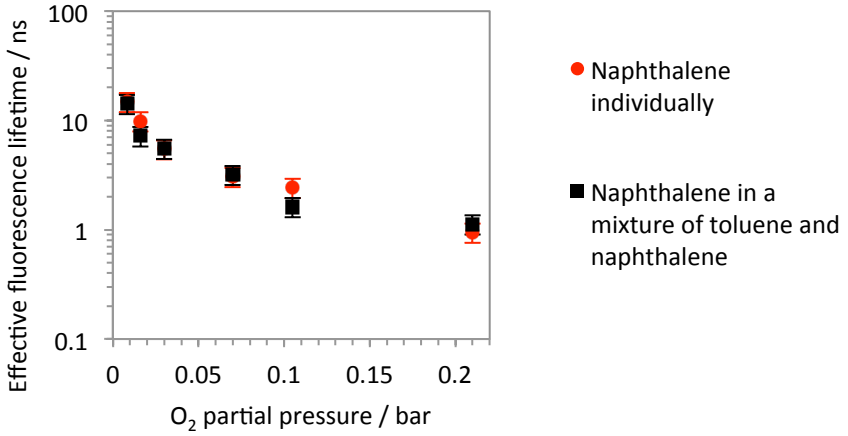

Figure 3-29: Effective fluorescence lifetimes of naphthalene individually (partial pressure of 0.4 mbar) and in a mixture of 0.9 mbar toluene and 0.009 mbar naphthalene in N_2/O_2 mixtures as a function of O_2 partial pressure in the range of 0–0.21 bar at 1 bar and 373 K.

3.5 Conclusions

After having briefly described the general photophysics of aromatic tracers, the results for the characteristics of the naphthalene-LIF signal have been presented under various conditions. The dependence of naphthalene fluorescence on temperature (in the 370–830 K range), pressure (in the 1–10 bar range), and O_2 partial pressure (in the 0–0.21 bar range) were in good agreement to data from the literature [77,78,87] that became available after our experiment was conducted. In addition, these results allow us to compare the naphthalene-LIF signal obtained with the individual tracers and in mixtures of naphthalene and toluene under similar experimental conditions using the same experimental setup. The fluorescence spectra of naphthalene were observed to be shifted towards shorter wavelengths in

the presence of toluene. However, this shift of 3.5 nm was the same for all conditions investigated (i.e., temperature, pressure, O_2 partial pressure) and therefore does not affect the temperature and O_2 partial pressure dependence of the naphthalene-LIF signal used in the two-tracer-LIF technique (cf. Chapter 5). In addition, the lower effective fluorescence lifetime of naphthalene in the presence of toluene is measured only in N_2 (Figure 3-27). In O_2, the effective fluorescence lifetime of naphthalene is not affected by the presence of toluene and the tracer mixture of toluene and naphthalene is therefore suitable for the application of the two-tracer LIF technique for quantitative measurements in practical environment in the presence of O_2.

4 Tracer-LIF temperature measurements in vaporized Diesel jets

Temperature images can be obtained from laser-induced fluorescence (LIF) (Chapter 2) of tracers naturally present or mixed in small proportions into the flow. The temperature-dependence of the collected LIF signal can be exploited to simultaneously measure temperature and fuel concentration. As mentioned in Chapter 2, tracers such as acetone, 3-pentanone, toluene, biacetyl, or naphthalene have been used for thermometry. The technique developed here is based on single-wavelength LIF excitation of toluene in the UV (e.g., 248, 266 nm) and uses the temperature dependence of toluene LIF- emission spectra. The main advantage of toluene over other tracers such as 3-pentanone for temperature measurements is that only one laser excitation is required, reducing experimental cost and complexity. Local variations in laser fluence and tracer concentration cancel when determining the ratio of the signal of two spectral ranges of the emission spectrum.

The objective here is to provide an optimized methodology for post-processing the LIF images as well as to determine the impact of errors on the temperature measurement. For this purpose, the application of the toluene-LIF thermometry is investigated in restrictive conditions such as in a vaporized Diesel spray, where high temperature levels and high temperature gradients occur. This chapter is an extension of the paper Tea et al. [89].

4.1 Toluene-LIF thermometry

4.1.1 Principle of the two-color toluene-LIF technique

The two-color toluene-LIF thermometry takes advantage of the temperature-dependent shape of the LIF emission spectra after ultraviolet (UV) excitation at 248 or 266 nm. The measurement strategy is described in Section 2.3.3. The toluene-LIF signal, which is red-shifted with increasing temperature, is collected in two distinct spectral ranges (Figure 4-1), the first around the emission peak at 280±10 nm (collection filter 1) and the second at longer wavelengths at 320±20 nm (collection filter 2). The ratio of the two collected signals depends on temperature. When calculating the LIF signal-ratio, variations in laser intensity, laser sheet profile, and toluene concentration cancel out. As a consequence, the two-color toluene-LIF technique can be applied in systems with inhomogeneous tracer distribution and a correction for the laser light sheet profile is no longer necessary.

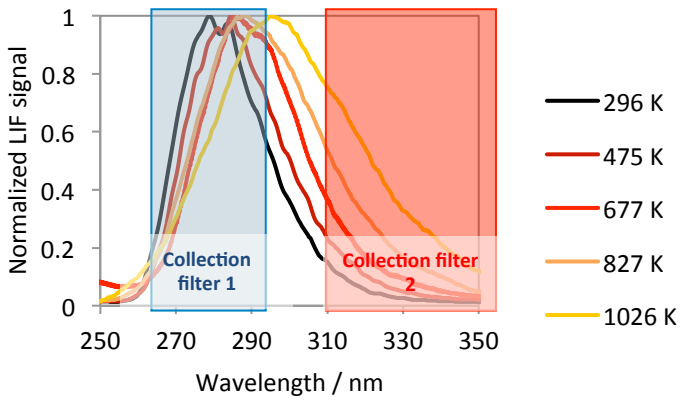

Figure 4-1: Toluene LIF-emission spectra [87] in N_2 at 1 bar for various temperatures and with the respective bandpass filters.

4.1.2 Validation and optimization

Two-color toluene-LIF thermometry has first been used in atmospheric-pressure flows [61,62], theoretically assessed [71], and then applied [62] to SI engine conditions. The reduction in signal strength with increasing temperature requires a detector with a high dynamic range in order to perform measurements over a wide temperature range without changing the experimental settings. This is a potentially limiting factor when applying this technique to Diesel sprays that feature high temperature gradients. However, with careful consideration of various aspects of the measurement technique, it is possible to optimize the toluene-LIF signal to enable measurements even in such challenging environments.

Excited aromatic molecules such as toluene undergo fast collisional quenching with O_2, leading to a reduction of the LIF signal as a function of O_2 partial pressure (Chapter 3). The O_2 quenching effects are problematic when performing temperature measurements using toluene LIF since the LIF signal is reduced in the presence of O_2 and the LIF signal-ratio depends on temperature and on O_2 partial pressure. In the present work, the two-color toluene-LIF technique was investigated under non-reactive conditions (i.e., in the absence of O_2 and the associated quenching effects) to optimize various aspects of the LIF technique and to develop a methodology for determining the measurement precision and accuracy.

4.2 Experiment

4.2.1 High-pressure high-temperature cell

Measurements were performed in an optically accessible, high-pressure, high-temperature cell ($V = 1400$ cm^3) (Figure 4-2), allowing the study of fuel sprays under well-controlled injection and bath-gas conditions that are representative of in-cylinder Diesel engine conditions. Flow in the initially quiescent gas is induced by the jet itself. For details concerning the cell and its operation, see [90]. A

single-hole (20 μm diameter) Bosch common-rail Diesel injector was mounted in the top plate of the cell directing the fuel jet downwards into the center of the chamber. Four sapphire windows of 100 mm diameter 20 mm thick were mounted on the remaining faces. The bath-gas temperature was measured with a K-type thermocouple (25 μm diameter bead) in the central region of the cell. The entire cell is electrically heated to 453 K to prevent water condensation at the inner surfaces.

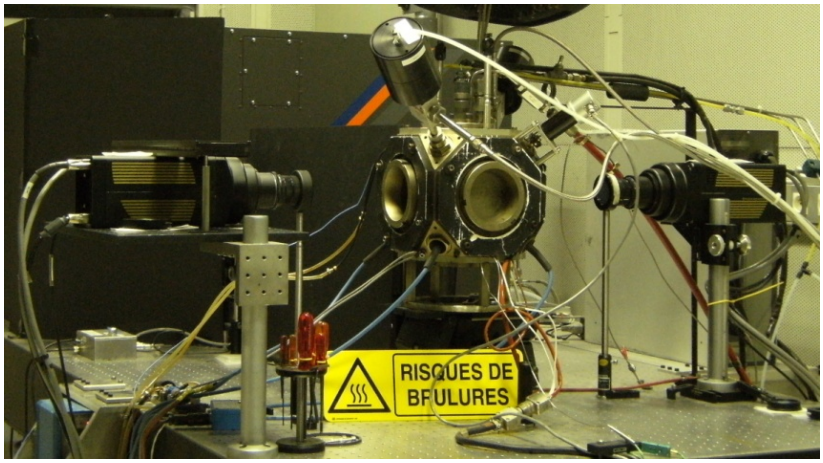

Figure 4-2: Photograph of the high-pressure high-temperature fuel injection cell with two intensified CCD cameras used for simultaneous acquisition of LIF images on the two spectral bands (collection filter 1 and 2 in Figure 4-1).

A pre-combustion of ethylene/hydrogen/oxygen/nitrogen mixtures provides high temperature and pressure conditions at the time of measurement [91]. Figure 4-3 shows the temporal variation of the pressure and temperature measured inside the cell. The pre-combustion mixture is introduced and homogenized inside the cell. The rapid pressure increase is due to the pre-combustion ignited with spark plugs located inside the cell. The progressive decrease of pressure is due to cooling of the burned gases by heat losses to the walls. The fuel is injected at a specified delay after the pre-combustion when the desired pressure and temperature are reached inside the cell. Alternatively, the composition of the combustible mixture can be adjusted so that a certain desired O_2 partial pressure is obtained in the burned gas after pre-combustion. For the experiments presented here, the pre-combustion mixture was chosen to completely consume O_2 providing inert conditions for the injected fuel. For all the tests presented here that required pre-combustion to reach high temperature, i.e., temperature and pressure ranging from 624 K and 46 bar to 728 K and 54 bar, a gas density of 25 kg/m^3 was used.

Fuel (i.e., *n*-dodecane (99.7% purity), doped with 10 vol.% toluene) was injected at a rail pressure of 1000 bar. An injection duration of 0.6 ms and a delay time of 1.5 ms (corresponding to the delay between the injector trigger signal and image acquisition) were selected to ensure that the fuel vapor cloud penetrated sufficiently within the cell for it to be excited by the full height of the laser sheet and that no liquid fuel was present in the zone illuminated by the laser sheet.

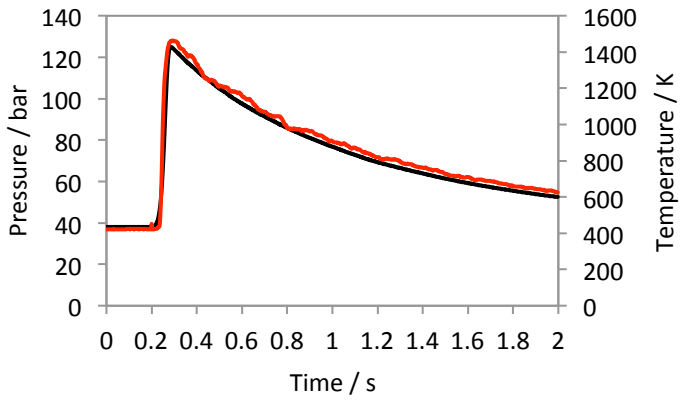

Figure 4-3: Typical pressure (black) and temperature (red) trace in the cell versus time during pre-combustion and cool down.

4.2.2 Optical arrangement

The optical arrangement for laser excitation and signal detections at the high-pressure high-temperature cell is shown in Figure 4-4. A KrF-excimer laser (Lambda Physik, CompexPro 102) was used for laser excitation at 248 nm. A vertical laser light sheet (47×0.4 mm²) entered the cell. Dark coated metal masks with vertical slots for passage of the laser beam were mounted on the inner sides of the laser entry and exit windows to reduce laser sheet flare. The LIF signal was collected through two opposite windows with two intensified CCD camera (Princeton PI-MAX, 1024×1024 pixels) equipped with custom high transmission optical filters ($T > 70\%$) and a fast UV-sensitive lens ($f = 45$ mm, $f_{\#} = 1.8$, EADS Sodern).

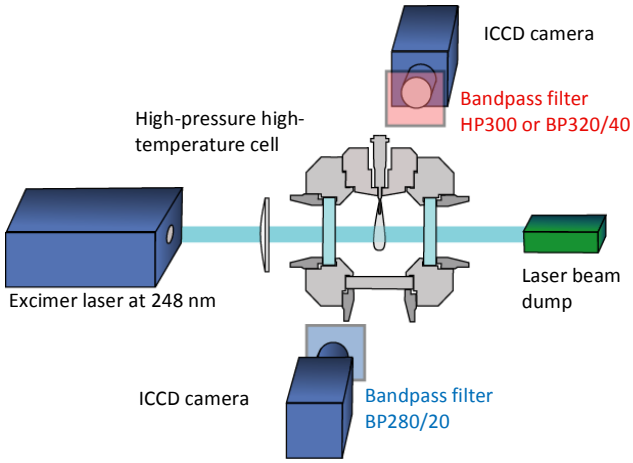

Figure 4-4: Schematics of the optical arrangement for two-color toluene-LIF temperature measurement on the high-temperature high-pressure cell.

Three bandpass filters (Semrock) were tested (Table 4-1). Figure 4-5 shows the spectral response of the entire detection system which consisted of the spectral quantum efficiency of the ICCD cameras (i.e., photosensitivity of the CCD) and the transmission characteristics of the bandpass filters, the UV lenses, and the sapphire windows. These data were provided by the manufacturer except for the sap-

phire windows whose transmission characteristics were measured by a spectrometer coupled to an optical fiber with a deuterium/halogen light source. The spectral response of the complete detection system was used in the calibration procedure described in Section 4.2.3.

Table 4-1: Characteristics of the bandpass filters used for two-color toluene-LIF thermometry.

	Collection filter characteristics	**Nomenclature**
Collection filter 1 Toluene-LIF emission peak	BP280 nm, FWHM = 20 nm	BP280-20
Collection filter 2 Long-wavelength toluene-LIF emission	BP320 nm, FWHM = 40 nm	BP320-40
	HP300 nm	HP300

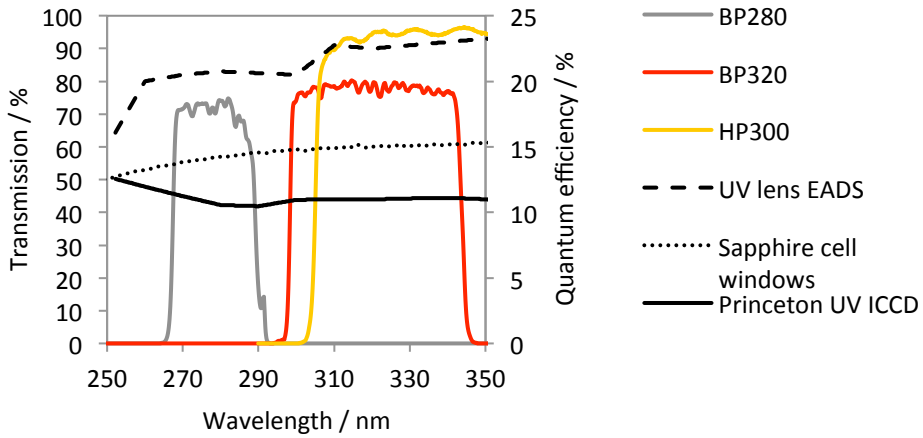

Figure 4-5: Spectral response of the entire detection system used for two-color toluene-LIF thermometry.

Two different experimental configurations were used in the present experiments that differ in the choice of optical filters used for LIF signal detection. The first set-up (denoted hereafter as configuration 1) was used for temperature measurements and enabled the detection of the toluene LIF signal in two different spectral intervals with one filter (BP280) centered at the toluene-LIF emission peak and with the other filter (HP300 or BP320) for the long-wavelength toluene-LIF emission. For configuration 2, identical filters (BP280) were used for both cameras to investigate various aspects of the measurement technique as will be discussed later in the report.

4.2.3 Temperature calibration

Unburned gas temperature measurements using two-color toluene LIF are based upon exploiting the temperature-dependence of the LIF emission spectra after ultraviolet (UV) excitation of toluene at 248 nm. The LIF signal-ratio from two different sections of the LIF emission spectrum must be determined. For imaging, two LIF images are captured simultaneously with two ICCD cameras that are equipped with appropriate (different) filters. A calibration enables to determine temperature from the LIF signal-ratio. The calibration is based on toluene-LIF emission spectra that are acquired under well-controlled conditions at different temperatures [62,64]. In the present work, spectrally-resolved in-cylinder measurements were used (Figure 4-6) where the temperature was determined from a ther-

modynamic analysis of the pressure trace [65,92]. When applying the calibration, the spectral response of the entire detection system (Figure 4-5) must be taken into account.

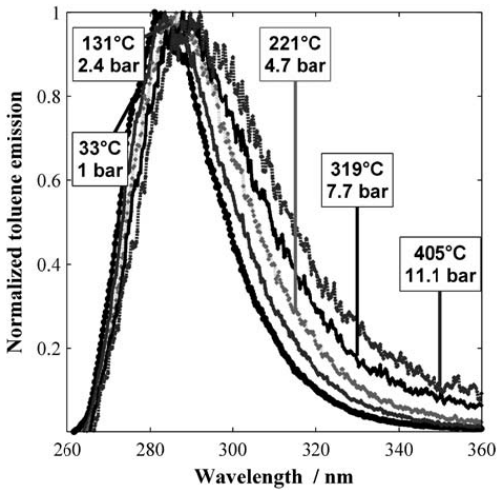

Figure 4-6: Normalized toluene-LIF emission spectra acquired in an optical engine in N_2 (graph from Devillers et al. [92]).

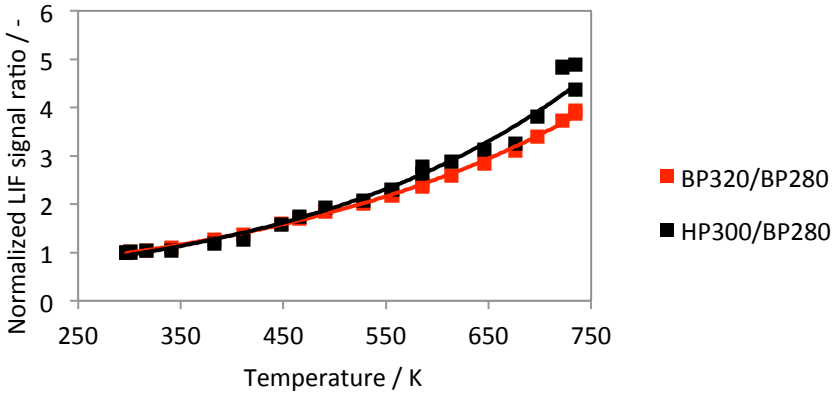

Figure 4-7: Dependence of the toluene-LIF signal ratio on temperature for the two-color LIF thermometry for 248 nm excitation and two filter pairs (BP320/BP280 and HP300/BP280). Symbols: Toluene-LIF signal ratio obtained from LIF spectra in N_2 (Figure 4-6) with the spectral response of the entire detection system (Figure 4-5). Lines: Interpolation by an exponential function.

The calibration method used here is based on previous application of the two-color toluene-LIF thermometry [62,64]. The toluene-LIF emission spectra at different temperatures (Figure 4-6) and the spectral response of the entire detection system (Figure 4-5) were combined to calculate the LIF signal-ratio of the two spectral ranges (collection filter 1 and 2 in Figure 4-1). Figure 4-7 shows the LIF signal-ratio calculated at various temperatures for two pairs of filters (BP320/BP280 and HP300/BP280) and normalized by the value at 300 K. The two pairs of filters which differ by the filters for the detection of signal in the long-wavelength tail of the toluene-LIF spectrum (HP300 and BP320) show different temperature-sensitivity. The temperature-sensitivity of the LIF signal-ratio is

improved with the highpass filter (HP300) compared to the bandpass filter (BP320) since the highpass filter (HP300) has a higher transmission and collects the LIF signal in a wider range of wavelengths.

The results presented in the following are for the pair of filter (BP280/20 and HP300) only.

4.2.4 Measurement conditions

Fuel quality and tracer concentration

Toluene was added to *n*-dodecane fuel, which was used as a non-fluorescing surrogate Diesel fuel for the application of the two-color LIF technique. Preliminary experiments were performed to select the toluene concentration and to investigate the spectroscopic purity of the *n*-dodecane (nominal purity of 99.7% as specified by the manufacturer) since impurities cause 'background' fluorescence. Figure 4-8 shows a comparison of the jet LIF images obtained with *n*-dodecane without tracer for two different fuel qualities (97.7 and 99.7% purity) and with a mixture of *n*-dodecane and toluene with various concentrations (3, 5, and 10 vol.%). The LIF-images were captured near the emission peak of toluene (BP280/20) with laser excitation at 248 nm.

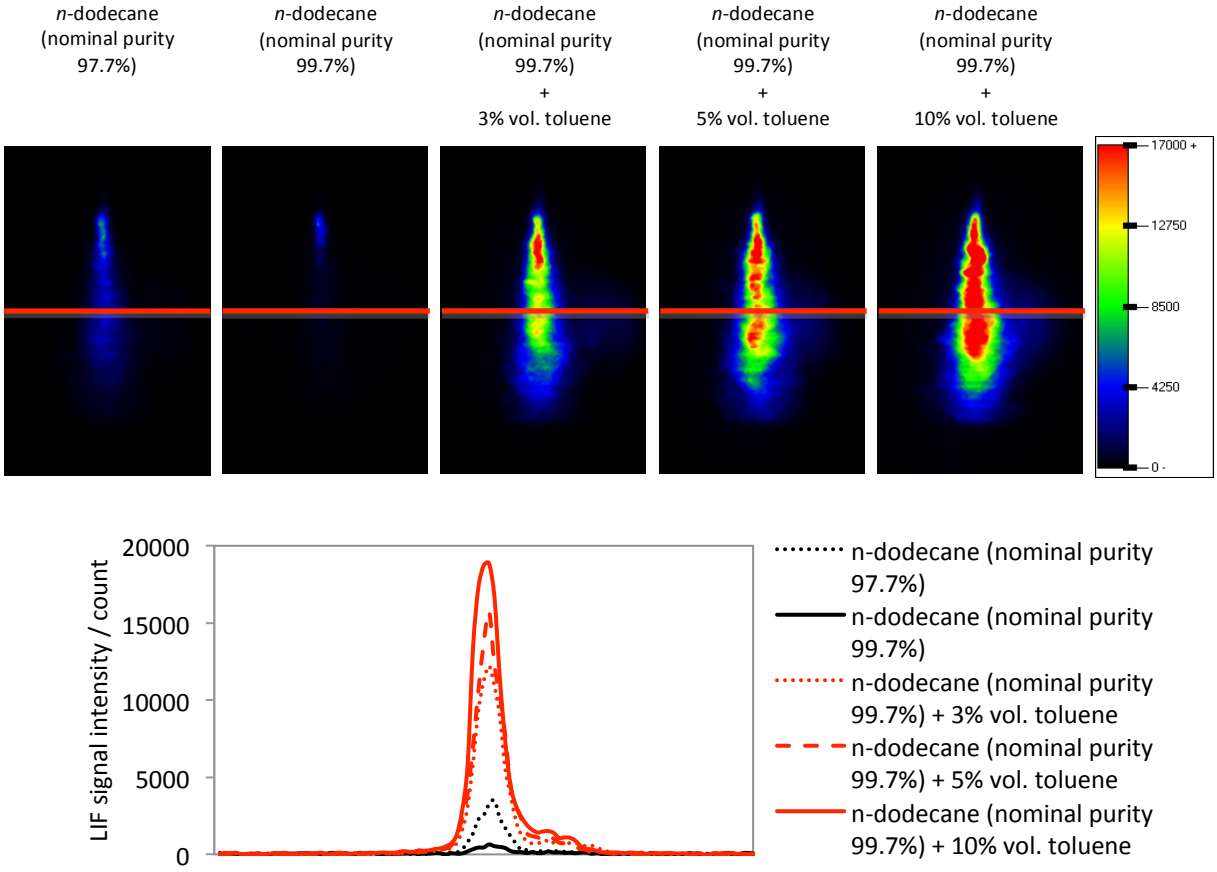

Figure 4-8: Upper row: Comparison of LIF images (ensemble-averaged from five single-shot images) of the jet obtained with neat *n*-dodecane and with the *n*-dodecane/toluene mixture. The LIF signals were collected near the toluene-LIF emission peak (BP280) in N_2, at 54 bar and 728 K, with laser excitation at 248 nm. Lower figure: Intensity profiles along the horizontal lines depicted on the upper LIF images.

Intensity profiles along the horizontal lines depicted on the LIF images are shown in the lower part of Figure 4-8. The 'LIF signal' level of neat *n*-dodecane confirmed to be lower for higher purity *n*-dodecane (99.7%). The background level was below 6% compared to the toluene-LIF signal for all measurement conditions and thus considered negligible. A toluene concentration of 10% was required to provide sufficient signal. Despite this high concentration, the measurements did not suffer from laser attenuation due to the small amount of fuel injected into the cell.

Optimization of the laser fluence

Toluene-LIF thermometry relies on photophysical processes occurring in the linear LIF regime. The laser fluence was adjusted to optimize the signal-to-noise ratio while remaining in the linear excitation regime. Toluene-LIF saturation is affected by temperature, pressure, and O_2 partial pressure [92]. With pure N_2, the saturation is reached at lower fluences for lower temperature and pressure, which might be explained by non-radiative de-activation processes promoted at higher temperature. For this reason, linearity tests were performed in N_2 at 1 bar and for a chamber temperature of 453 K (corresponding to the minimum temperature in the electrically-heated cell without pre-combustion). The fuel-tracer mixture was injected 20 s prior to image acquisition, providing enough time for creating a spatially-homogeneous mixture within the cell. The toluene-LIF (BP280) intensity was measured (with 248 nm excitation) as a function of fluence (Figure 4-9). To maximize LIF signals, the highest value of laser fluence was employed while ensuring that measurements were performed in the linear LIF regime, i.e., at 58 mJ/cm^2 laser fluence.

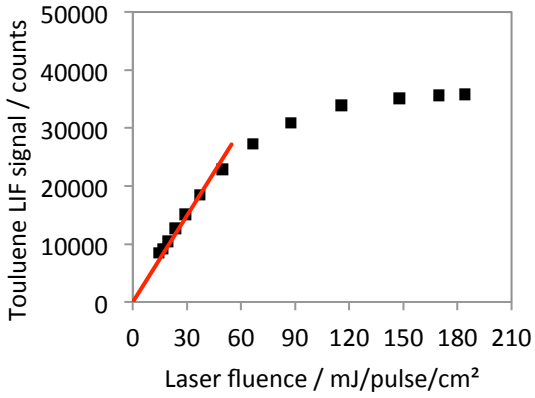

Figure 4-9: Fluence dependence of the toluene-LIF signal intensity for laser excitation at 248 nm in N_2 at 1 bar and 453 K, with detection at the emission peak of toluene (BP280).

Experimental methodology

Prior to each series of temperature measurements with configuration 1, configuration 2 was used for a series of standardization experiments. Therefore, the cell was homogeneously filled with vaporized fuel/tracer mixture. LIF images of the laser sheet profiles were then acquired with both cameras. The comparison of the pair of images allowed to correct for variations in pixel-to-pixel sensitivity of both

cameras, as discussed later. After acquiring images of homogeneous toluene distributions, LIF images in the Diesel jet (624 K and 46 bar ambient conditions) were measured after pre-combustion. As discussed later, the pair of single-shot LIF images detected in the identical spectral band served as reference images to perform (1) spatial mapping of the entire series of images and (2) to calibrate differences in the overall sensitivity of the two CCD cameras.

Filters were then used according to configuration 1 for two-color temperature measurements. Background images were acquired under the same cell conditions but without fuel injection. In addition, dark current background was subtracted. The image pairs obtained with fuel injection were then corrected for variations in pixel sensitivity and for spatial overlap using the data obtained from configuration 2. Additionally, the images were filtered for noise reduction as described in more detail in Section 4.3. Finally, the LIF-ratio image was determined which was then converted into a temperature image using the calibration data. An example of toluene-LIF images and the resulting temperature distribution is presented in Figure 4-10.

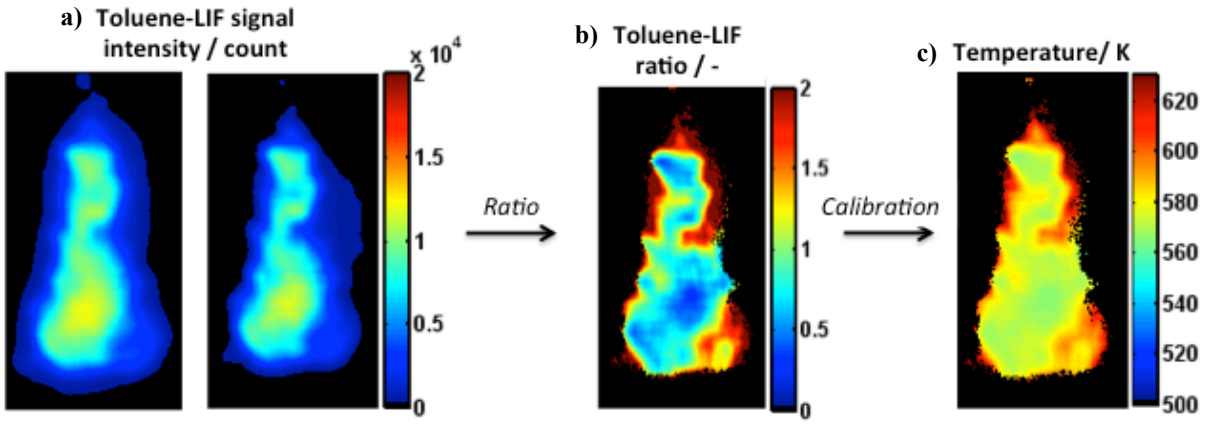

Figure 4-10: a) Toluene-LIF images obtained with the 300 nm highpass filter (left) and the 280 nm bandpass filter (right). b) Toluene LIF-ratio images. c) Resulting temperature distribution at 624 K and 46 bar ambient conditions.

4.3 Results and discussion

4.3.1 Image post-processing routine

Various aspects of the data processing were investigated using the LIF images obtained with configuration 2. Theoretically, both acquired images should be identical besides factors that would be attributed to different detector sensitivities or optical efficiencies. A plot of the pixel intensity of one camera on the *y*-axis versus that of the second camera on the *x*-axis (i.e., a pixel intensity correlation plot) should therefore result in a straight narrow line. Figure 4-11, however, shows significant dispersion around the mean which is due to imperfect superposition of the two images, variations in pixel-to-pixel sensitivity for both cameras, and shot noise. Additionally, the two detection paths (including

windows, filters and lenses) might have slight spatial variations in transmission properties. The image pair can thus be used to optimize image superposition, standardize the sensitivity of both detection systems, and evaluate the sources of various measurement uncertainties and their effects on the precision of the technique.

Image superposition

Calculating the LIF-intensity ratio relies on an accurate superposition of the two images. A poor spatial adjustment introduces significant errors in the temperature measurement. In the present work, the superposition was initially achieved by using a reference grid imaged by both cameras. A comparison of the two images yields a transformation matrix that is then applied to adjust one image relative to the other in terms of translation, rotation and scaling. The transformation matrix is given by the following expression:

$$T = \begin{bmatrix} sc & -ss & 0 \\ ss & sc & 0 \\ t_x & t_y & 1 \end{bmatrix}$$
$$sc = scale * \cos(angle) \qquad (4.1)$$
$$ss = scale * \sin(angle)$$

The variable *scale* specifies the scalar factor, *angle* the angle of rotation, t_x the displacement along the x-axis and t_y the displacement along the y-axis in the image.

Figure 4-11a reveals significant dispersion in the scatter plot (σ_I) even though the standard transformation matrix has been applied. Discretization of the scatter plot in the x-axis (using an interval width of 100 counts) enabled the determination of the mean (yellow dots) and the ±2σ standard deviation (red dots) as shown in Figure 4-11. The magnitude of the dispersion (σ_I) was used as criterion to further optimize the transformation matrix. Each term (*scale*, *angle*, t_x, t_y) of the initial transformation matrix described in eq. (3.1) was modified successively in order to obtain the minimum σ_I. The optimization of the transformation matrix was leading to a σ_I that was reduced by 70% (Figure 4-11b).

The methodology of optimizing the transformation matrix improved significantly the image superposition quality compared to the common approach using the initial transformation matrix generated by the grid images. However, this procedure was not totally optimized since the problem depends on four dependent parameters (*scale, angle,* t_x, t_y) while they were assumed to be independent. The methodology of optimizing the superposition of the LIF images can be further improved by taking into account the interdependency of the transformation matrix parameters (i.e., solve a problem with four variables). In the present work, the transformation matrix optimization was satisfactory as a first approximation with the dispersion criterion (σ_I) in Figure 4-11 b) that was significantly decreased by 70%.

Flat-field correction

The differences in the pixel sensitivities of both cameras also contribute to the dispersion. The correction procedure was based on acquiring toluene-LIF images in homogeneous conditions (i.e., homogeneous temperature and toluene concentration distribution) inside the cell, using configuration 2. Because both images should be identical (in the absence of shot noise), it was possible to determine differences in sensitivity on a pixel-by-pixel basis from averaged images (ensemble-averaged from 20 single-shot images to reduce shot noise). The correction was performed by multiplying one of the Diesel jet LIF images by this correction image. The additional effect of this correction can be seen by comparing Figure 4-11b and c. The dispersion (σ_I) was again reduced by 5% after applying the reference ratio image, showing that although shot noise tends to reduce the efficiency of this correction, the effect on measurement precision is beneficial.

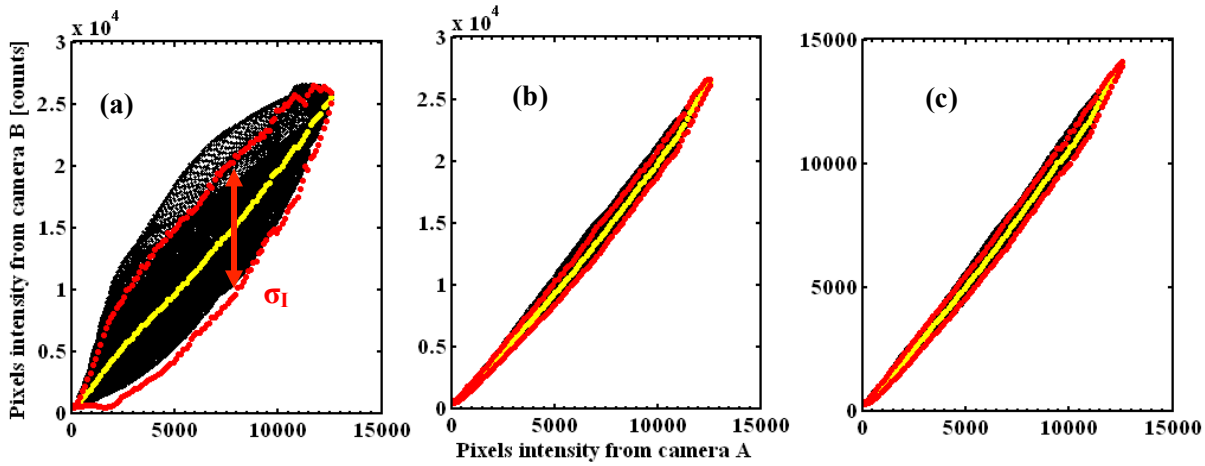

Figure 4-11: Signal intensity correlation for an image pair obtained in configuration 2. (a) After spatial adjustment from reference grid image. (b) After optimization of the spatial adjustment. (c) After optimization of the spatial adjustment and flat field correction. For symbols and color see text.

Adjustment of the camera sensitivity

The pair of Diesel-jet LIF images obtained with configuration 2 was also used to correct for differences in sensitivity between the two detectors. The mean values, represented by yellow dots in Figure 4-11c, reveal the difference in sensitivity of one detector relative to the other (which deviates slightly from a constant factor as a function of intensity). The resulting function was thus used to correct the LIF ratios when processing the images from configuration 1. With this methodology the fluorescence ratio becomes independent of sensitivity differences of the two cameras. The temperature-versus-LIF-intensity-ratio calibration curve derived from toluene emission spectra and corrected by the transmission characteristics of the collection optics (Figure 4-5) can therefore be *directly* applied to the LIF-ratio images and does not require an additional calibration measurement at conditions where the temperature is known. The calibration method is described in Section 3.2.3. With the two detectors matched in sensitivity, the technique does not require in situ calibration for the determination of temperature.

4.3.2 Error analysis – Determination of random error

Methodology for determining random error

The error sources that affect the precision (random error) of the measurement include errors due to imperfect superposition (spatial mapping) of the two images, differences in pixel-to-pixel sensitivity of the two cameras and camera shot noise. Because the comparison of the two LIF images in the jet from configuration 2 (i.e., identical optical filters) is also affected by these error sources, it can be used to determine the measurement precision as follows.

A pair of toluene-LIF images of the Diesel jet is acquired using configuration 2 which was then used to determine a LIF-ratio image. For all pixels, the LIF ratio should be unity as long as significant signal is measured. This is, however, not the case and there is some dispersion of the ratio (Figure 4-12). The magnitude of this dispersion (σ_R) indicates the contribution of the different error sources discussed before. This analysis of the ratio image is similar to the image-pair analysis displayed in Figure 4-11, except that the magnitude of the dispersion is expressed in terms of the ratio. This is more convenient because the measured temperature is directly related to the LIF ratio by using the toluene LIF calibration data.

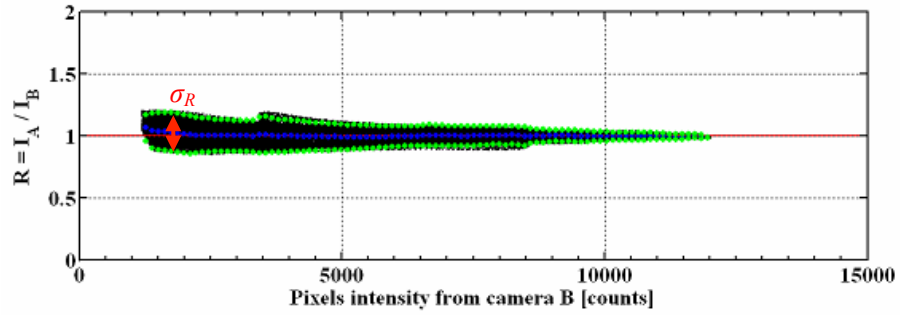

Figure 4-12: Signal intensity correlation between LIF-ratio image and LIF-intensity image with configuration 2.

In the present experimental set-up, the following expression (Eq. (3.2)) corresponds to the fit related temperature (in Kelvin), *T*, and the LIF signal ratio, *R,* defined as the inverse function of the interpolated curves shown in Figure 4-7.

$$T = (278\times \ln(R) + 544)\ \mathrm{K} \tag{4.2}$$

Temperature image is calculated by implementing eq. (1.3) and (1.4) into the LIF-ratio image. The dispersion of the LIF ratio can be expressed in terms of a dispersion in temperature (Eq. (3.3)):

$$dT = 278\ \mathrm{K}\times(dR/R) \tag{4.3}$$

The measurement precision (statistical error) was then determined from the LIF-ratio image obtained in configuration 2 using Eq. (3.4):

$$\sigma_T = 278\ \mathrm{K}\times(\sigma_R/R) \tag{4.4}$$

where σ_T is the temperature measurement precision and σ_R the standard deviation of the values of R in the ratio image.

An example of the evolution of σ_T versus the signal intensity of one of the image pairs obtained in configuration 2 is presented in Figure 4-13. The values presented in this figure were obtained after applying the various correction procedures described above. Additionally, both images were numerically filtered to reduce the effects of shot noise; two types of filter were investigated, a 'median filter' and a 'mean filter'. The filter box-size was 2×2 mm^2 as discussed in more detail in the following. The results show that the statistical error is maximal for low levels of LIF signal, around 23 K and decreases to below 10 K in regions of the jet where the LIF signal intensity is maximal. This is consistent with the relative contribution of shot noise in the regions of low or high signal intensity. These results also show the difficulty of applying the two-color toluene-LIF thermometry for measurements in a Diesel jet configuration. In the jet periphery, the measurement precision is low as a result of low fuel concentration and high temperature which leads to a decrease in LIF signal strength.

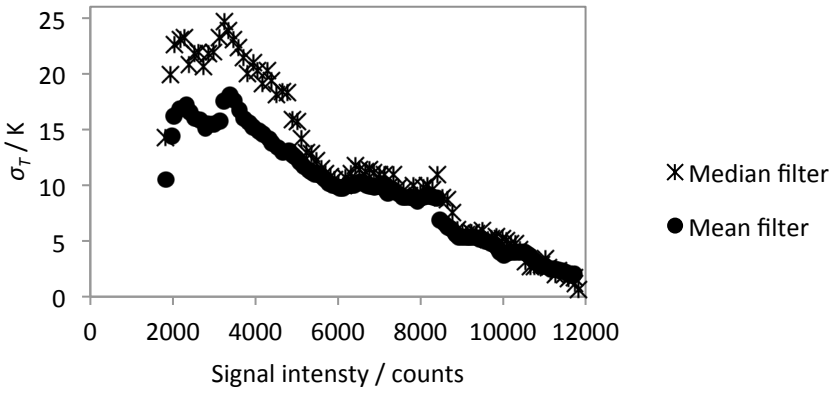

Figure 4-13: Statistical error σ_T as a function of signal intensity for an image pair obtained in configuration 2.

Numerical filtering and random error

After optimizing the image superposition and applying the flat-field correction, the main contributor to statistical error is shot noise. In order to reduce its contribution, the LIF images were numerically filtered. In the present work, the effects of the type of the numerical filter and its filter box-size were investigated. Figure 4-14 shows the evolution of the maximum measurement statistical error σ_{TM} as a function of the filter box-size for the two types of filters. The value of σ_{TM} presented in this figure corresponds to the maximum value obtained in the LIF ratio image, corresponding to regions of low signal intensity in the images as shown Figure 4-13 (in Figure 4-13, σ_{TM} is approximately 23 K with the 'mean average' filter). The filter box-size used for filtering is expressed in mm^2 (rather than in pixels, 1 pixel corresponds to 0.08 mm). Figure 4-14 shows that the statistical error σ_{TM} decreases with increasing filter box-size and is lower with the 'averaging filter'. It shows that there is a compro-

mise between measurement precision and spatial resolution. In the present work a filter box-size of 2×2 mm^2 was selected.

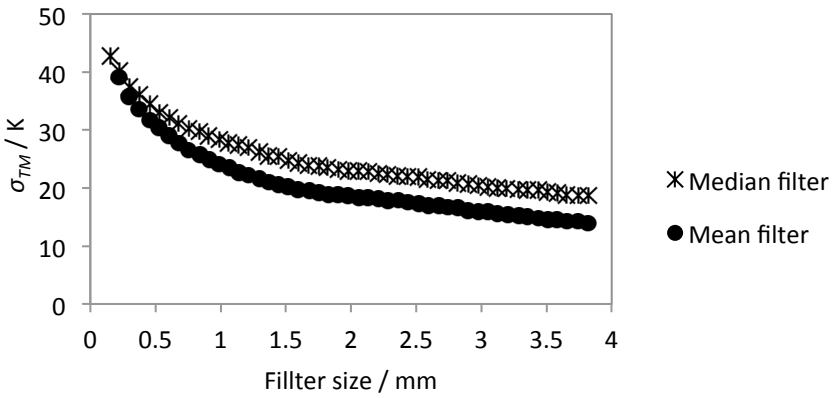

Figure 4-14 Evolution of the maximal measurement statistical error as a function of the filter box-size, for two types of numerical filters, calculated with an image pair obtained in configuration 2.

4.3.3 Error analysis – Systematic error evaluation

In order to evaluate the accuracy of the temperature measurement (systematic error), it was necessary to compare the temperatures measured by the two-color toluene LIF technique against a known (reference) temperature measurement. The bath-gas temperature T_{TC} (measured by a thermocouple) in the central zone of the cell prior to fuel injection was used as a reference. When measurements were carried out in fully homogeneous mixtures within the electrically-heated cell at 453 K, the homogeneous toluene-LIF temperature data can be directly compared to T_{TC} and thus allows to determine the measurement accuracy at this low temperature.

Reference measurements at higher temperature, however, could not be realized in the same way. Therefore, a different strategy was developed that is based on fuel injection into the hot bath gas that was heated by pre-combustion. In this configuration, thermocouple measurements (T_{TC}) can only provide information on the ambient temperature in the absence of a jet, hence the ambient temperature outside the jet boundaries. However, the two-color toluene LIF technique can only provide temperature information (T_{LIF}) inside the jet. Therefore, a specific strategy was used to enable an indirect comparison (Figure 4-15). The ambient temperature T_{TC} provided by the thermocouple measurement was used to derive temperature within the spray T_{AM} using an adiabatic mixing model. This model is based on the assumption of adiabatic mixing between the fuel and ambient air and requires the ambient temperature measured by the thermocouple as input, as well as the estimation of the fuel concentration inside the jet that was deduced from single-line measurements of toluene LIF. This analysis was performed with a relatively long delay between the end of injection and image acquisition to ensure sufficient time for complete evaporation to prevent interference from liquid fuel.

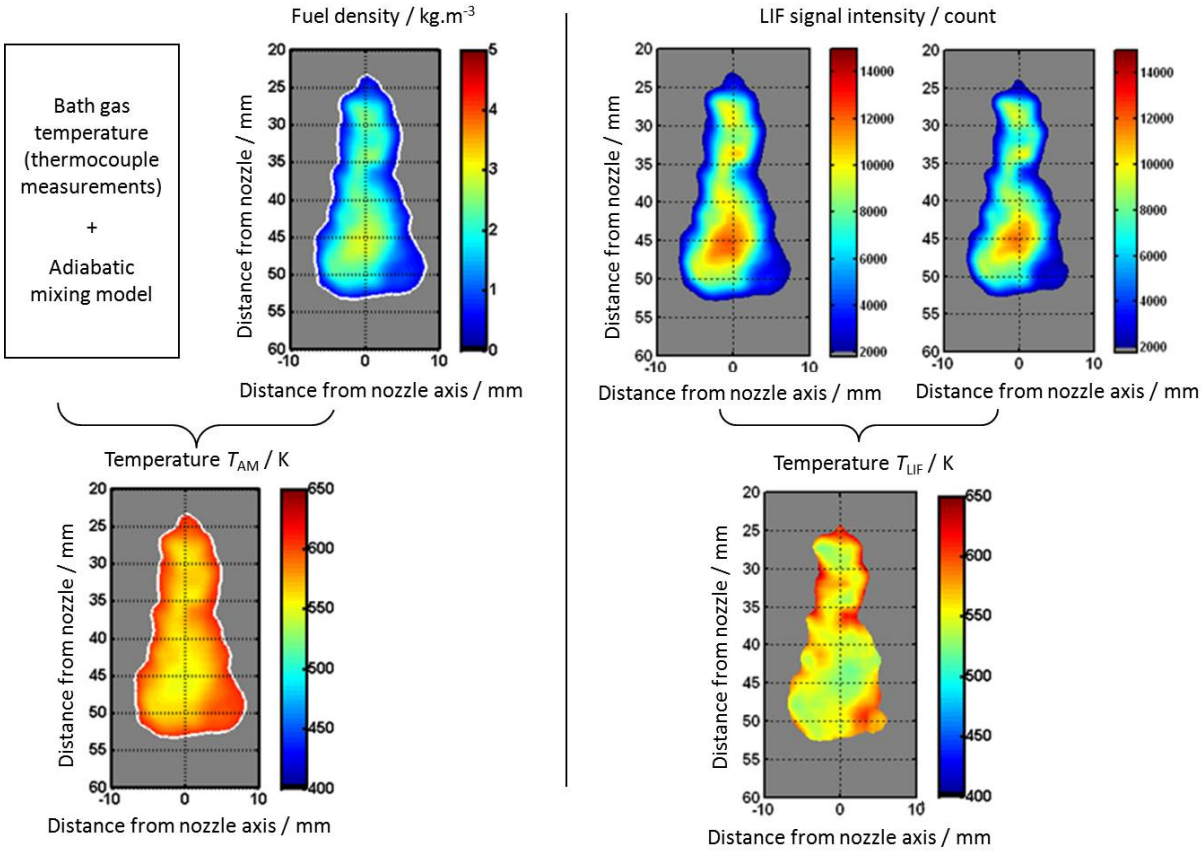

Figure 4-15: Comparison of temperature measured by two-color LIF (T_{LIF}) and reference temperature measurement (T_{AM}) to evaluate the measurement accuracy. Left: Reference temperature within the spray T_{AM} derived from thermocouple measurements of the ambient temperature by using an adiabatic mixing model and an estimation of the fuel concentration inside the jet (single-line measurement of toluene LIF). Right: Temperature within the spray T_{LIF} using two-color LIF thermometry.

In a zeroth-order approximation, LIF intensities obtained with the HP 300 filter were interpreted as maps of fuel number densities. In toluene-LIF images, the signal intensity S_{fl} is at each point (x,y) proportional to the product of the number density n_{tol}, the absorption cross-section σ_{abs} and the fluorescence quantum yield Φ_{fl} of the fluorescence species and finally the laser intensity E_{laser} [26]:

$$S_{fl}(x,y) = \eta\, E_{laser}(x,y) n_{tol}(x,y) \sigma_{abs}\big(T(x,y)\big) \phi_{fl}\big(T(x,y)\big) \qquad (4.5)$$

with η a proportionality factor taking into account the optical characteristics of the set-up (i.e., detection efficiency).

By assuming the same behavior between the fuel (*n*-dodecane) and the tracer (toluene) in terms of droplet formation, evaporation, convection and diffusion [93], the toluene-LIF signal intensity is proportional to the fuel concentration. However, the tracer-LIF signal depends on local temperature, pressure, and the bath gas composition (mainly O_2 partial pressure). In the present experiment, spatial homogeneity of pressure is assumed and there was no O_2 left in the ambient gas. Therefore, the fuel concentration in the jet can be obtained from the toluene-LIF image by considering only the temperature

and the laser sheet profile. Temperature influence was in a first step neglected and the toluene-LIF signal was expressed as uniquely proportional to fuel concentration:

$$S_{\mathrm{fl}}(x,y) = \eta' \, E_{\mathrm{laser}}(y) c_{\mathrm{fuel}}(x,y) \tag{4.6}$$

The toluene-LIF signal in volume I_v is directly related to the corresponding fuel mass M by the proportional factor η'. Therefore, η' can be calculated with the following expression:

$$\eta' = I_v / M \tag{4.7}$$

The LIF signal volume I_v represents the intensity in the volume and was obtained by rebuilding the 3D images of the jet from available 2D images based on the assumption of an axisymmetric jet:

$$I_v = \iiint_{-\pi}^{\pi} \frac{S_{fl}(x,y)}{E_{laser}(y)} \, x \, d\theta \, dy \, dx = 2\pi \iint \frac{S_{fl}(x,y)}{E_{laser}(y)} \, x \, dy \, dx \tag{4.8}$$

After evaluating the corresponding fuel mass M, the fuel concentration distribution c_{fuel} is calculated from the toluene-LIF signal with the following expression:

$$c_{\mathrm{fuel}} = \frac{S_{\mathrm{fl}}(x,y)}{\eta' \, E_{\mathrm{laser}}(y)} \tag{4.9}$$

The toluene-LIF signal was thus interpreted as maps of fuel number density assuming spatially invariant fluorescence quantum yields according to [93] which is based on a comparison of local intensities to those measured after injection of a known fuel mass. The local temperature can be obtained from the local fuel concentration by calculating the fuel mass-related evaporative cooling via the adiabatic mixing model [13]. By assuming adiabatic mixing between the fuel (doped with toluene) and the ambient, the adiabatic mixing temperature T_{AM} was calculated using thermodynamic equilibrium. T_{AM} was determined from the following expression [13] based on energy conservation:

$$\int_{T_{\mathrm{AM}}}^{T_{\mathrm{TC}}} C_{p,\mathrm{a}} dT = (F/A)_m \left[\int_{T_{\mathrm{fl,ini}}}^{T_{\mathrm{int}}} C_{p,\mathrm{fl}} dT + h_{v,T_{\mathrm{ini}}} + \int_{T_{\mathrm{int}}}^{T_{\mathrm{AM}}} C_{p,\mathrm{fv}} dT \right] \tag{4.10}$$

The term $\int_{T_{\mathrm{AM}}}^{T_{\mathrm{TC}}} C_{p,\mathrm{a}} dT$ expresses the decrease of thermal energy of the ambient gases during transfer energy with the fuel. The ambient gases temperature drops from the initial temperature T_{TC} (measured by thermocouple) to the adiabatic mixing temperature T_{AM}. $C_{p,\mathrm{a}}$ is the ambient gas molar specific heat. The term $(F/A)_m$ expresses the fuel/air ratio by mass which is related to the fuel concentration ($\rho_{\mathrm{fuel}} = m_{\mathrm{fuel}}/V$) by using the ideal gas law. The term $\left[\int_{T_{\mathrm{fl,ini}}}^{T_{\mathrm{int}}} C_{p,\mathrm{fl}} dT + h_{v,T_{\mathrm{ini}}} + \int_{T_{\mathrm{int}}}^{T_{\mathrm{AM}}} C_{p,\mathrm{fv}} dT\right]$ expresses the increase in thermal energy during energy exchange with the ambient gases when the fuel temperature rises from $T_{\mathrm{fl,ini}}$ (initial fuel temperature) to the adiabatic mixing temperature T_{AM} passing through the intermediate temperature T_{int} where the change of state from liquid to gas occurs. $C_{p,\mathrm{fl}}$ and $C_{p,\mathrm{fv}}$ are the molar specific heat of the liquid and gas fuel respectively. $h_{v,T_{\mathrm{ini}}}$ expresses the molar heat transfer coefficient.

The adiabatic mixing temperature T_{AM} gives an evaluation of the local temperature in the fuel jet where all fuel is vaporized. Using expression (3.10), the temperature distribution in the jet (T_{AM}) was determined from the fuel concentration c_{fuel}. The resulting zeroth-order temperature field (T_{AM}) was used to replace the initial assumption of constant fluorescence quantum yields by temperature-dependent values leading to a first-order correction in local fuel mass. This again led to improved temperatures and this procedure was carried on in an iterative way until no further changes occurred. The result was a temperature map from single-line LIF with adiabatic-mixing assumption that will be denoted hereafter as T_{AM}.

Various sources of uncertainty remain in this procedure. Firstly, uncertainties arise from the determination of the injected fuel mass. The injected fuel mass was calculated as follow:

$$M = 0.6 \times \rho_{fuel} \times Q_{inj} \times t_{inj} \tag{4.11}$$

with ρ_{fuel} the fuel density (770 kg/s), Q_{inj} the flow injection rate (12 mm^3/ms) and t_{inj} the injection duration (900 µs). The collected LIF signal does not represent the entire jet since only a slice of the jet was illuminated by the laser light sheet and a threshold was used to extract the signal from noise which is causing signal loss. The visible part of the jet (i.e., the fluorescing part) was evaluated 60% of the jet total volume and thus the fuel mass *M* was evaluated 60% of the total injected fuel mass. Uncertainties arise also from the effect of temperature on the fluorescence yields. However, the main source of uncertainty might be due to the adiabatic mixing model itself. The model is based on the hypothesis that mixing and evaporation is adiabatic, which in the present experiment is a reasonable assumption since neither significant wall heat losses nor radiative heat losses are expected. However, errors are likely due to an incorrect determination of the boundary conditions: the ambient temperature and the temperature of the pure vaporized fuel. The uncertainty of the ambient temperature T_{TC} is given by the accuracy of the thermocouple measurement. A value of 473 K was selected according to the thermodynamic model presented in [13]. Consequently, the error of this temperature determination is believed to increase with increasing deviation from ambient temperature T_{TC} and, thus, fuel concentration. The temperature distribution in the jet determined by T_{AM} is expected to be more accurate in the region of the jet where the temperature is close to the ambient temperature T_{TC}.

A comparison is made between the two-line LIF temperatures (T_{LIF}) and the temperatures derived from the single-line LIF using an adiabatic mixing model (T_{AM}), within the high-temperature regions of the jet that are located close to the jet periphery. Around these regions the temperature is close to the ambient/bath gas temperature (T_{TC}) which is therefore expected to be reasonably accurate. The results of this comparison derived from six individual measurements are shown in Figure 4-16. It reveals that below 700 K, measurement accuracy (systematic error) determined from the difference between T_{LIF} and T_{AM} at the edge of the jet is better than ±30 K. A more accurate determination of the measurement systematic error would require a higher number of samples for statistical analysis. For temperatures higher than 700 K, the difference between the two temperatures increases significantly. This deteriora-

tion of the measurement accuracy at high temperature is probably due to a significant decrease of the toluene-LIF signal, resulting in a reduced signal-to-noise ratio from 10 to 5 in the jet periphery at ambient temperature of 624 and 728 K, respectively. Higher signal-to-noise levels would be required to enable temperature measurements at higher temperatures.

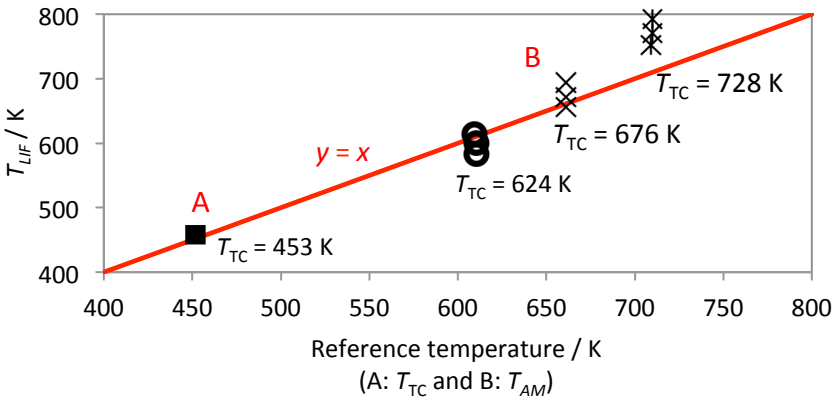

Figure 4-16: Comparison between results of two-color LIF thermometry (T_{LIF}) with A: thermocouple (T_{TC}) measurements in the electrically-heated cell, and B: single-line LIF measurements with the adiabatic mixing model (T_{AM}) applied to the jet periphery where the fuel concentration equals 0.4 kg/m^3. Measurements with different bath gas temperatures (T_{TC}) at 624 K, 676 K and 728 K. Injection duration 600 µs, detection 1.5 ms after start of injection.

4.3.4 Discussion

Diesel jet temperatures corresponding to one injection event (i.e. single-shot LIF images) obtained by LIF imaging (T_{LIF}) are compared to the reference temperature (T_{AM}) derived from thermocouple measurements of the ambient temperature by using an adiabatic mixing model and an estimation of the fuel concentration inside the jet (cf. Section 4.3.3) in Figure 4-17. Unlike Figure 4-16 where the temperature was calculated within the periphery of the jet at a given fuel concentration, the data presented in Figure 4-17 corresponds to temperature measurements which have been made within the entire jet with variable fuel concentrations. For a given range of T_{AM} values corresponding to specific locations in the image, mean averaged and standard deviations of T_{LIF} values in the corresponding locations in the image are presented. The results from one injection event presented here are typical for the results obtained for other injection events. The results reveal satisfactory agreement when comparing the average temperature measured by LIF imaging with the corresponding T_{AM} value although higher discrepancies are observed at lower temperatures. These results show that the temperatures determined via single-line LIF imaging with the adiabatic mixing model are comparable to the results of the two-color LIF thermometry. The discrepancy observed at lower temperatures is attributed to the fact that the adiabatic mixing model yields increasing errors with increasing fuel concentration and, thus, decreasing temperature. The temperature standard deviations determined from the two-color LIF themometry (T_{LIF}) compared to T_{AM} are consistent with the statistical error evaluation in Figure 4-13.

In particular, in the lower temperature regions of the jet the standard deviation is below 10 K while it increases to 30 K in the higher temperature zones. These values compare well with estimates of the statistical error presented earlier (Figure 4-13) and thus indicate that the major source of error when comparing the two methods is most likely due to this statistical error.

As a result, it seems reasonable to conclude that in the configuration studied here, local temperature fluctuations in the jet are most likely due to the presence of fuel concentration fluctuations arising from temperature inhomogeneities, which are related to the mixing process. Overall, the initial results are promising and indicate that the two-color toluene-LIF thermometry is a highly valuable tool for temperature imaging and, thus, an aid for gaining an improved understanding of the mixing and auto-ignition processes in Diesel jets.

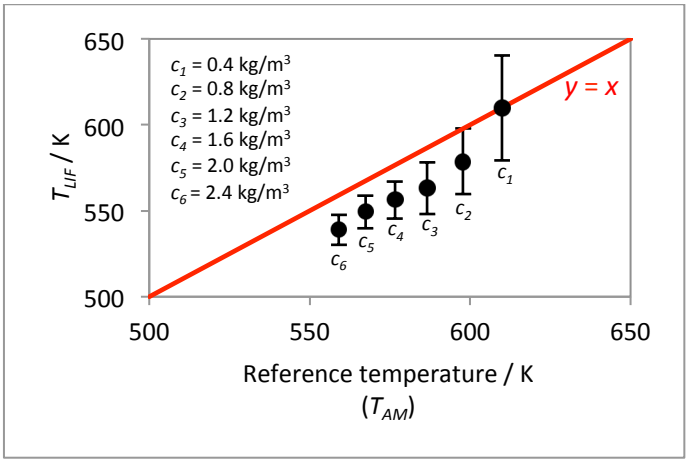

Figure 4-17: Comparison of LIF ratio temperature (T_{LIF}) and T_{AM} in the whole jet at different fuel concentrations (c) for one injection event with an ambient temperature of 624 K (T_{TC}). The circles correspond to average T_{LIF} values over a range of T_{AM}, while the crosses correspond to the standard deviation.

4.4 Conclusions

Measurements of unburned gas temperature in an evaporating Diesel spray have been performed using two-color toluene-LIF temperature imaging. Various aspects of the technique were studied and a detailed uncertainty analysis has been performed. Using single-wavelength excitation at 248 nm and two-color detection, the measurement precision (σ) of the technique is in the 20–40 K range.

Various sources of random and systematic errors were examined and methods are reported which help to significantly improve measurement precision and accuracy. In particular, improved data processing algorithms have been developed including for example, an iterative optimization procedure which allows precise superposition of the LIF image pair. Flat field image corrections are also performed to compensate for variations in pixel-to-pixel sensitivity of the two detectors. Finally, the calibration procedure also takes into account the spectral characteristics of the various optical components (i.e., windows, optical filters, lenses and spectral response of the image intensifiers).

The measurement accuracy was evaluated by comparing the temperature measured by the two-color toluene LIF technique with a known ambient/bath gas temperature measurement. A straightforward comparison was possible for one temperature (453 K) within the electrically-heated cell under homogeneous conditions without pre-combustion. At higher temperatures an indirect comparison was performed between the jet temperatures derived from the two-color LIF ratio with those derived from a single-color LIF measurement using an adiabatic mixing model.

The results reveal that toluene two-color LIF thermometry has limitations at temperatures above 700 K. It might be possible to perform measurements at higher temperatures by using higher laser fluence in a partially-saturated situation to improve LIF signal-to-noise ratio, thus giving up some of the spectroscopic rigidity. Furthermore, the results presented suggest that local temperature fluctuations in the Diesel jet are most likely due to the presence of fuel concentration fluctuations arising from temperature inhomogeneities which are related to the mixing process.

In the present work, experiments were performed in conditions close to mixing adiabatic conditions which enabled the validation of the technique. An application of the technique appears to be promising for more complex, i.e., non-adiabatic conditions as well.

5 Multi-parameter two-tracer-LIF measurements in Diesel jets

5.1 Tracer-LIF for multi-parameter measurements

Fuel concentration measurements using tracer-LIF have previously been investigated and the results were discussed in Chapter 2. However, tracer LIF is generally sensitive to temperature and in some cases (e.g., aromatic tracers) to O_2 partial pressure. As a consequence, the use of tracer-LIF to measure fuel concentration with a high degree of precision additionally requires knowledge of gas-phase temperature and in some cases of O_2 partial pressure, which also can be determined from the effects of temperature and O_2 on the tracer-LIF signal. These requirements formed the basis of the work described in the present chapter where the objective was to evaluate the possibility to measure simultaneously the gas-phase temperature and O_2 partial pressure using a two-tracer three-color LIF technique.

5.1.1 Measurement strategy for 2D imaging of temperature and O_2 partial pressure

The use of two tracers with LIF signal collection within three distinct spectral ranges using three appropriate optical filters and three detectors potentially allows the simultaneous measurement of temperature and O_2 partial pressure as described in Chapter 2. The criteria and justification for the selection of the two tracers toluene and naphthalene used in this study were discussed in Chapter 2. The fluorescence emission spectra principle for the two-tracer three-color LIF method developed in the present work is illustrated in Figure 5-1, corresponding to a mixture with a 99:1 ratio of toluene and naphthalene in N_2 at 1 bar and 370 K. The LIF signal was normalized to the emission peak of naphthalene. The collection filters 1, 2, and 3 indicate the three spectral ranges where the LIF signal is collected.

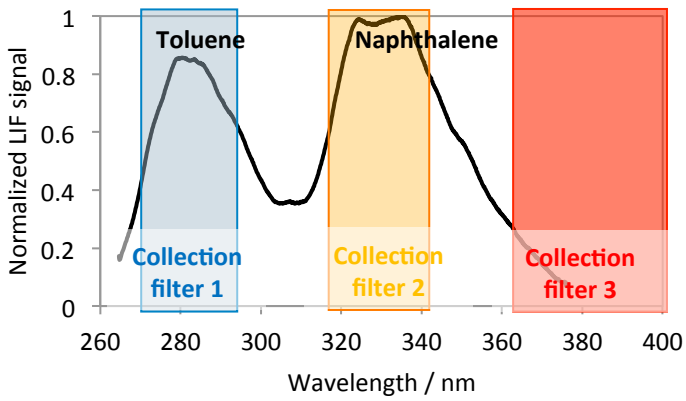

Figure 5-1: Fluorescence emission spectra of the two-tracer mixture with a 99:1 ratio of toluene and naphthalene in N_2 at 1 bar and 370 K with the respective bandpass filters.

Measurement of temperature

In the present work, the temperature measurement was based on the redshift of the LIF signal of naphthalene with increasing temperature. The principle of this temperature measurement technique (two-color LIF thermometry) was described in Chapter 4 for toluene. The LIF signal is collected in two distinct spectral ranges (Figure 5-1), the first around the emission peak at 330±10 nm (collection filter 2) and the second at longer wavelengths at 370±15 nm (collection filter 3). In a mixture of toluene and naphthalene, the LIF signals of both tracers are red-shifted to longer wavelengths with increasing temperature. Both tracers could theoretically be used for two-color LIF thermometry. However, naphthalene was better suited than toluene (in the present mixture) because its detection was less affected by interference from toluene LIF while a toluene-based measurement would have been significantly influenced by the naphthalene-LIF signal. The ratio of the two collected signals (collection filters 2 and 3 in Figure 5-1) was used to determine temperature after calibration from reference measurements (cf. Chapter 4). As a first approximation, the LIF signal-ratio can be assumed to be independent of the O_2 partial pressure.

Measurement of the O_2 partial pressure

Excited aromatic molecules such as toluene and naphthalene undergo fast collisional quenching with O_2 leading to a reduction of the LIF signal as a function of O_2 partial pressure. The O_2 partial-pressure measurement was based on exploiting the difference in the sensitivity of toluene and naphthalene LIF on O_2 quenching. The LIF signals of each tracer were collected near their respective emission peaks (Figure 5-1) at 280±10 nm in the case of toluene (collection filter 1) and 330±10 nm in the case of naphthalene (collection filter 2). The ratio of the two collected signals could then be used to determine O_2 partial pressures after calibration and correction for temperature dependences which were determined from two-color LIF thermometry measurements using naphthalene (cf. Chapter 4). The calibration is based on reference measurements of naphthalene and toluene LIF signals for various O_2 partial pressures and temperatures. Figure 5-2 shows a schematic of the measurement strategy for the two-tracer three-color LIF technique using toluene and naphthalene.

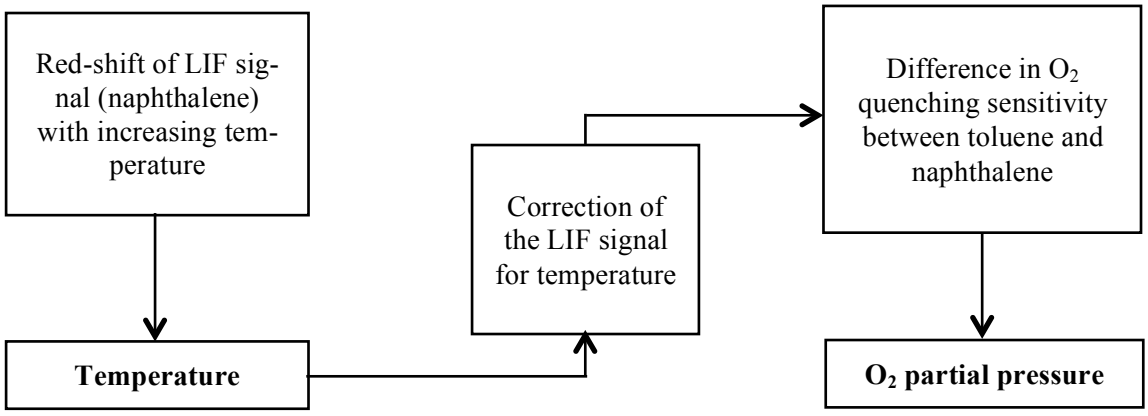

Figure 5-2: Temperature and O_2 partial pressure measurement strategy

5.1.2 Validation approach

The two-tracer three-color LIF technique was applied in the high-pressure high-temperature cell (described in Chapter 4) to perform an initial validation of the experimental approach. The cell provides a well-controlled injection and bath-gas conditions that are representative of in-cylinder engine conditions. Furthermore, it enables single-parameter variations for temperature and O_2 partial pressure. *n*-Dodecane (Diesel surrogate) doped with a mixture of naphthalene and toluene tracers was used in the experiments. The relative proportions of toluene and naphthalene were adjusted to ensure comparable signal-to-noise ratios for both tracers.

Three cameras would have been required for the simultaneous acquisition of LIF images corresponding to the three spectral ranges (collection filters 1, 2 and 3 in Figure 5-1). However, due to time and equipment limitations, it was not possible to install a three-camera experiment in the present work. An alternative, simplified experimental configuration was used which required a single intensified CCD camera only. As a result, the simultaneous acquisition of LIF images of the three spectral ranges was not possible and the analysis was based on ensemble-averaged LIF images of subsequently acquired data. As will be discussed in more details later, this approach generated difficulties due to the deviation from linear response of the LIF signal in the respective channels on the respective quantities (temperature and O_2 partial pressure), higher shot-to-shot fluctuations of average quantities, leading to an increase of the measurement uncertainty, especially for small samples. However, despite these limitations, the experimental configuration was found suitable to perform an initial evaluation of the methodology.

The LIF signals of toluene and naphthalene and the respective calculated LIF signal-ratios obtained in the jet were compared to experimental and simulation data reported in previous work [25,72,78,85,88,87]. Seven different optical filters were tested each one covering one of the three collection spectral ranges (collection filter 1, 2, and 3 in Figure 5-1) in order to determine the optimal combination of filters. Furthermore, laser excitation at 248 and 266 nm was used (not simultaneously) to investigate the appropriate excitation wavelength(s) for toluene LIF. For naphthalene LIF 266 nm excitation was used only.

5.2 Experiment

5.2.1 Optical arrangement

The optical arrangement for laser excitation and signal detection at the high-pressure high-temperature cell is shown in Figure 5-3. A KrF-excimer laser (Lambda Physik, CompexPro 102) and a frequency-quadrupled Nd:YAG laser (Quanta-Ray INDI Series) were used for laser excitation at 248 and 266 nm, respectively. For each laser, a vertical laser light sheet (34×0.3 mm²) entered the cell. Dark coated metal masks with vertical slots allowing the passage of the laser beam were mounted on the inner

sides of the laser entry and exit windows to reduce laser sheet flare. The LIF signal was collected through a third window located at 90° with an intensified CCD camera (Princeton PI-MAX, 1024×1024 pixels) equipped with custom high transmission optical filters (T > 70%) and a fast UV sensitive lens (f = 45 mm, $f_{\#}$ = 1.8, EADS Sodern). Seven band-pass filters (Semrock) were tested (Table 5-1) and their transmission characteristics are shown in Figure 5-4. A power meter was used to measure the laser pulse energy corresponding to each LIF image acquisition on a single-shot basis to correct for laser energy variations.

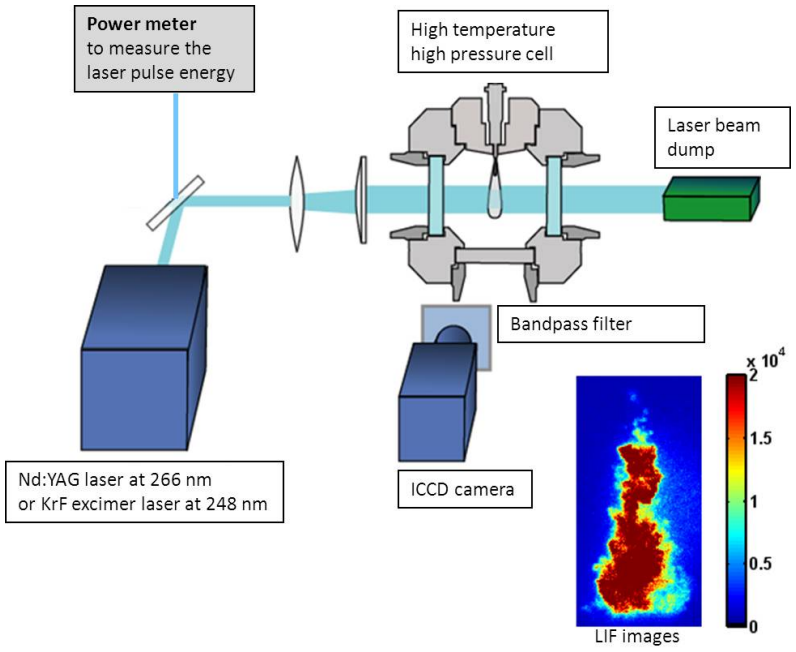

Figure 5-3: Schematics showing the optical arrangement for subsequent two-tracer three-color LIF measurements on the high-temperature high-pressure cell.

Table 5-1: Characteristics of the bandpass filters used for two-tracer three-color LIF measurements.

Tracer fluorescence signal collection	**Collection filter characteristics**	**Nomenclature**
Collection filter 1 Toluene-LIF emission peak	(1) BP280 nm, FWHM = 20 nm	BP280-20
	(2) BP292 nm, FWHM = 27 nm	BP292-27
Collection filter 2 Naphthalene-LIF emission peak	(3) BP335 nm, FWHM = 7 nm	BP335-07
	(4) BP340 nm, FWHM = 12 nm	BP340-12
	(5) BP340 nm, FWHM = 26 nm	BP340-26
Collection filter 3 Long-wavelength naphthalene-LIF emission	(6) BP370 nm, FWHM = 36 nm	BP370-36
	(7) BP376 nm, FWHM = 20 nm	BP376-20

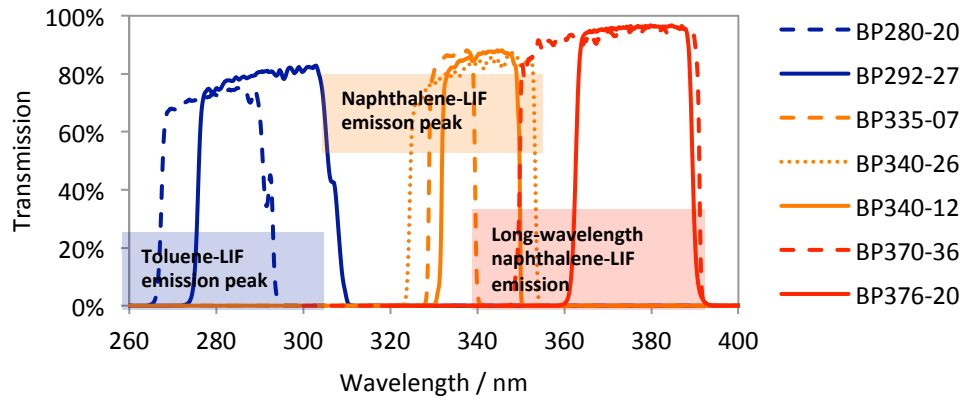

Figure 5-4: Transmission characteristics of the bandpass filters used for two-tracer three-color LIF measurements.

5.2.2 Experimental conditions

Camera linearity

The linearity of the response of the camera to incident light intensity must be ensured for quantitative LIF imaging. The linearity of the CCD was guaranteed by the manufacturer that measured the linearity of the output signal as a function of exposure time. However, linear response for the intensifier was not ensured, which could cause a non-linear response of the detector already below the CCD saturation limit of 16 Bit pixel digitization. Saturation of the intensifier can be observed when using high-gain settings or for specific conditions related to the experiments (e.g., strong background signal, high signal gradients). Based on our experience from toluene-LIF temperature measurements on the high-pressure high-temperature cell (Chapter 4), it was decided to maintain LIF signals below a threshold of 30000 counts in order to ensure a linear camera response. However, this approach clearly placed a restriction on the detected LIF signal level which limited the dynamic range of the acquired signals and therefore limited LIF measurement sensitivity in the present experiment.

Fuel quality and tracer concentration

Toluene and naphthalene were added to *n*-dodecane which was used as non-fluorescing surrogate Diesel fuel for the application of the two-tracer three-color LIF technique. The spectroscopic purity of *n*-dodecane (nominal purity of 99.7% as specified by the manufacturer) was verified as described in Chapter 4 to ensure that the measured LIF signal in the jet is a result of toluene and naphthalene tracer LIF. Figure 5-5 shows a comparison of the jet LIF images obtained with *n*-dodecane without tracers and with a mixture of *n*-dodecane, toluene, and naphthalene. The LIF images were captured near the emission peak of toluene (BP280/20) with laser excitation at 248 nm. Intensity profiles along the horizontal lines depicted on the LIF images are shown in the lower part of Figure 5-5. The background level (i.e., 'LIF signal' level of neat *n*-dodecane) was below 6% compared to the tracer-LIF signal and thus considered negligible. A total combined tracer (toluene and naphthalene) concentration of 10%

was required to provide sufficient signal. Despite this high concentration, the measurements did not suffer from laser attenuation due to the small amount of fuel injected into the cell.

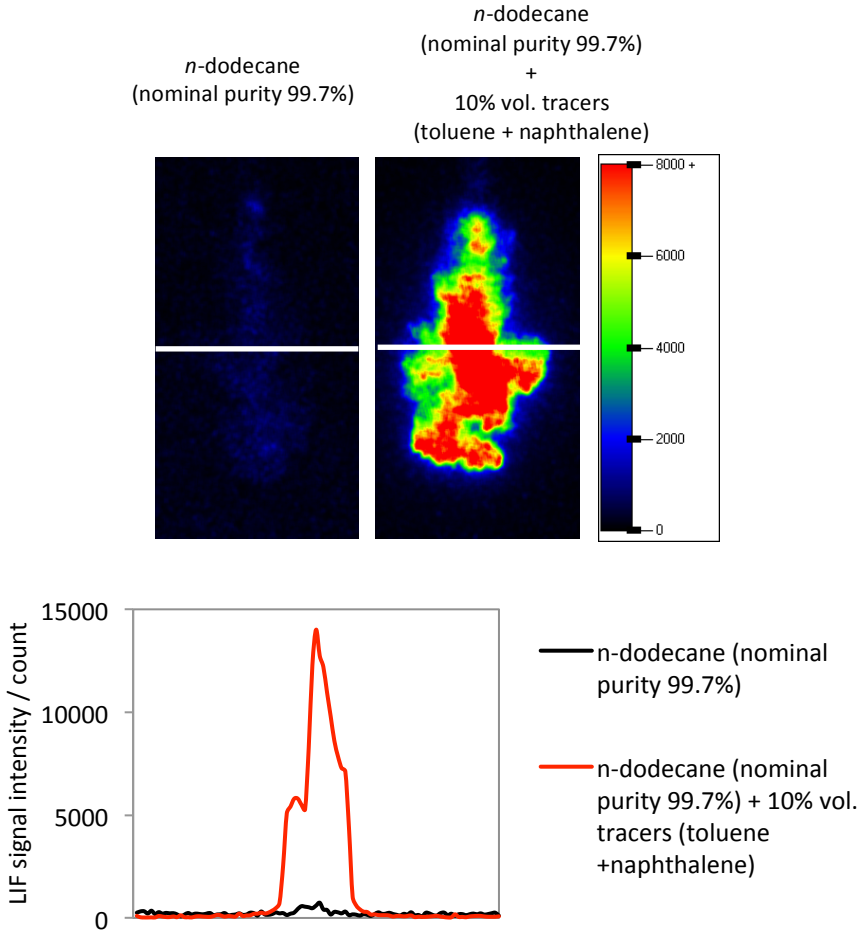

Figure 5-5: Upper figures: Comparison of LIF images of the jet obtained with neat *n*-dodecane and with the *n*-dodecane/toluene/naphthalene mixture. The LIF signals were collected near the emission peak for toluene (BP280/20) at 600 K and 0.46 bar O_2 partial pressure and with laser excitation at 248 nm. Lower figure: Intensity profiles along the horizontal lines depicted on the upper LIF images.

In addition, the relative proportions of toluene and naphthalene added to dodecane were adjusted to ensure comparable LIF signal intensities for both tracers. Figure 5-6 shows the LIF images captured around the emission peak of toluene (BP280/20) and naphthalene (BP320/26) for 266-nm excitation. LIF signal intensities were compared at 600 K and 0.46 bar O_2 partial pressure (i.e., at the lowest temperature and O_2 partial pressure investigated where the LIF signals were expected to be the highest in the present experiment) for a mixture of dodecane with 9.8 vol.% toluene and 0.2 vol.% naphthalene.

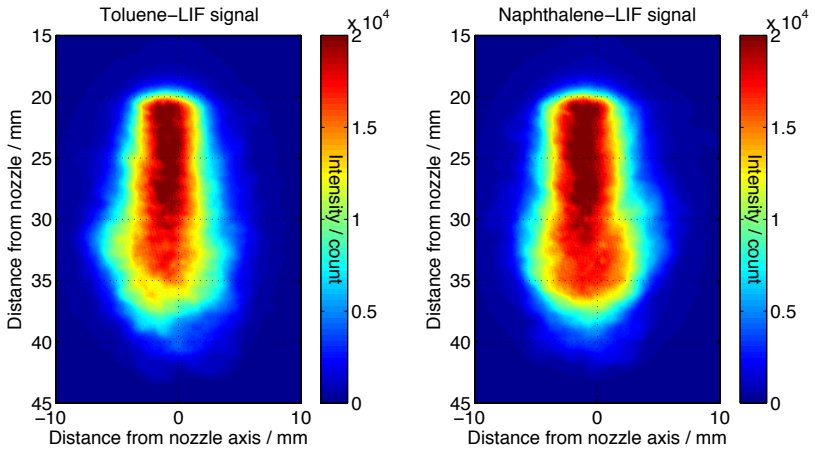

Figure 5-6: LIF images (ensemble-averaged from 20 images) obtained with dodecane with 9.8 vol.% toluene and 0.2 vol.% naphthalene, for excitation at 266 nm, at 600 K and 0.46 bar O_2 partial pressure. Left: LIF signal of toluene (BP292/27). Right: LIF signal of naphthalene (BP340/26).

Optimization of laser fluence

The laser fluence was also adjusted to optimize the signal-to-noise ratio while remaining in the linear excitation regime. Linearity tests were performed as described in Chapter 4 in N_2 at 3 bar and for a chamber temperature of 453 K (corresponding to the minimum temperature in the electrically-heated cell without pre-combustion). Fuel-tracer mixtures were injected 20 s prior to image acquisition, allowing enough time for creating a spatially homogeneous mixture within the cell. Toluene (BP292/27) and naphthalene (BP340/26) LIF-intensities were measured with 248- and 266-nm excitation as a function of fluence (Figure 5-7).

The linearity curves for toluene and naphthalene are shown in Figure 5-8 for laser excitation at 248nm (left) and 266 nm (right). To maximize LIF signals, the highest value of laser fluence was employed while ensuring that measurements were performed in the linear fluorescence regime for both tracers. In the present experiment, the selected laser fluence was 98 and 39 mJ/cm^2 for laser excitation wavelengths corresponding to 248 and 266 nm, respectively.

For a same concentration of tracer in the cell, the LIF signals behavior of toluene and naphthalene change with the laser excitation wavelength (Figure 5-8). Same LIF signal level for toluene and naphthalene and same saturation level were observed at 266 nm. However, the LIF signal of naphthalene was lower than toluene at 248 nm and the naphthalene LIF reaches saturation for higher fluence compared to toluene.

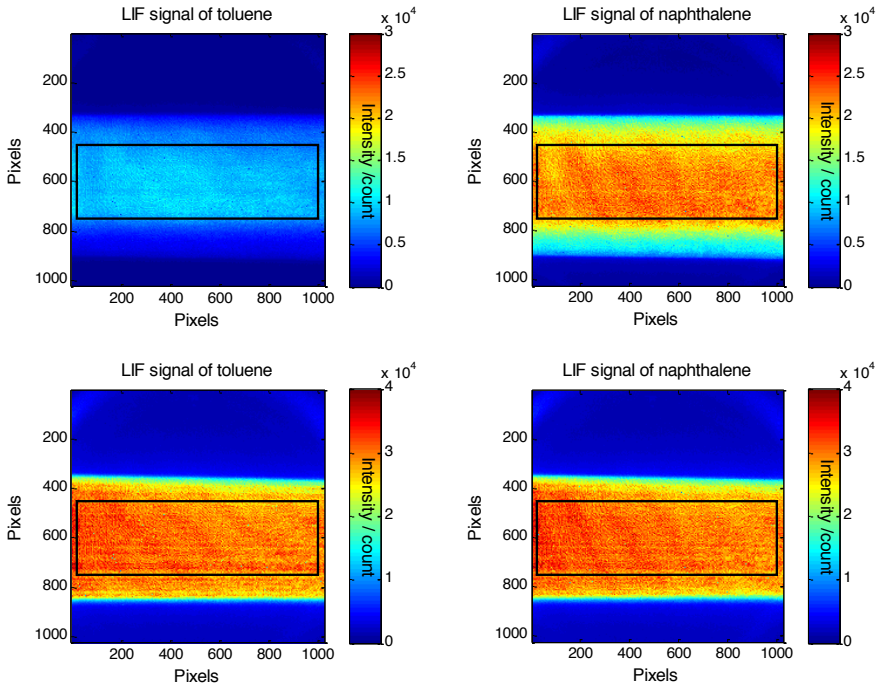

Figure 5-7: LIF images (ensemble-averaged from 30 single-shot images) of a spatially homogeneous distribution of the dodecane/toluene/naphthalene mixture in N_2 at 3 bar and 453 K, for laser excitation at 248 nm (upper row) and 266 nm (lower row), for a laser fluence of 177 mJ/cm^2. Optical filters: BP292/27 (toluene) and BP340/26 (naphthalene). The black square marks the region of interest.

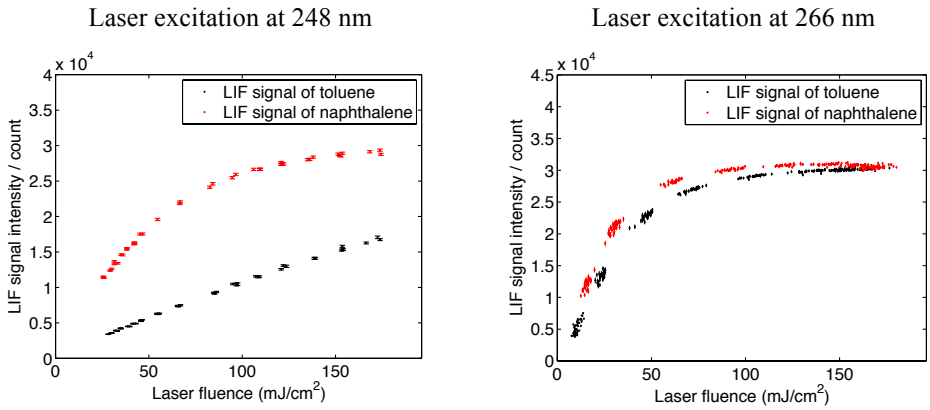

Figure 5-8: Fluence dependence of the toluene- and naphthalene-LIF signal intensity for the two-tracer mixture for laser excitation at 248 nm (left) and 266 nm (right) in N_2 at 3 bar and 453 K with detection at the emission peaks of toluene (BP292-27) and naphthalene (BP340-26).

Cell conditions

The high-pressure high-temperature cell described in Chapter 4 was used to evaluate the performance of the two-tracer three-color LIF technique. The main objective was to quantify the effects of temperature and O_2 partial pressure on the toluene- and naphthalene-LIF signals. An ambient bulk gas density of 22.8 kg/m^3 was used for all the tests requiring pre-combustion to reach the target temperature and pressure conditions. All core temperatures, pressures and O_2 partial pressures used are given in Table

5-2. A single-hole (90 μm diameter) Bosch common-rail Diesel injector was mounted in the top plate of the cell directing the fuel jet downwards into the center of the chamber.

Table 5-2: Conditions investigated in the high-pressure high-temperature cell.

		O_2 mole fraction	**0.01**	**0.05**	**0.1**	**0.15**	**0.21**
Toluene LIF emission peak Bandpass filter BP280/20 Laser excitation at 248 nm	T = 600 K	O_2 partial pressure (bar)	0.42	2.08	4.13	6.15	8.54
	p = 41 bar	Number of LIF images	5	5	20	20	5
	T = 650 K	O_2 partial pressure (bar)	0.46	2.26	4.49	6.68	9.27
	p = 45 bar	Number of LIF images	5	5	5	5	5
	T = 700 K	O_2 partial pressure (bar)	0.49	2.44	4.84	7.21	10.00
	p = 48 bar	Number of LIF images	5	5	5	5	5
	T = 750 K	O_2 partial pressure (bar)	-	-	5.20	-	-
	p = 52 bar	Number of LIF images	-	-	5	-	-
Toluene LIF emission peak Bandpass filter BP292/27 Laser excitation at 266 nm	T = 600 K	O_2 partial pressure (bar)	0.42	2.08	4.13	6.15	8.54
	p = 41 bar	Number of LIF images	20	20	5	5	5
	T = 650 K	O_2 partial pressure (bar)	0.46	2.26	4.49	6.68	9.27
	p = 45 bar	Number of LIF images	5	5	5	5	5
	T = 700 K	O_2 partial pressure (bar)	0.49	2.44	4.84	7.21	10.00
	p = 48 bar	Number of LIF images	5	5	5	5	5
	T = 750 K	O_2 partial pressure (bar)	-	-	5.20	-	10.74
	p = 52 bar	Number of LIF images	-	-	5	-	5
Naphthalene LIF emission peak Bandpass filter BP335/07 Laser excitation at 266 nm	T = 600 K	O_2 partial pressure (bar)	0.42	2.08	4.13	6.15	8.54
	p = 41 bar	Number of LIF images	5	20	5	5	5
	T = 650 K	O_2 partial pressure (bar)	0.46	2.26	4.49	6.68	9.27
	p = 45 bar	Number of LIF images	5	5	5	5	5
	T = 700 K	O_2 partial pressure (bar)	0.49	2.44	4.84	7.21	10.00
	p = 48 bar	Number of LIF images	5	5	5	5	5
	T = 750 K	O_2 partial pressure (bar)	-	-	5.20	-	10.74
	p = 52 bar	Number of LIF images	-	-	5	-	5
Naphthalene LIF emission peak Bandpass filter BP340/12 Laser excitation at 266 nm	T = 600 K	O_2 partial pressure (bar)	0.42	2.08	4.13	6.15	8.54
	p = 41 bar	Number of LIF images	5	5	5	5	10
	T = 650 K	O_2 partial pressure (bar)	0.46	2.26	4.49	6.68	9.27
	p = 45 bar	Number of LIF images	5	5	5	5	10
	T = 700 K	O_2 partial pressure (bar)	0.49	2.44	4.84	7.21	10.00
	p = 48 bar	Number of LIF images	5	5	5	5	10
	T = 750 K	O_2 partial pressure (bar)	-	-	5.20	-	10.74
	p = 52 bar	Number of LIF images	-	-	5	-	5
Naphthalene LIF emission peak Bandpass filter BP340/26 Laser excitation at 266 nm	T = 600 K	O_2 partial pressure (bar)	0.42	2.08	4.13	6.15	8.54
	p = 41 bar	Number of LIF images	20	20	5	5	5
	T = 650 K	O_2 partial pressure (bar)	0.46	2.26	4.49	6.68	9.27
	p = 45 bar	Number of LIF images	5	5	5	5	5
	T = 700 K	O_2 partial pressure (bar)	0.49	2.44	4.84	7.21	10.00
	p = 48 bar	Number of LIF images	5	5	5	5	5
	T = 750 K	O_2 partial pressure (bar)	-	-	5.20	-	10.74
	p = 52 bar	Number of LIF images	-	-	5	-	5
Naphthalene LIF emission long wave-length rang Bandpass filter BP370/36 Laser excitation at 266 nm	T = 600 K	O_2 partial pressure (bar)	0.42	2.08	4.13	6.15	8.54
	p = 41 bar	Number of LIF images	5	20	5	5	5
	T = 650 K	O_2 partial pressure (bar)	0.46	2.26	4.49	6.68	9.27
	p = 45 bar	Number of LIF images	5	5	5	5	5
	T = 700 K	O_2 partial pressure (bar)	0.49	2.44	4.84	7.21	10.00
	p = 48 bar	Number of LIF images	5	5	5	5	5
	T = 750 K	O_2 partial pressure (bar)	-	-	5.20	-	10.74
	p = 52 bar	Number of LIF images	-	-	5	-	5
Naphthalene LIF emission long wave-length range Bandpass filter BP376/20 Laser excitation at 266 nm	T = 600 K	O_2 partial pressure (bar)	0.42	2.08	4.13	6.15	8.54
	p = 41 bar	Number of LIF images	15	15	10	5	10
	T = 650 K	O_2 partial pressure (bar)	0.46	2.26	4.49	6.68	9.27
	p = 45 bar	Number of LIF images	5	5	5	5	5
	T = 700 K	O_2 partial pressure (bar)	0.49	2.44	4.84	7.21	10.00
	p = 48 bar	Number of LIF images	5	5	5	5	5
	T = 750 K	O_2 partial pressure (bar)	-	-	5.20	-	10.74
	p = 52 bar	Number of LIF images	-	-	5	-	5

Injection conditions

The two-tracer fuel mixture (dodecane with 9.8 vol.% toluene and 0.2 vol.% naphthalene) was injected at a rail pressure of 1200 bar. An injection duration of 1 ms and a delay time of 1.5 ms (corresponding to the delay between the injector trigger signal and image acquisition) were selected to ensure that the fuel vapor cloud penetrated sufficiently within the cell for it to be excited by the full height of the laser sheet and that no liquid fuel was present in the zone illuminated by the laser sheet.

5.2.3 Image post-processing

Background images (ensemble-averaged from three single-shot images) were subtracted from single-shot LIF images, which were then normalized to the laser-pulse energy (simultaneously recorded during image acquisition) to correct for laser fluctuations. For the seven bandpass filters that were tested, the four ambient temperatures and five O_2 partial pressures investigated in the high-pressure high-temperature cell, five single-shot LIF images were acquired (cf. Table 5-2). The acquisition of a single-shot LIF image at fixed ambient conditions required pre-combustion of the ambient gas mixture to reach high-pressure and high-temperature conditions which were a time consuming process taking into account the number of parameter variations that were investigated. Therefore, only five images were acquired for each test condition, which was a necessary trade-off and enabled investigation of the large number of test conditions. From a statistics point of view the acquisition of only five LIF images was a limiting factor (cf. Section 5.2.4) for the ensemble-average based analysis that was performed. A higher number of LIF images (up to twenty single-shot images) were acquired for a selected number of conditions (cf. Table 5-2) in order to assess the influence of sample number on LIF image shot-to-shot fluctuations and determined the required sample number to ensure convergence of a cumulative average (described in detail in Section 5.3.1).

The LIF signal was acquired in the vapor phase in a region of the jet where LIF signal-to-noise was sufficiently high and characterized by low shot-to-shot image fluctuations for a given experimental condition. The region of interest (ROI), black rectangle in Figure 5-9) was carefully selected. The ensemble-averaged image (left in Figure 5-9) was used to optimize the position of the ROI to ensure sufficient signal-to-noise, while the corresponding LIF image of the relative standard deviation for the 20 single-shot images (right in Figure 5-9) was used to quantify shot-to-shot fluctuations. In the present work, the LIF signal was investigated by determining the mean value of the LIF signal in the ROI for all single-shot LIF images acquired.

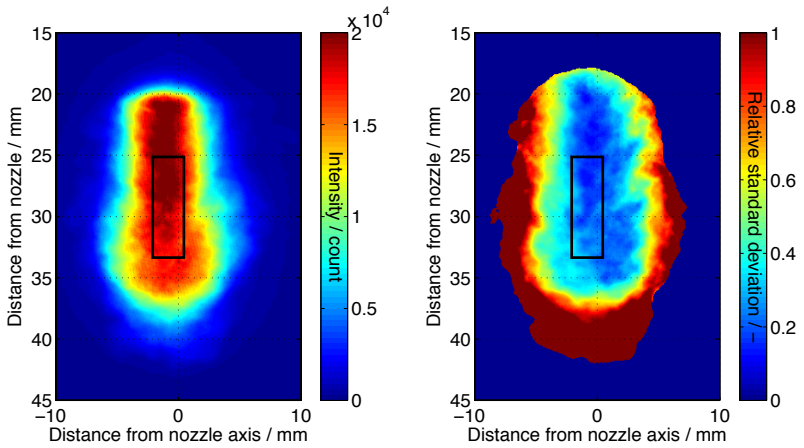

Figure 5-9: LIF images acquired near the emission peak of toluene (BP292-27) at 600 K and 0.46 bar O_2 partial pressure. Left: Ensemble-averaged from 20 single-shot LIF images. Right: Relative standard deviation from 20 single-shot images obtained by calculating the ratio between the standard deviation image and the ensemble-averaged image.

5.2.4 Study of the experimental sensitivity (fluctuations)

Because of the turbulent nature of the jet, the fuel concentration and temperature distribution inside the vaporized jet were, however, not strictly identical for consecutive experiments, resulting in shot-to-shot fluctuations between LIF images. These fluctuations were quantified by calculating the relative mean value in the ROI (black rectangle in Figure 5-9) for all single shot-to-shot LIF images (Figure 5-10). The relative mean value was defined as the ratio between the mean value calculated in the ROI to the average of all mean values obtained for the series of LIF images acquired under identical experimental conditions (i.e., comparable bandpass filters, temperatures, and O_2 partial pressures). The majority of the data are distributed around unity and within a maximum variation of ±60%.

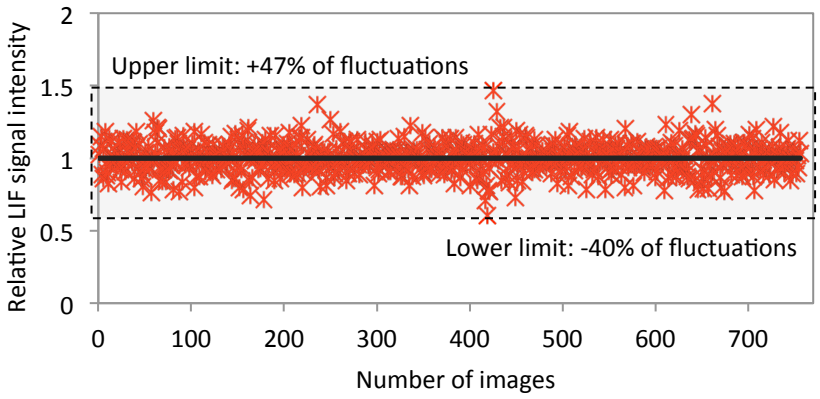

Figure 5-10: Relative mean value over the ROI (cf. Figure 5-9) for all single-shot images. The relative mean value is defined as the ratio of the mean value over the ROI and the averaged mean value for LIF single-shot images obtained under identical conditions.

The histogram of all relative mean values obtained in the present experiment (Figure 5-11) also shows the distribution of the data around unity and a 2σ standard deviation at 20% providing information on shot-to-shot fluctuations between the LIF images, which was assumed to correspond to the single LIF signal measurement relative uncertainty in the present experiment.

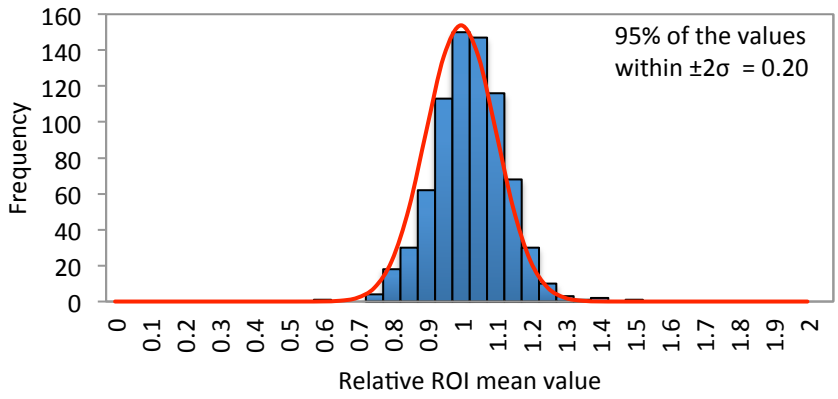

Figure 5-11: Histogram of the relative mean value of the LIF signal (for the ROI shown in Figure 5-9) for all LIF single-shot images acquired.

To determine the impact of the size of the ROI size its dimensions were varied (Figure 5-12). The histogram of the relative mean values calculated in the smaller ROI shown in Figure 5-13 reveals a comparatively high 2σ standard deviation (80%), which confirmed that there was no benefit of reducing the ROI size compared to the initial ROI size shown in Figure 5-9.

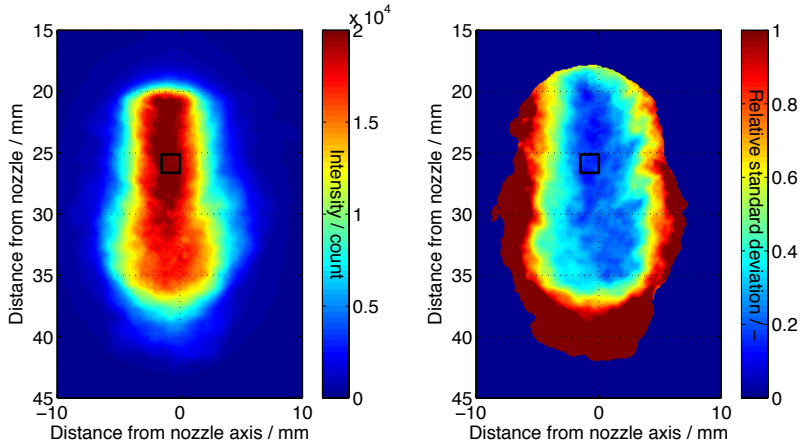

Figure 5-12: LIF images showing reduced ROI size acquired near the emission peak of toluene (optical filter BP292-27) at 600 K and 0.41 bar O_2 partial pressure. Left: LIF image ensemble-averaged from 20 single-shot images. Right: Relative standard deviation image over 20 single-shot images obtained by calculating the ratio between the standard deviation image and the ensemble-averaged image.

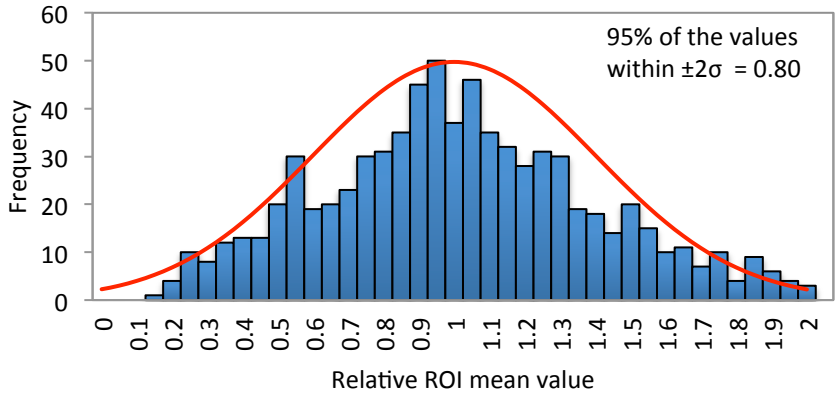

Figure 5-13: Histogram of the relative mean value of the LIF signal for the smaller ROI size (illustrated in Figure 5-12) for all LIF single-shot images acquired.

In the present work, at least five single-shot LIF images were acquired at each experimental condition investigated and up to 20 single-shot images were acquired for a selected number of experimental conditions (Table 5-2). The cumulative relative mean value in the ROI (illustrated in Figure 5-9) was calculated for 20 single-shot LIF images acquired at a given experimental condition in an attempt to determine the required sample number to perform a robust ensemble-averaged analysis. The cumulative relative mean values reveal convergence for a sample of number between 15 and 20 single-shot images (Figure 5-14). The acquisition of a sample number greater than 20 single-shot images might have enabled a conclusion to be made on the minimum sample number required for each experimental condition investigated.

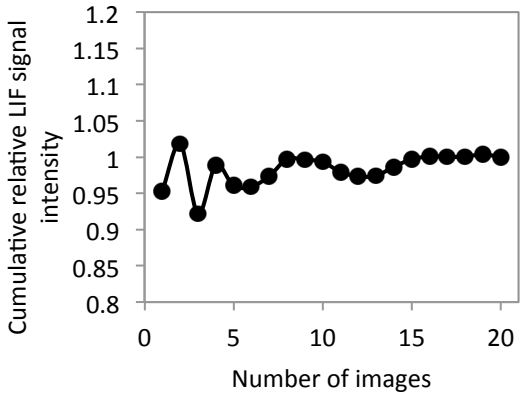

Figure 5-14: Cumulative relative LIF signal calculated in the ROI illustrated in Figure 5-9 for LIF images obtained at 600 K and 0.41 bar O_2 partial pressure with laser excitation at 266 nm and for the collection filter BP292-27.

5.3 Results and discussion

5.3.1 Determination of LIF signal measurement uncertainty

The LIF signal was calculating by averaging the mean value of the LIF signal in the ROI (Figure 5-9) for all single-shot LIF images acquired under identical experimental conditions (i.e., bandpass filters, temperatures, and O_2 partial pressures). The uncertainty of the LIF signal measurement (ΔI_{LIF}) was defined as the standard uncertainty for a level of confidence of 95%:

$$\Delta I_{\mathrm{LIF}} = \frac{2\sigma}{\sqrt{N}} \tag{5.1}$$

with σ the standard deviation and N the number of single-shot LIF images used for the averaging (Table 5-2).

For the application of the two-tracer three-color LIF technique, LIF ratios are calculated with the LIF signals measured on the three spectral ranges (collection filters 1, 2 and 3 in Figure 5-1) to determine temperature and O_2 partial pressure. A general definition of the LIF ratio is given by the following equation with LIF signal $I^{\mathrm{a}}_{\mathrm{LIF}}$ and $I^{\mathrm{b}}_{\mathrm{LIF}}$ collected in two distinct spectral ranges:

$$R_{\mathrm{LIF}} = \frac{I^{\mathrm{a}}_{\mathrm{LIF}}}{I^{\mathrm{b}}_{\mathrm{LIF}}} \tag{5.2}$$

The LIF signal ratio measurement uncertainty (ΔR_{LIF}) was obtained from the propagation of the LIF signal (ΔI_{LIF}) using the following equation:

$$\Delta R_{\mathrm{LIF}} = R_{\mathrm{LIF}} \sqrt{\left(\frac{\Delta I^{\mathrm{a}}_{\mathrm{LIF}}}{I^{\mathrm{a}}_{\mathrm{LIF}}}\right)^2 + \left(\frac{\Delta I^{\mathrm{b}}_{\mathrm{LIF}}}{I^{\mathrm{b}}_{\mathrm{LIF}}}\right)^2} \tag{5.3}$$

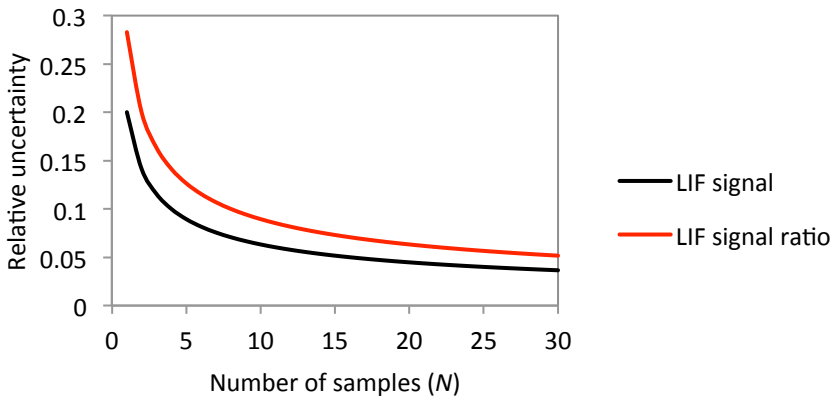

Figure 5-15: Dependence of the relative uncertainty (2σ) with the number of single-shot LIF images for the ensemble-averaged analysis. Relative uncertainty of the LIF signal (black line) and the LIF signal ratio (red line).

Figure 5-15 shows the dependence of the relative measurement uncertainty of the LIF signal ($\Delta I_{LIF}/I_{LIF}$) and the LIF signal ratio ($\Delta R_{LIF}/R_{LIF}$) on the number of single-shot LIF images used for

the ensemble-averaged analysis. The single LIF signal relative measurement uncertainty was evaluated at 20% (Figure 5-11) and the relative uncertainty of the LIF signal for higher number of single-shot LIF images was calculated with equation (5.1). The relative uncertainty of the LIF signal ratio was then derived using eq. (5.2). The relative uncertainties of the LIF signal and the LIF signal ratio were halved by increasing the number of single-shot LIF images from 5 to 20 for the ensemble-averaged analysis. For the majority of the measurements, 5 single-shot LIF images were acquired at each experimental condition investigated. The results in the following sections therefore will be presented with an uncertainty evaluated for 5 samples ($N = 5$).

5.3.2 Temperature dependence

In the present work, the temperature measurement was based on the red-shift of the naphthalene-LIF signal with increasing temperature (cf. Section 5.1.1) for 266 nm laser excitation. The LIF signal was detected in two distinct spectral bands (collection filter 2 and 3 in Table 5-1) which ratio depends on temperature. The naphthalene-LIF signal in the 320–350 nm range (near the emission peak) was collected by the bandpass filters BP335/07, BP340/12, and BP340/26 and in the 350–390 nm spectral range by the bandpass filters BP370/30 and BP376/20 filters.

The temperature dependence of the naphthalene-LIF signal ratio was investigated in the high-pressure high-temperature cell for O_2 mole fraction of the ambient gas varying between 0.01 and 0.21 at total pressures in the 41–52 bar range (i.e., for O_2 partial pressures in the 0.5–9.6 bar range). The naphthalene-LIF signal ratio (calculated as described in Section 5.3.1) increases with increasing temperature for all pair of bandpass filters investigated (Figure 5-16) and for all O_2 partial pressures, confirming that the red-shift of the naphthalene-LIF signal depends on temperature.

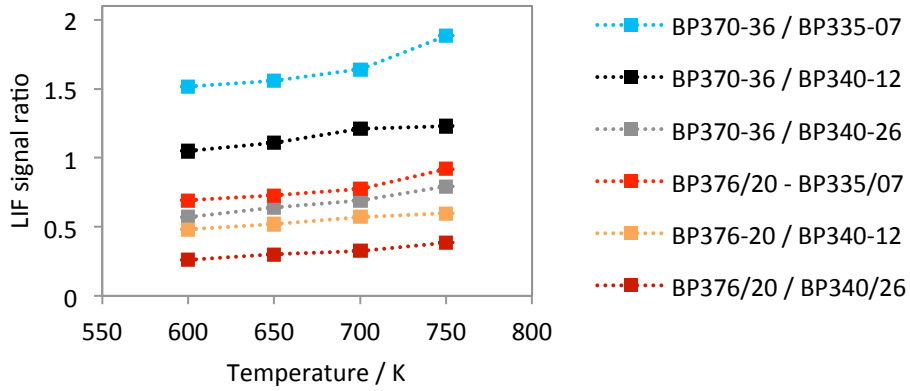

Figure 5-16: Temperature dependence of the naphthalene-LIF signal ratio measured in the vaporized jet in the 600–750 K temperature range at ambient pressures varying between 41 and 52 bar, O_2 partial pressure of 9.6 bar, and for various bandpass filter pairs.

The naphthalene-LIF signal ratio measured in the vaporized jet did not reveal any notable dependence on O_2 partial pressure for the range of temperatures investigated (Figure 5-17, right). The investigation

of the naphthalene-LIF signal in Chapter 3 showed a red-shift of the LIF spectra with increasing O_2 partial pressure with a saturation of the effect above 0.1 bar. Since the naphthalene-LIF signal characterizes the red-shift of the LIF spectra, the naphthalene-LIF signal ratio was expected to be independent of O_2 partial pressures above 0.1 bar. In the present experiment, a clear constant behavior of the LIF signal ratio for O_2 partial pressures varying in the 0.5–9.6 bar range (in the 600–750 K temperature range) could not be measured since the sensitivity of the detection system (using subsequently recorded averaged individual measurements for the respective bandpass channels) was not sufficient to avoid high statistical errors. The limited sensitivity of the detection system was mainly due to the use of a single CCD camera for detection of the naphthalene-LIF signal at distinct spectral bands that required an evaluation of averaged information from not directly correlated measurements. In addition, the low number of samples ($N = 5$) did not allow to perform a robust ensemble-averaged analysis. Although a temperature dependence of the LIF signal ratio was detected (Figure 5-17, left), the variability of the LIF signal ratio with O_2 partial pressure prevented the naphthalene-LIF thermometry from providing any reliable quantitative temperature measurement in the present experiments. However, these preliminary results reveal the potential of the naphthalene-LIF thermometry at high temperatures (in the 600–750 K range) and high O_2 partial pressures (in the 0.5–9.6 bar range) from simultaneously acquired LIF image pairs from two spectral bands (i.e., with two cameras simultaneously) to improve the overall precision of the measurements.

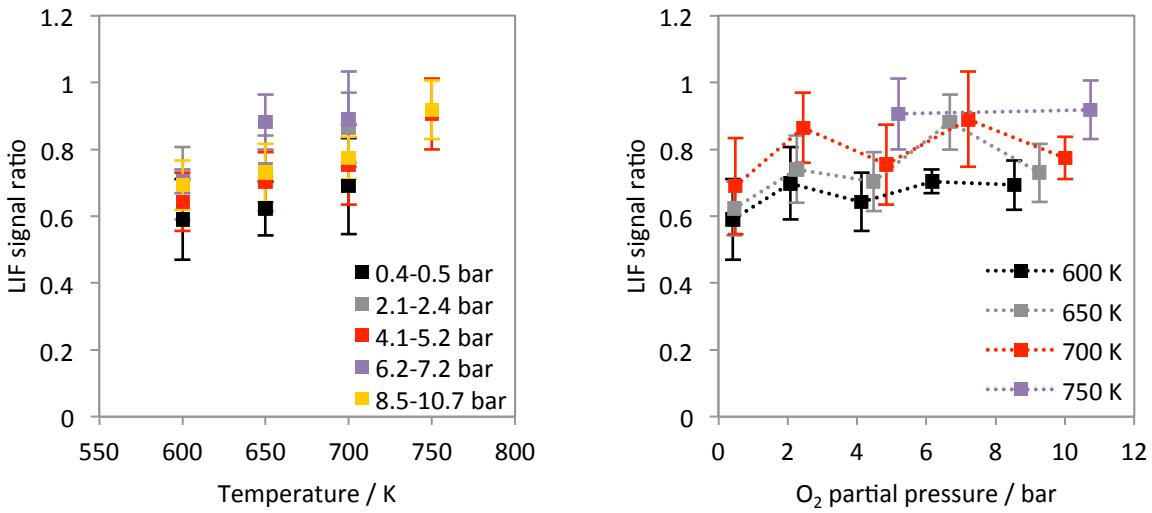

Figure 5-17: Naphthalene-LIF signal ratio measured in the vaporized jet with the bandpass filter pair BP376-20/BP335-07. Left: Temperature dependence of naphthalene-LIF ratio for various O_2 partial ranges in the 0.4–10.7 bar range. Right: Dependence of the naphthalene-LIF signal ratio on O_2 partial pressure for temperatures in the 600–750 K range.

The behavior of the naphthalene-LIF signal ratio with temperature and O_2 partial pressure was investigated with the naphthalene-LIF spectra measured in previous work [78] for 266 nm laser excitation.

Based on peak-normalized fluorescence spectra (Figure 5-18, left), the temperature dependence of the naphthalene-LIF ratio (Figure 5-18, right) was calculated for the respective optical filters (Table 5-1) using their transmission characteristics shown in Figure 5-4. However, this investigation of naphthalene-LIF spectra is limited to O_2 partial pressures below 0.21 bar (Figure 5-19) and the measurements in the high-pressure high-temperature cell (in the 0.5–9.6 bar) could not be directly compared with the results of naphthalene-LIF spectra [78] (i.e. in the 0–0.17 bar O_2 partial pressure range). The LIF signal ratio increases when the temperature is increased, i.e., from 0.59 at 600 K to 0.92 at 750 K at high O_2 partial pressure (in the vaporized jet). At low O_2 partial pressure (investigated with LIF spectra) the LIF signal ratio increases from 0.48 to 0.70 at 0 bar O_2 partial pressure (in nitrogen) and from 0.62 to 0.99 at 0.17 bar O_2 partial pressure by increasing the temperature from 600 to 750 K. The variation of the LIF-signal ratio at low O_2 partial pressures (i.e., 47% at 0 bar O2 partial pressure and 60% at 0.17 bar O2 partial pressure) are comparable to the variation measured at higher O_2 partial pressures (i.e., 56% in the 0.5–9.6 bar O_2 partial pressure range) between 600 and 750 K. The temperature dependence observed at low O_2 partial pressures was maintained at higher O_2 partial pressures.

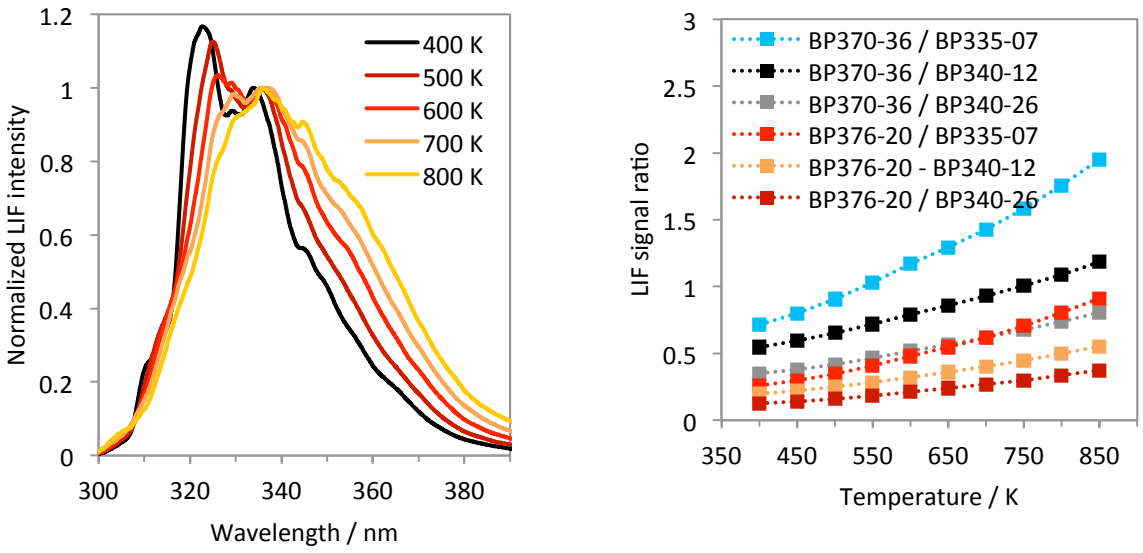

Figure 5-18: Two-color naphthalene-LIF thermometry for 266-nm excitation in N_2. Dependence of the naphthalene-LIF signal ratio on temperature (right) based on peak-normalized fluorescence spectra [78] given per unit number density of naphthalene in N_2 for various temperatures (left). Collection filters: BP370/36, BP376/20 (in the 320–350 nm range, near the emission peak) and BP335/07, BP340/12, and BP340/26 (in the 350–390 nm spectral range).

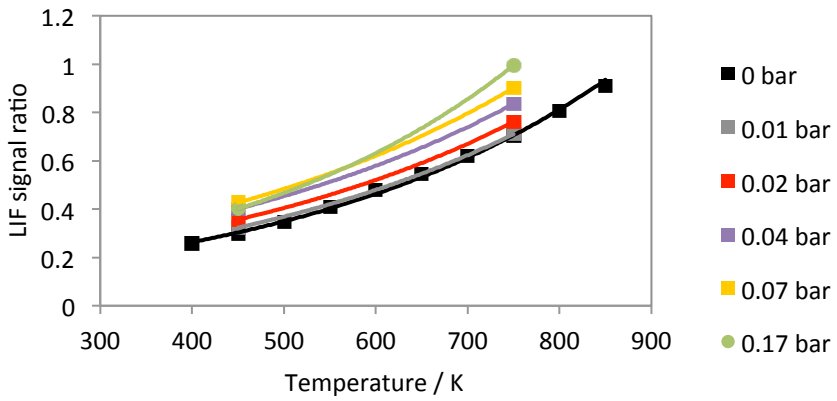

Figure 5-19: Dependence of the naphthalene-LIF signal ratio on O_2 partial pressure for 400–850 K with the bandpass filter pair BP376-20/BP335-07.

5.3.3 O_2 partial-pressure dependence

The two-tracer three-color LIF technique using toluene and naphthalene can be used for measuring O_2 partial pressure by exploiting the different sensitivity of the two tracers on O_2 quenching (cf. Chapter 2 and 3). The ratio of the LIF signal collected around the emission peaks of the two tracers depends on O_2 partial pressure and also on temperature. The temperature can be measured by two-color LIF thermometry using naphthalene (cf. Section 5.3.2).

Photophysical measurements on toluene and naphthalene in previous work [25,72,85, 87,88] resulted in a description of toluene and naphthalene LIF spectra and effective fluorescence lifetimes over a wide range of temperature, pressure, and O_2 partial pressure. In addition, semi-empirical photophysical models were developed and validated using these fluorescence data [25,72,85, 87,88]. However, this investigation of LIF signals is limited to O_2 partial pressure below 2.1 bar. In the present work, the models [25,72,85, 87,88] predicting the toluene and naphthalene-LIF signals were – as a zeroth-order approach to comparing experimental and simulated data – extrapolated to higher O_2 partial pressure (up to 11 bar) and the measurements in the high-pressure high-temperature cell were used to compare with the results of the extrapolated models.

Toluene-LIF signal

The dependence of the toluene-LIF signal on O_2 partial pressure was investigated in the high-pressure high-temperature cell for 248- and 266-nm excitation and for ambient temperatures in the 600–700 K range. The O_2 mole fraction of the ambient gas was varied between 0.01 and 0.21 at total pressures in the 41–52 bar range which enabled an investigation of the toluene-LIF signal (measured in the vaporized jet) for O_2 partial pressures in the 0.5–11 bar range. The toluene-LIF signal (as described in Figure 5-9) decreases with increasing O_2 partial pressure for all temperatures investigated (Figure 5-20), confirming that toluene is strongly affected by collisional quenching by O_2. Figure 5-20 shows a rela-

tively weak temperature dependence that should be examined in future experiments and modeling efforts.

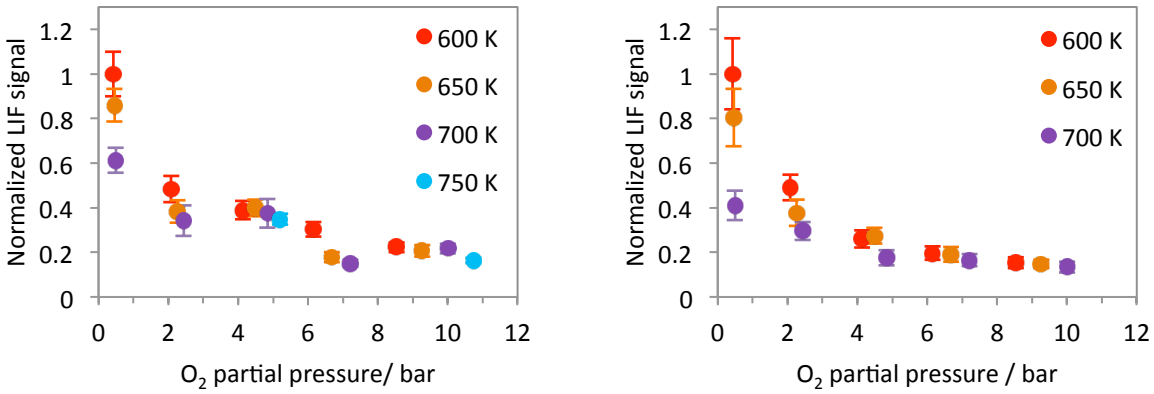

Figure 5-20: Dependence of the toluene-LIF signal on O_2 partial pressure measured in the vaporized jet in the 600–750 K temperature range at ambient pressures varying between 41 and 52 bar. LIF signal normalized to the signal intensity obtained for the minimum O_2 partial investigated (0.5 bar) at 600 K. Left: 266-nm excitation, bandpass filter BP292/27. Right: 248-nm excitation, bandpass filter BP280/20.

The dependence of the toluene-LIF signal (measured in the vaporized jet) on O_2 partial pressure was compared to data from previous work [25,72,85,88] in the 580–730 K temperature range. Faust et al. [85,88] measured toluene-LIF lifetimes with 266-nm excitation and for O_2 partial pressures from 0 to 2.1 bar (Figure 5-21). With the LIF lifetime being proportional to the fluorescence quantum yield (cf. Chapter 3), the expected toluene-LIF signal (Figure 5-22) was calculated from LIF-lifetime measurements [85,88] by correcting for the absorption cross-section which varies with temperature [25,72]. A model developed by Koban et al. [25,72] enabled the prediction of toluene-LIF signal intensities for O_2 partial pressures in the range 0 to 2.1 bar and for excitation at 266 nm (Figure 5-22) and 248 nm (Figure 5-23). For 266-nm excitation, the model [25,72] reveals good agreement with the toluene-LIF signal based on LIF-lifetime measurements [85,88] for 580–630 K although discrepancies are observed for temperatures above 680 K (Figure 5-22). Therefore, the data from previous work [25,72,85,88] was used exclusively for a comparison at a temperature of 580 K (Figure 5-24 and Figure 5-25) which corresponds to an ambient temperature of 600 K within the cell during injection since the temperature in the central zone of the jet is approximately 20–30 K lower (cf. Section 4) compared to the average gas temperature within the cell.

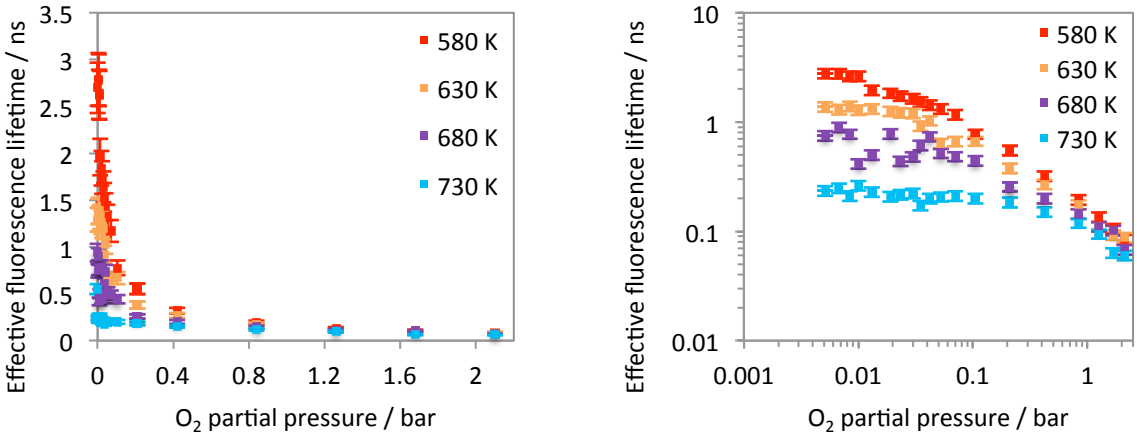

Figure 5-21: Dependence of toluene-LIF lifetimes on O_2 partial pressure at 580–730 K with 266-nm excitation [85,88].

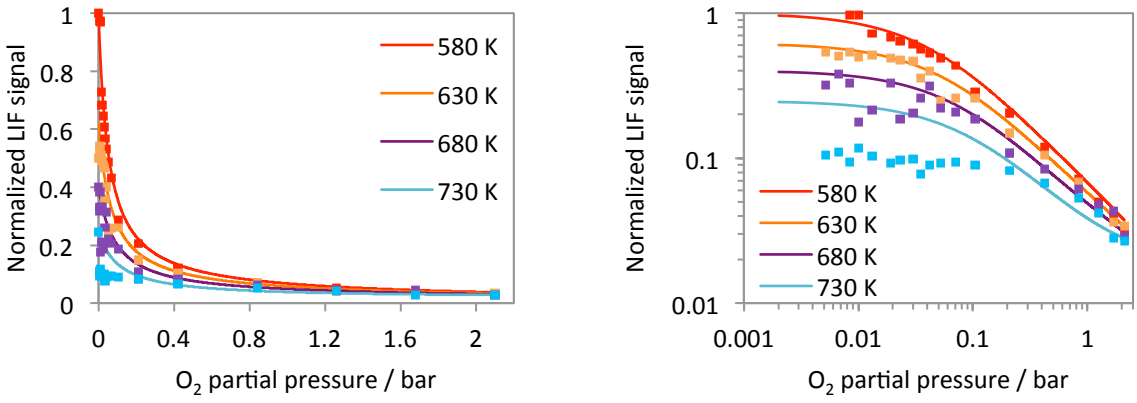

Figure 5-22: Dependence of the toluene-LIF signal (per unit number density) on O_2 partial pressure for 580–730 K and 266-nm excitation. Toluene-LIF signal is normalized to the intensity obtained in N_2 at 580 K. Lines: Koban model [25,72]. Points: derived from LIF-lifetimes measurements [85,88].

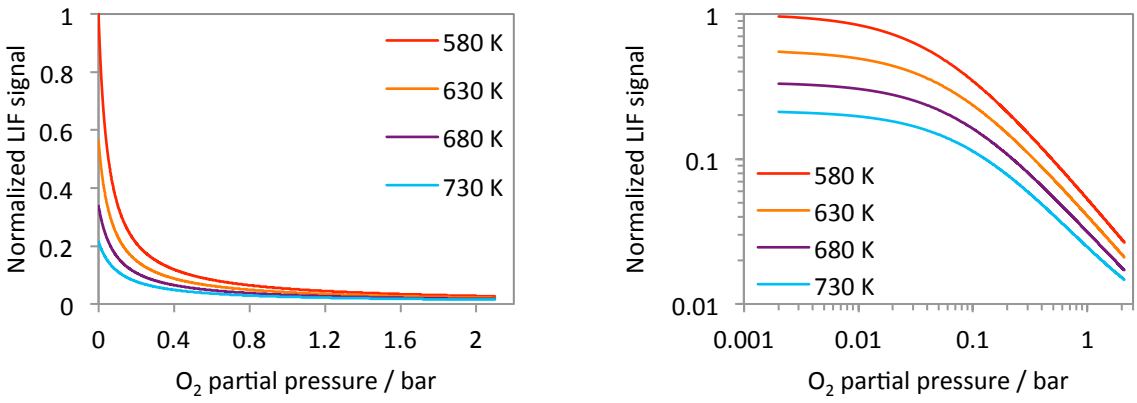

Figure 5-23: Dependence of the toluene-LIF signal (per unit number density) on O_2 partial pressure at 580–730 K and 248-nm excitation (Koban model [25,72]). Toluene-LIF signal normalized to the intensity obtained in N_2 at 580 K.

The toluene-LIF signal from previous work [25,72,85,88] was acquired up to a maximum O_2 partial pressure of 2.1 bar. In the high-pressure high-temperature cell, toluene-LIF measurements in the jet were performed from 0.5 to 11 bar O_2 partial pressure. To enable a comparison of these data, the Koban model [25,72] was extrapolated to O_2 partial pressures up to 11 bar – far above its previously validated range (Figure 5-24 and Figure 5-25). The dependence of the toluene-LIF signal on O_2 partial pressure investigated in the vaporized jet reveals good agreement with the predictions using the extrapolated Koban model for both excitation wavelengths.

However, the toluene-LIF signal in the vaporized jet for the lowest O_2 partial pressure (0.5 bar) investigated in the high-temperature high-pressure cell was measured at a lower value than expected relatively to measurements at higher O_2 partial pressures (Figure 5-24 and Figure 5-25). It was possible to adjust the composition of the pre-combustion gases to obtain the desired O_2 mole fraction during fuel injection. At the time that these experiments were performed, however, it was not possible to work with pre-combustion gas mixtures that consume O_2 completely. The lowest achievable O_2 mole fraction was 0.01 which was difficult to control accurately and therefore resulted in high uncertainties (e.g., an uncertainty of ±0.01 in O_2 mole fraction corresponds to an uncertainty of ±0.4 bar for the O_2 partial pressure at 41 bar and 600 K).

The good agreement between measurements and extrapolated model predictions observed at higher O_2 partial pressures indicates that the simplification of the Koban model which neglects the effects of pressure on the relative fluorescence quantum yield [25,72] remains valid for higher O_2 partial pressures up to 11 bar. Even if O_2 quenching effect on the toluene-LIF signal appears to saturate at higher O_2 partial pressures (in the O_2 partial pressure 1–11 bar range), the influence of the total pressure appears to be negligible compared to the effect of O_2 quenching. The extrapolated Koban model well predicts the toluene-LIF signal at higher O_2 partial pressures up to 11 bar (in the temperature range of 580–680 K).

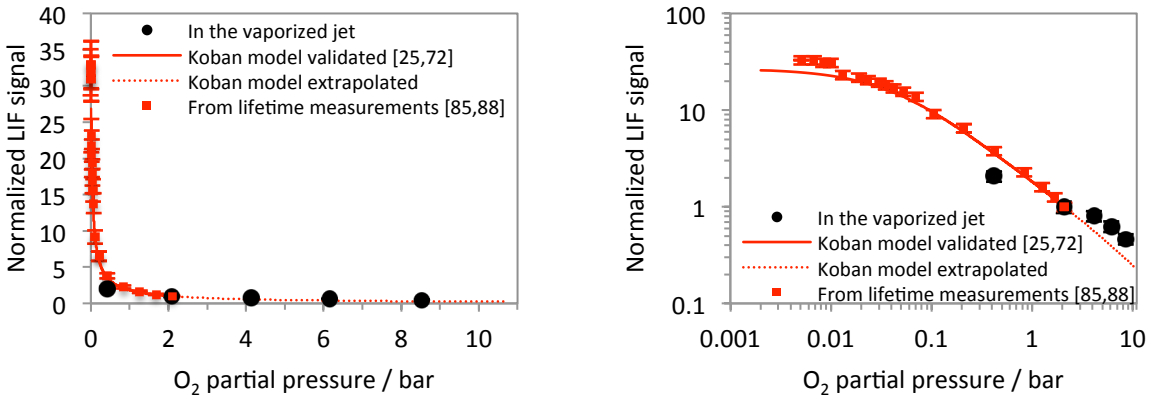

Figure 5-24: Dependence of the toluene-LIF signal on O_2 partial pressure in the vaporized jet at 600 K, 41 bar, and 266-nm excitation (black points). Comparison to the Koban model (solid lines) [25,72] and the extrapolated Koban model (dashed lines). Data based on fluorescence lifetime measurements [85,88] (red symbols). LIF signal normalized to the intensity at 2.1 bar O_2 partial pressure.

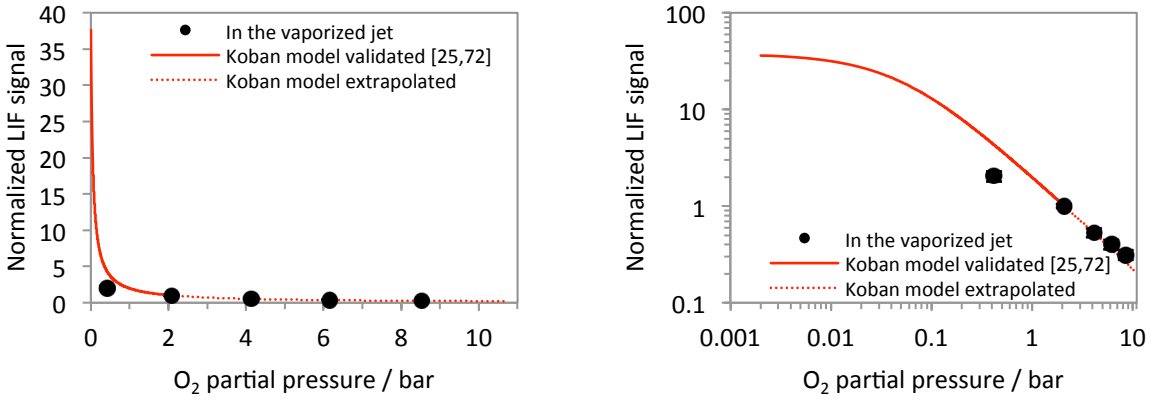

Figure 5-25: Dependence of the toluene-LIF signal on O_2 partial pressure in the vaporized jet at 600 K, 41 bar, and 248-nm excitation (black points). Comparison to the Koban model (solid lines) [25,72] and the extrapolated Koban model (dashed lines). LIF signal normalized to the intensity at 2.1 bar O_2 partial pressure.

Naphthalene-LIF signal

For naphthalene, similar investigations as for toluene were performed with 266-nm excitation. The naphthalene-LIF signal decreases with increasing O_2 partial pressure for all temperatures investigated (Figure 5-26), indicating that naphthalene LIF is strongly affected by collisional quenching by O_2. The naphthalene-LIF signal was not temperature dependent in the investigated range (Figure 5-26) except for the lowest O_2 partial pressure of 0.5 bar.

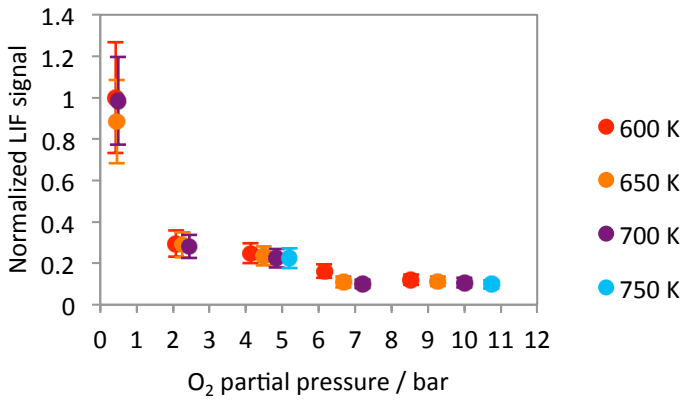

Figure 5-26: Dependence of the naphthalene-LIF signal on O_2 partial pressure at 600–750 K and 41–52 bar, 266-nm excitation, bandpass filter BP340/26. The LIF signal is normalized to the signal intensity obtained for the minimum O_2 partial investigated (0.5 bar) at 600 K.

The naphthalene-LIF signal measured in the jet does not depend on the bandpass filters (BP335/07, BP340/12, BP340/26) as shown in Figure 5-27 at 600 K and the same behavior was observed at higher temperatures (650, 700, and 750 K).

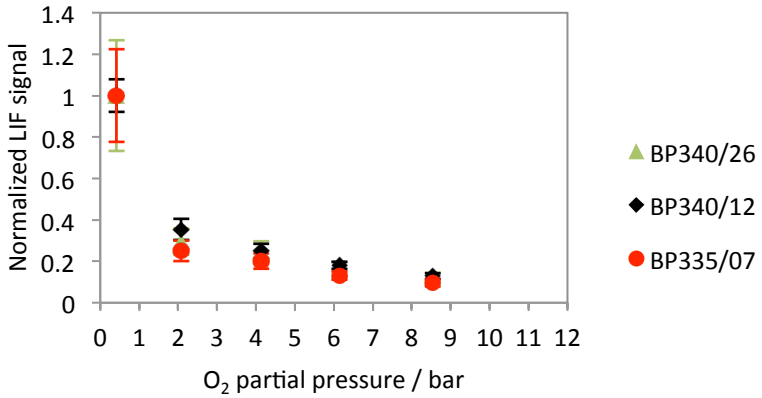

Figure 5-27: Dependence of the naphthalene-LIF signal on O_2 partial pressure at 600 K and 41 bar with 266-nm excitation. The LIF signal is normalized to the signal intensity obtained for the minimum O_2 partial investigated (0.5 bar). Comparison of the BP335/07, BP340/12, and BP340/26 bandpass filters.

The naphthalene-LIF signal measured in the vaporized jet over a range of O_2 partial pressures was compared to data from previous work [87,88] in the 580 to 730 K range. Faust et al. [87,88] measured naphthalene-LIF lifetimes (266-nm excitation) with O_2 partial pressures from 0 to 2.1 bar (Figure 5-28). With the LIF lifetime being proportional to the LIF quantum yield (cf. Chapter 3), the naphthalene-LIF signal (Figure 5-29) was obtained from lifetime measurements [87,88] by considering the absorption cross-section is constant with temperature [78]. A model developed by Faust et al. [87,88] allows to predict the naphthalene-LIF signal intensities for O_2 partial pressures between 0 and 0.21 bar and for 266-nm excitation (Figure 5-29). This model [87,88] was validated at 1 bar for O_2 partial pressures between 0 and 0.21 bar.

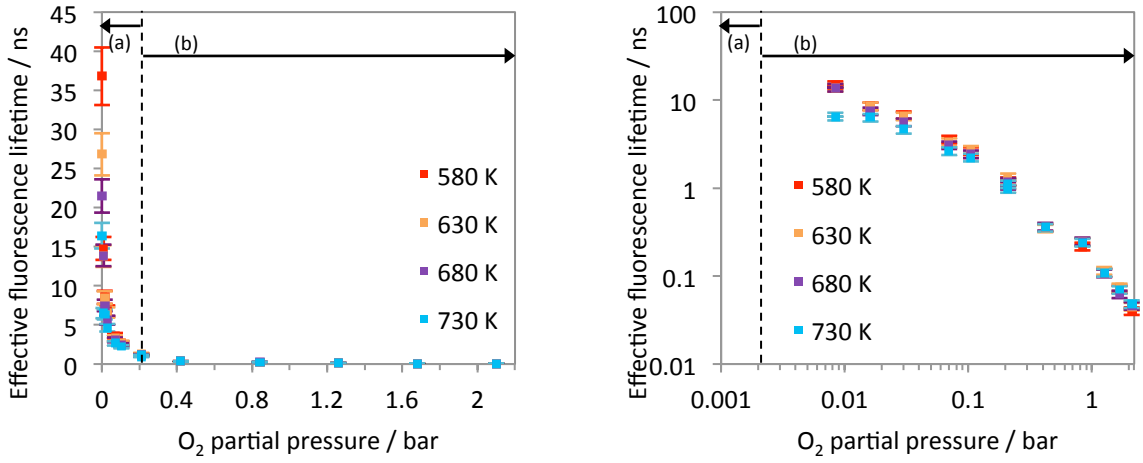

Figure 5-28: Dependence of the effective naphthalene-LIF lifetime on O_2 partial pressure for 580–730 K. Lifetime measurements obtained (a) at 1 bar by varying the amount of O_2 in N_2 [87] and (b) in air by varying the total pressure between 1 and 10 bar [88].

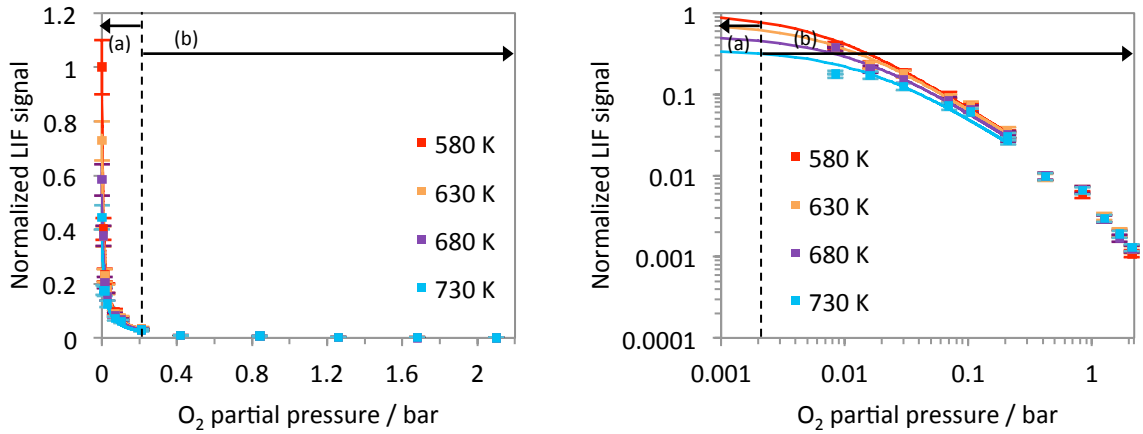

Figure 5-29: Dependence of the naphthalene-LIF signal (per unit number density) on O_2 partial pressure at 580–730 K and 266-nm excitation. Naphthalene-LIF signals are normalized to the intensity obtained in N_2 at 580 K. Lines: Faust model [87,88]. Symbols: Data based on fluorescence lifetime measurements [87,88]. Lifetime measurements obtained (a) at 1 bar by varying the amount of O_2 in N_2 [87] and (b) in air by varying the total pressure between 1 and 10 bar [88].

The naphthalene-LIF signal at 600 K was compared to results from model predictions [87,88] and to data from LIF-lifetime measurements at 580 K (Figure 5-30). To cover a comparable range of O_2 partial pressures as for the experiments, the model was extrapolated up to 11 bar. The normalized naphthalene-LIF signal intensities measured in the jet for O_2 partial pressures in the range 0.5 to 11 bar (i.e., O_2 mole fractions from 0.01 to 0.21 at total pressures from 41 to 52 bar) reveal a good agreement with the Faust model [87,88] (Figure 5-30).

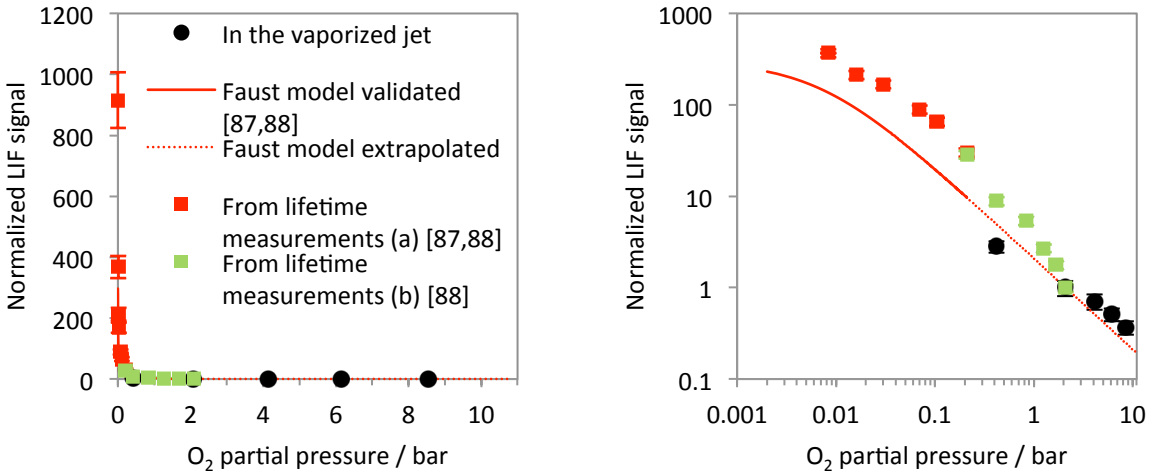

Figure 5-30: Dependence of the naphthalene-LIF signal on O_2 partial pressure at 600 K and 41 bar, with 266-nm excitation and the BP340/26 filter. Comparison to Faust model (solid line) [87,88] and the extrapolated Faust model (dashed line). Data based on LIF-lifetime measurements [87,88] for 1 bar and various N_2/O_2 bath gas compositions (red symbols) (a) and for 1–10 bar at 580 K (green symbols) (b). LIF signal normalized to the intensity at 2.1 bar O_2 partial pressure.

LIF signal ratio of toluene and naphthalene

The O_2 quenching effects on fluorescence are more significant for naphthalene compared to toluene (cf. Chapter 2), which was confirmed at high pressure as shown in Figure 5-20 for toluene and in Figure 5-26 and Figure 5-27 for naphthalene. Due to differences in the sensitivity of toluene and naphthalene LIF on quenching by O_2, the ratio of both LIF signals depends on O_2 partial pressure and also on temperature. For 266-nm excitation, the normalized naphthalene- and toluene-LIF signal ratio (Figure 5-31) increases with O_2 partial pressures while temperature effects were not detectable within our experiment in the 600–750 K range. The LIF signal ratio was also investigated for various pairs of bandpass filters (Figure 5-32). The highest sensitivity on O_2 partial pressure was obtained with the BP292/27 and BP335/07 bandpass filter pair at 600 K with an increase of the LIF signal ratio by 132% when the O_2 partial pressure increased from 0.4 to 8.5 bar. Similar observations were made at temperatures up to 750 K.

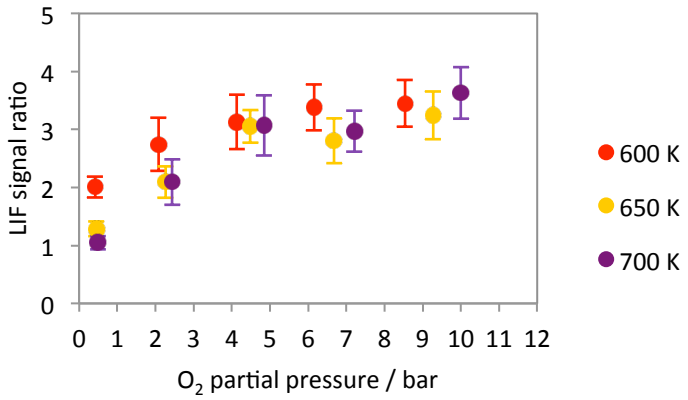

Figure 5-31: Dependence of the toluene- and naphthalene-LIF signal ratio (266-nm excitation) on O_2 partial pressure at 600–750 K with the BP292/27 and BP340/12 bandpass filters.

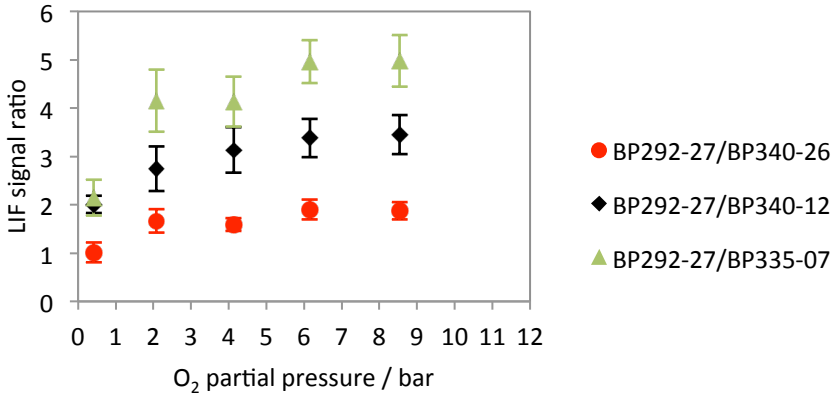

Figure 5-32: Dependence of the toluene- and naphthalene-LIF signal ratio (266-nm excitation) on O_2 partial pressure at 600 K for various bandpass filter pairs (BP292-27/BP340-26, BP292-27/BP340-12, BP292-27/BP335-07).

The LIF signal ratio of toluene and naphthalene with 266-nm excitation measured in the jet was compared to the LIF signal ratio (Figure 5-33) calculated based on LIF-lifetime measurements and model predictions [25,72,85, 87,88]. In Figure 5-33, the LIF signal ratio increases with increasing O_2 partial pressure with a reduced effect at higher temperatures in the 580–730 K range. The LIF signal ratio depends strongly on O_2 partial pressure for low O_2 partial pressures below 0.10 bar. However, this dependence tends to saturate for O_2 partial pressures above 0.10 bar for all temperatures investigated.

The LIF signal ratios calculated with the LIF lifetime measurements agree with the model [25,72,85, 87,88] for O_2 partial pressures between 0 and 0.21 bar but deviate above (Figure 5-30). The Koban model (toluene-LIF signal) was validated for O_2 partial pressures up to 2.1 bar, whereas the Faust model (naphthalene-LIF signal) was limited to O_2 partial pressures below 0.21 bar. The Faust model was extrapolated to higher O_2 partial pressures but the LIF-lifetime measurements based data were lower than the predictions (Figure 5-30).

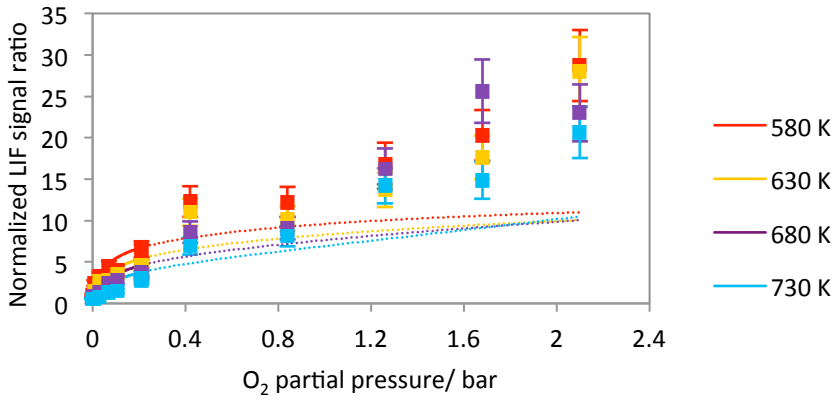

Figure 5-33: Dependence of the toluene- and naphthalene-LIF signal ratio (266-nm excitation) on O_2 partial pressure for 580–750 K. The LIF signal ratios are normalized to the value obtained in N_2 at 580 K. Lines: Ratios based on simulations for naphthalene and toluene up to 0.21 bar [25,72,85, 87,88]. Dashed lines: Ratios based on extrapolated models [25,72,85, 87,88]. Symbols: Data based on LIF lifetimes [25,72,85, 87,88].

The LIF signal ratio obtained in the jet at a temperature of 600 K was compared to model predictions and to the data derived from lifetime measurements at 580 K [25,72,85, 87,88] (Figure 5-34). The LIF signal ratio measured in the jet reveals good agreement with the model predictions (extrapolated to higher O_2 partial pressures) between 0.5 and 11 bar. Based on the measurements in the present work, the model [25,72,85, 87,88] describes the toluene- and naphthalene-LIF signals and the ratio of the two sufficiently well up to 11 bar. These results reveal the dependence of the LIF signal ratio of toluene and naphthalene for 266-nm excitation on O_2 at high O_2 partial pressures. The LIF signal ratio depends strongly on the O_2 partial pressure before the effect saturated at approx. 2.1 bar O_2 partial pressure. The impact on the precision of the two-tracer LIF technique to determine the O_2 partial pressure is discussed in Section 5.3.4.

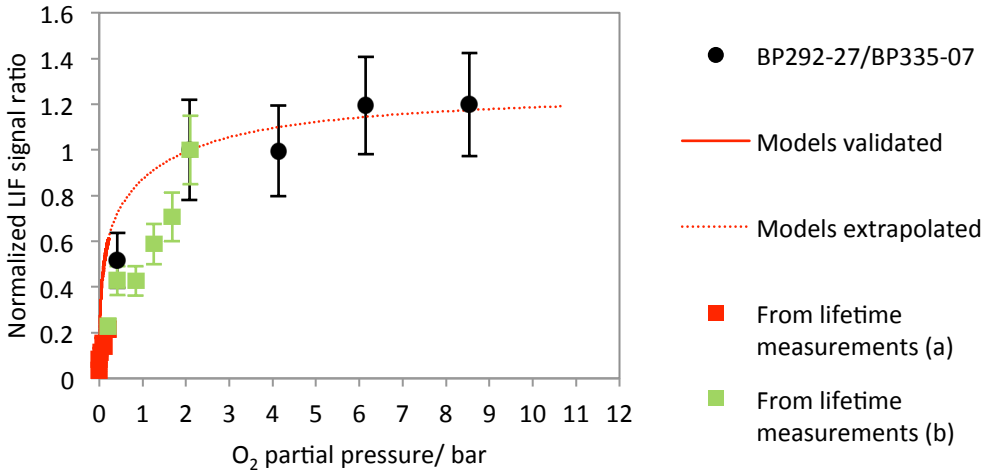

Figure 5-34: Dependence of the toluene- and naphthalene-LIF signal ratio on O_2 partial pressure at 600 K and 41 bar with 266-nm excitation. Comparison to the models [25,72,85, 87,88] (solid line) and the extrapolated models (dotted line). Data based on LIF-lifetime measurements [25,72,85, 87,88] for 1 bar and various N_2/O_2 bath gas compositions (red symbols) (a) and for 1–10 bar in air at 580 K (green symbols) (b). The LIF signal ratio is normalized to its value at 2.1 bar O_2 partial pressure.

The LIF signal ratio of toluene (248-nm excitation) and naphthalene (266-nm excitation) measured in the vaporized jet did not reveal any notable dependence on O_2 partial pressure for the range of temperatures (Figure 5-35) and optical filters (Figure 5-36) investigated. The comparison of the results with models employed at higher O_2 partial pressures up to 11 bar (Figure 5-37) reveals good agreement with the model predictions in terms of independence of the LIF ratio on the O_2 partial pressure.

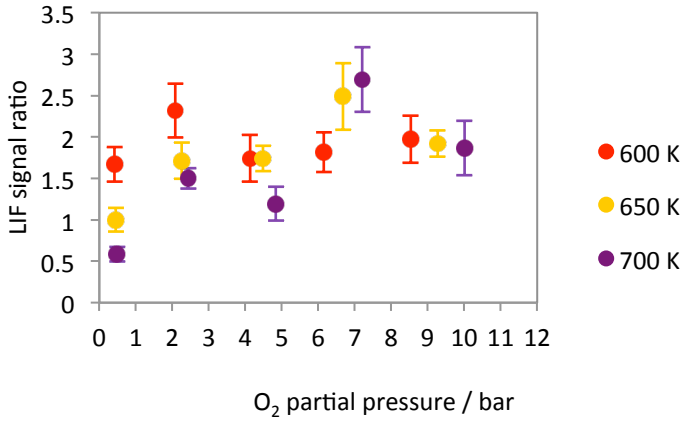

Figure 5-35: Dependence of the LIF signal ratio of toluene (248-nm excitation) and naphthalene (266-nm excitation) on O_2 partial pressure at 600–750 K with the BP280/20 and BP340/12 filters.

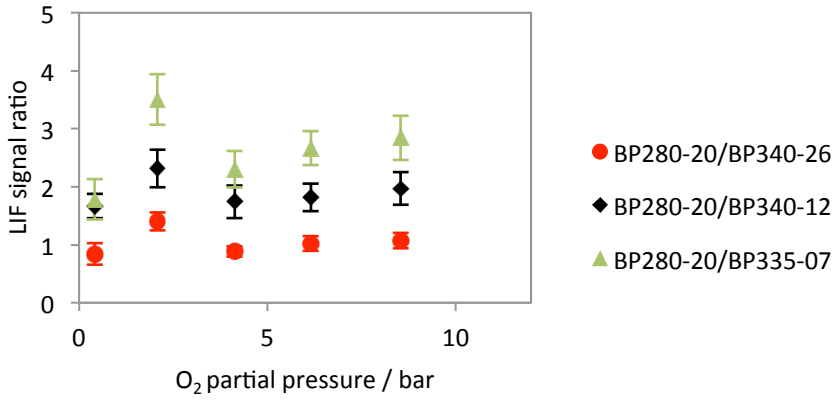

Figure 5-36: Dependence of the LIF signal ratio of toluene (248-nm excitation) and naphthalene (266-nm excitation) on O_2 partial pressure at 600 K for various filter pairs. The LIF signal ratio is normalized to the value obtained for the minimum O_2 partial investigated (0.5 bar) at 600 K.

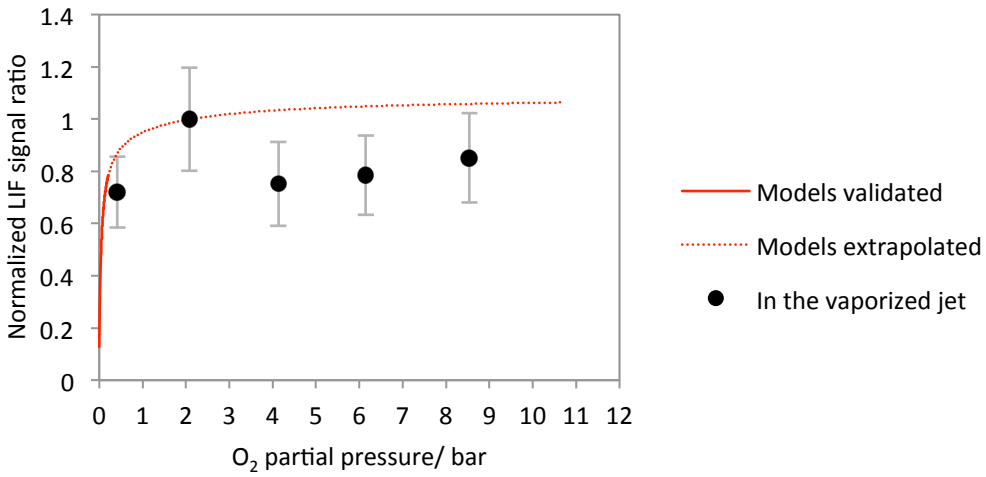

Figure 5-37: Dependence of the toluene- and naphthalene-LIF signal ratio (266-nm excitation) on O_2 partial pressure at 600 K and 41 bar. Comparison of simulated signal ratios based on the models [25,72,85, 87,88] (solid line) and the extrapolated models (dotted line). The LIF signal ratio is normalized to its value at 2.1 bar O_2 partial pressure.

5.3.4 Discussion

The two-tracer three-color LIF technique was applied in the high-pressure high-temperature cell to evaluate the experimental methodology and quantify the effects of temperature and O_2 partial pressure on toluene- and naphthalene-LIF signals. This study was performed with a simplified experimental configuration based on a single ICCD camera for subsequent detection of the images at three distinct spectral ranges: This approach significantly increased the single shot-to-shot fluctuations between LIF images to 20% because of the turbulent nature of the jet. From a statistics point of view the acquisition of only 5 LIF images for each test condition was an additional limiting factor for the ensemble-average based analysis. The relative uncertainty of the LIF signal ratio due to the shot-to-shot fluctuations be-

tween the LIF images (around 13% for $N = 5$, cf. Figure 5-15) contributed to significantly increase the random error resulting to a low degree of precision for the measurement technique. This can be improved by using simultaneous detection of the three bandpass-filtered images with three cameras simultaneously. The relative uncertainty of the LIF signal ratio would then be reduced to a systematic error that will remain due to superposition of the three LIF images, the flat field correction and adjustment of the camera sensitivity, and the influence of shot noise (cf. Chapter 4). This systematic error can be evaluated by following the experimental methodology (using identical filters applied to each camera) presented in Chapter 4 for the two-color LIF thermometry method using the toluene tracer. LIF images acquired simultaneously with the three cameras equipped with identical filters can be used to determine the systematic error based on the differences between the LIF images that remain after all corrections (i.e., image superposition, flat field correction, camera sensitivity adjustments) and after application of the calibration curves [89].

The relative uncertainty of the LIF signal ratio was evaluated at 5–10% (cf. Chapter 4) for simultaneous acquisition of the LIF images for calculating the LIF ratio. In case of subsequent acquisition of the LIF images, the relative uncertainty is increased with the additional uncertainty due to the shot-to-shot fluctuations to 15–20%. The precision of the two-tracer three-color LIF technique to measure temperature and O_2 partial pressure measurements is analyzed based on the spectral characterization of toluene and naphthalene as a function of temperature and O_2 partial pressure and the relative uncertainty of the LIF signal ratio. This precision analysis provides insight into the feasibility of using the two-tracer three-color LIF technique in conditions typical of IC engines.

Temperature measurement precision

The principle of the temperature measurement based on two-color LIF thermometry using naphthalene as tracer is described in Section 5.1.1. The naphthalene-LIF signal is collected near the emission peak (filter 2) and at longer wavelengths (filter 3) while the ratio of both signals quantifies the red-shift occurring with increasing temperature and depends on temperature. For naphthalene, this temperature dependence (investigated in Chapter 3) can be described by an exponential function:

$$R_T = ae^{bT} \tag{5.4}$$

The coefficients *a* and *b* depend on the filters used (Table 5-3).

Table 5-3: Coefficients *a* and *b* in eq. (5.4) describing the dependence of the LIF signal ratio on temperature for different bandpass filter pairs.

	BP370/36 BP335/07	BP370/36 BP340/12	BP370/36 BP340/26	BP376/20 BP335/07	BP376/20 BP340/12	BP376/20 BP340/26
a	0.4176	0.505	0.4722	0.3231	0.4002	0.3742
b	0.0022	0.0017	0.0019	0.0029	0.0023	0.0025

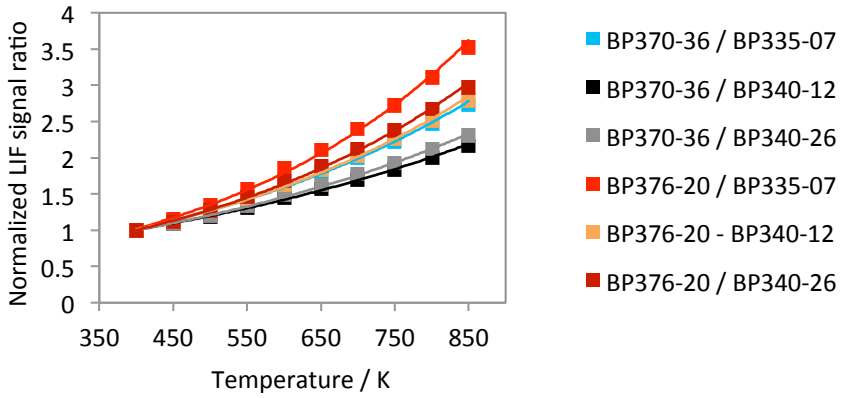

Figure 5-38: Dependence of the naphthalene-LIF signal ratio on temperature for the two-color LIF thermometry for 266-nm excitation and for various bandpass filter pairs (cf. Figure 5-4, Figure 5-18). Symbols: Naphthalene-LIF signal obtained from fluorescence spectra at 1 bar in N_2 [78]. Lines: Interpolation by an exponential function.

The relation between the relative uncertainty of the LIF signal ratio ($\Delta R_T/R_T$) and the temperature measurement precision ΔT is obtained by calculating the derivative of eq. (5.4):

$$\Delta R_T/R_T = b\,\Delta T \tag{5.5}$$

The temperature measurement precision (ΔT) depends on the coefficient b and the relative uncertainty of the LIF signal ratio ($\Delta R_T/R_T$) as shown in Figure 5-39. The BP376/20, BP335/05 filter pair provides the highest degree of temperature measurement precision compared to other pairs of filters investigated. The relative uncertainty of the LIF signal ratio ($\Delta R_T/R_T$) is mostly related to the set-up of the detection system (i.e., number of cameras used for signal detection in the respective spectral ranges of interest). The use of one camera (subsequent measurements) provides a relative uncertainty of the LIF signal ratio ($\Delta R_T/R_T$) of 15–20%, which corresponds to a temperature measurement precision of approximately 50–70 K (BP376/20, BP335/05 filter pair). The use of two cameras (simultaneous measurements) improves the relative uncertainty of the LIF signal ratio ($\Delta R_T/R_T$) significantly, to as low as 5–10% (cf. Chapter 4), which results in a temperature measurement precision of 20–35 K (BP376/20, BP335/05 filter pair).

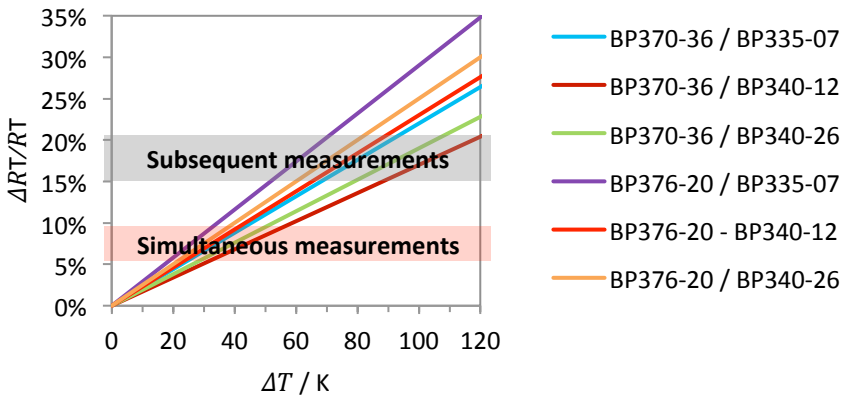

Figure 5-39: Relation the temperature measurement precision (ΔT) between the relative uncertainty of the LIF signal ratio ($\Delta R_T/R_T$) and in the 400−850 K temperature range, for the two-color LIF thermometry using naphthalene with 266-nm excitation and for various pairs of filters (cf. Figure 5-4).

O_2 partial pressure measurement range

The dependence of the toluene- and naphthalene-LIF signal ratio on the O_2 partial pressure at 580 K is shown in Figure 5-34 for 266-nm excitation of both tracers and in Figure 5-37 for 248-nm excitation of toluene and 266-nm excitation of naphthalene. The LIF signal ratio measured in the jet at 41−52 bar revealed good agreement with model predictions [25,72,85, 87,88] at higher O_2 partial pressures up to 11 bar (Section 5.3.3). Therefore, the dependence of the LIF signal ratio on the O_2 partial pressure at 580 K obtained with the extrapolated models [25,72,85, 87,88] was used for investigating the dependence of the relative uncertainty of the LIF signal ratio on O_2 partial pressure (Figure 5-40) that was obtained by calculating the derivative of the curve describing the dependence of the LIF signal ratio on O_2 partial pressure in Figure 5-34 and Figure 5-37. The O_2 partial pressure range that can be measured is limited by a maximum value that depends on the relative uncertainty of the LIF signal ratio as shown in Figure 5-41. The use of a single intensified CCD camera (subsequent measurements) results in a relative uncertainty of the LIF signal ratio ($\Delta R/R$) of 15–20%, which enables O_2 partial pressure measurements up to 0.07 bar. The simultaneous use of two cameras reduces the relative uncertainty of the LIF signal ratio ($\Delta R/R$) down to 5–10% (cf. Chapter 4), which enables O_2 partial pressure measurements up to 0.33 bar. This analysis was also performed for a variation of temperatures in the range 350−950 K (Figure 5-42). The O_2 partial pressure can be measured using the two-tracer LIF technique, over a wider O_2 partial pressure range at higher temperatures (e.g., the relative uncertainty of the LIF signal ratio ($\Delta R/R$) of 5% obtained for simultaneous measurement enables O_2 partial pressure measurements up to 1.2 bar at 680 K).

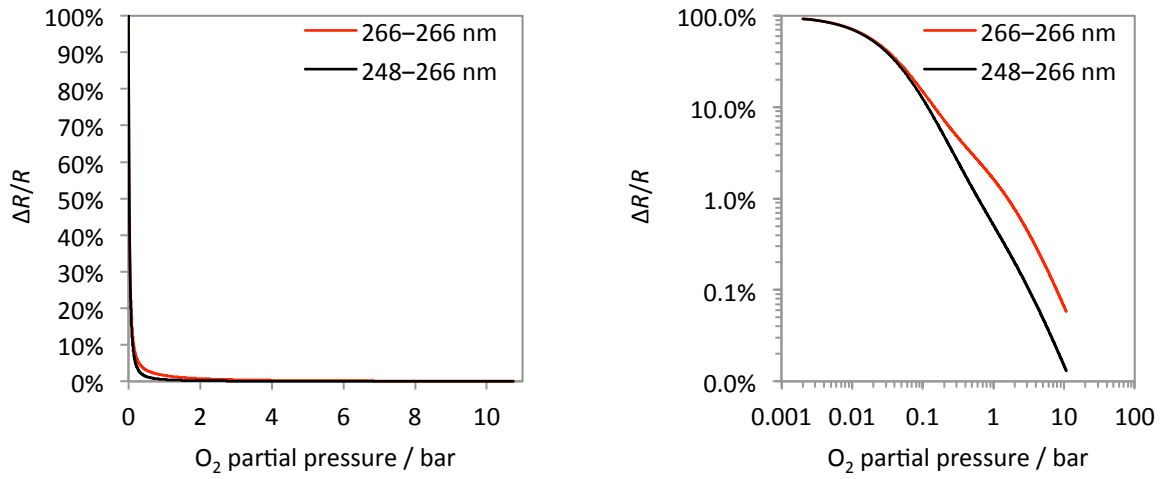

Figure 5-40: Dependence of the relative uncertainty of the LIF signal ratio (toluene- and naphthalene-LIF signal ratio) on O_2 partial pressure at 580 K. Relative uncertainty of the LIF signal ratio derived from model predictions [25,72,85, 87,88] (Figure 5-34 and Figure 5-37). 266–266 nm: 266-nm excitation of both tracers. 248–266 nm: 248-nm excitation of toluene and 266-nm excitation of naphthalene.

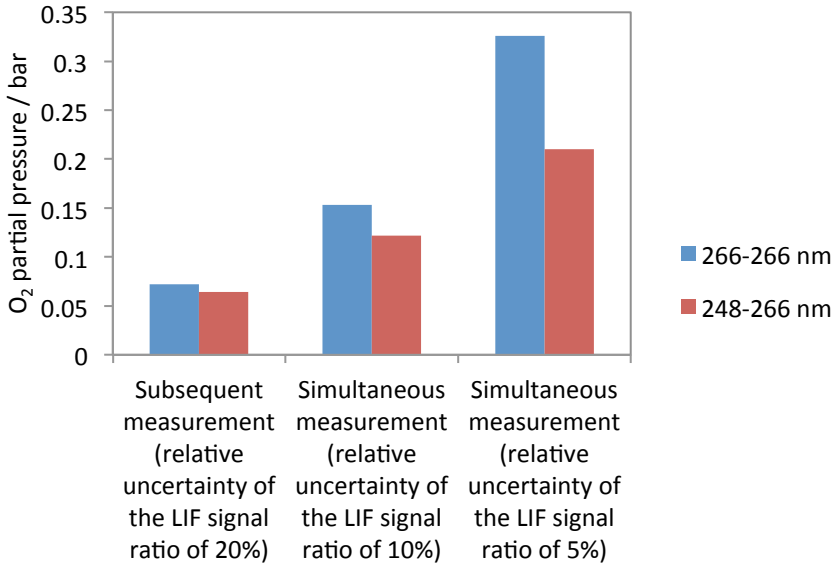

Figure 5-41: Maximum measurable O_2 partial pressure using the two-tracer LIF technique at 580 K for various relative uncertainty of the LIF signal ratio (Figure 5-40). 266–266 nm: 266-nm excitation of both tracers. 248–266 nm: 248-nm excitation of toluene and 266-nm excitation of naphthalene.

The range of measurable O_2 mole fractions using the two-tracer LIF technique depends on the maximum measureable O_2 partial pressure which itself depends on the relative uncertainty of the LIF ratio and the temperature as shown in Figure 5-42 and on the total pressure as shown in Figure 5-43. For example, O_2 mole fractions in the range 0 to 0.21 can be measured at 30 bar total pressure provided the O_2 partial pressure is measurable up to 6.3 bar.

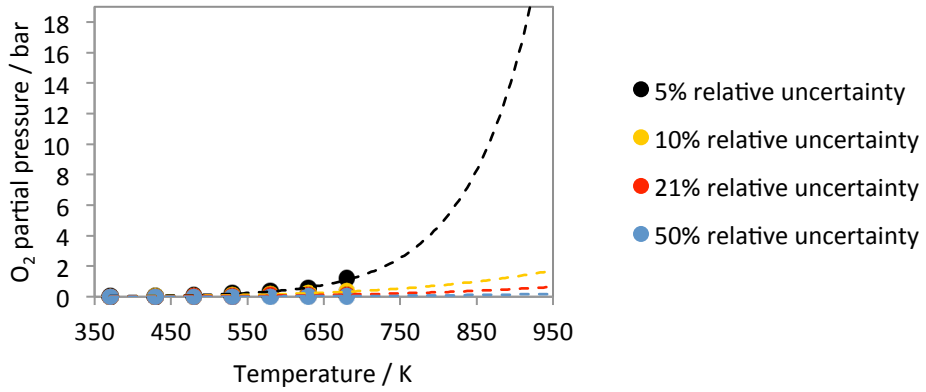

Figure 5-42: Maximum measurable O_2 partial pressure using the two-tracer LIF technique as a function of temperature for various relative uncertainty of the LIF signal ratio and for 266-nm excitation.

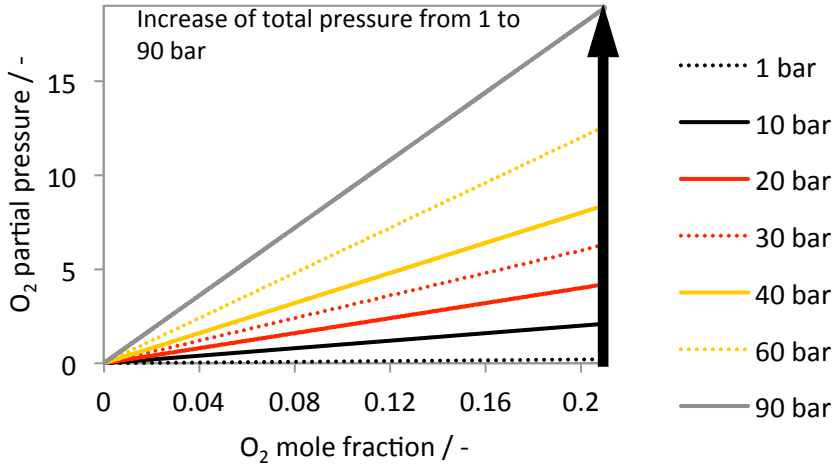

Figure 5-43: O_2 partial pressures as a function of O_2 mole fraction for varying total pressures in the range 1 to 90 bar which are representative of in-cylinder engine conditions.

The relative uncertainty of the LIF signal ratio tends to increase with increasing temperature as a result of the significantly reduced LIF signal-to-noise ratio which is highly temperature-dependent (cf. Chapter 4). Figure 5-45 depicts the range of O_2 mole fractions that can be measured using the two-tracer LIF technique (with toluene and naphthalene) for a wide range of temperatures, total pressures and for four different scenarios. The objective here is to attempt to determine the measurable O_2 mole fraction using the tracer-LIF technique. The four scenarios are based on four different hypotheses with regards to the influence of the temperature-dependence on the relative uncertainty of the acquired LIF signal ratio described in Table 5-4.

Table 5-4: Comparison of three scenarios (from "best-case" to "worst-case") that reveal the level of assumed relative uncertainty of the LIF signal ratio using a two-tracer LIF technique based on temperature-dependences.

	Relative uncertainty of the LIF signal ratio			
	Two cameras (simultaneous measurements)			**One camera (subsequent measurements)**
Temperature range	**Scenario 1 ("best case")**	**Scenario 2 (intermediate)**	**Scenario 3 ("worst-case")**	**Scenario 4**
350–600 K	5%	5%	5%	20%
600–800 K	5%	Linear increase from 5 to 10%	Linear increase from 5 to 10%	20%
800–950 K	5%	10%	Linear increase from 10 to 50%	20%

Scenario 1 can be considered as a highly optimistic or "best-case" scenario since the relative uncertainty of the LIF signal ratio is assumed constant at 5% in the temperature range 350–950 K. In reality, measurements described previously in this thesis revealed a significant increase in relative uncertainty with increasing temperature. Scenario 2 is an intermediate case where a 5% relative uncertainty in the LIF signal ratio measurement is assumed for the 350–600 K range. Thereafter, a linear increase of the relative uncertainty from 5% up to a maximum of 10% is assumed in the temperature range 600–800 K while a 10% uncertainty is assumed for temperatures above 800 K. The "worst-case" scenario 3 is based on identical assumptions as scenario 2 in the temperature range 350–800 K. However, from 800 to 950 K, the relative uncertainty of the measured LIF ratio is assumed to increase linearly from 10 to 50%.

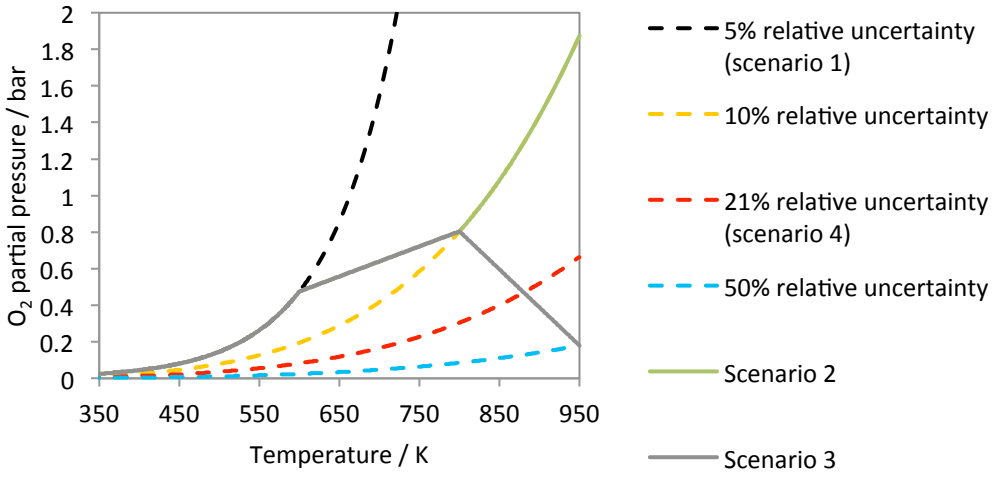

Figure 5-44: Maximum measurable O_2 partial pressure using the two-tracer LIF technique (toluene and naphthalene tracers and 266-nm excitation) as a function of temperature for various assumed levels of relative uncertainty of the LIF signal ratio for the four different scenarios described in Table 5-4. The curves representing the relative uncertainty of 5, 10, 21, and 50% are interpolated as shown in Figure 5-42.

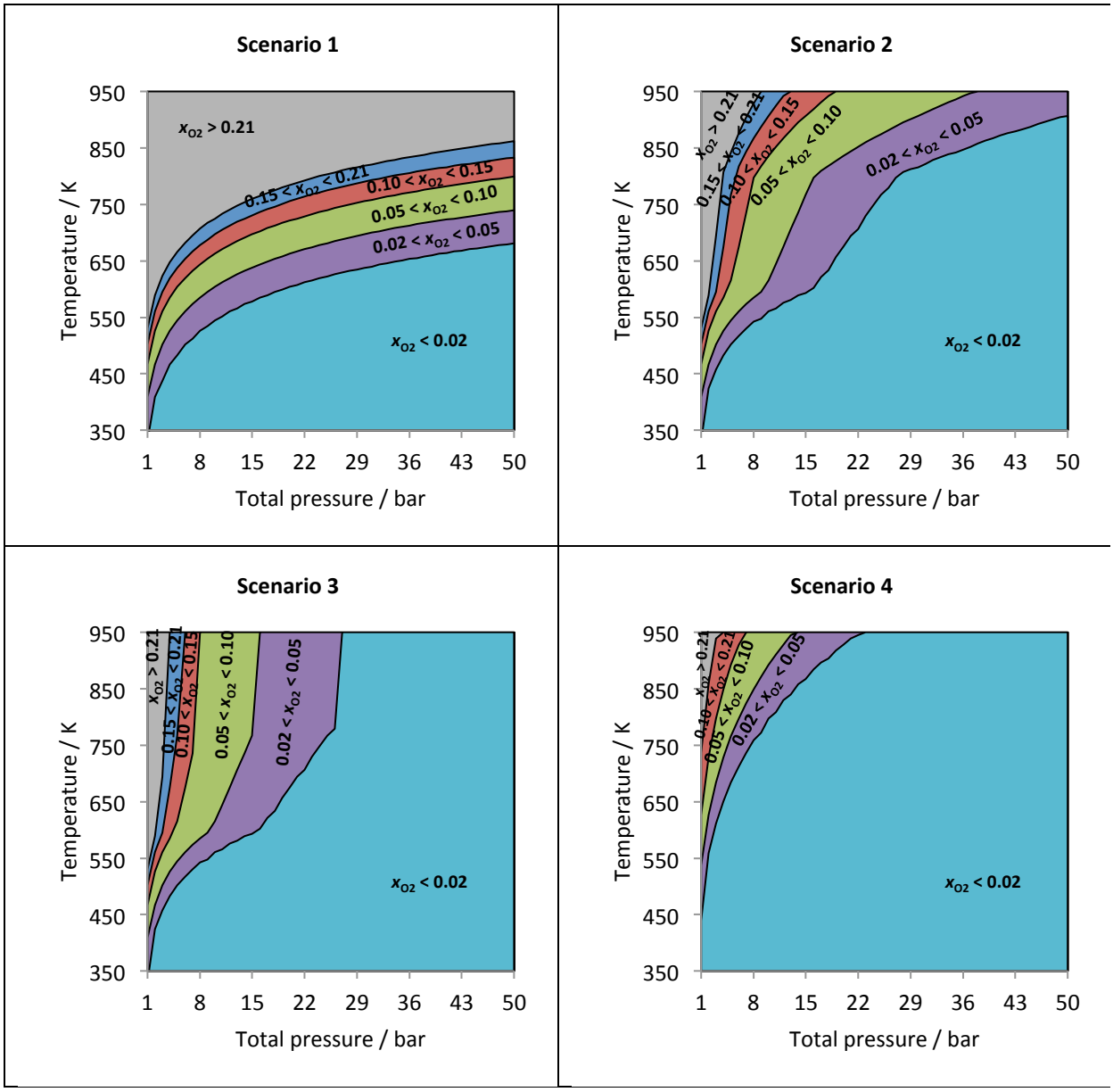

Figure 5-45: 2D maps showing the measurable range of O_2 mole fractions (x_{O2}) using the two-tracer LIF technique. Measurements depend on temperature and total pressure. The maps correspond to the four scenarios (from "best-case" to "worst-case") defined in Table 5-4 and Figure 5-44.

In summary, measurements of O_2 mole fraction in the range 0 to 0.21 are feasible using a two-tracer LIF technique with toluene and naphthalene under atmospheric conditions in the 500–950 K range. Such measurements would require the use of two cameras (scenarios 1, 2, and 3). The analysis reveals that in order to be able to measure a wide range of O_2 mole fractions, it is necessary to obtain higher temperatures at high pressures. For example, for the “best-case” scenario 1, temperatures above 800 K would be required at a total pressure of 40 bar to be able to measure O_2 mole fractions in the 0–0.21 range. However, based on the results of the present study, it has been shown that the relative uncertainty of the LIF ratio increases significantly at high temperature. In this context, scenario 3, although considered "worst-case", is expected to be closer to reality compared to scenario 1. Taking this into

account, the results shown in Figure 5-45 reveal that the two-tracer LIF approach (using toluene and naphthalene) is highly limited for measurements in an IC engine environment.

5.4 Conclusions

In the present work, the two-tracer three-color LIF technique was applied in a high-pressure high-temperature cell to evaluate the experimental methodology. Ideally, three intensified CCD cameras were required for simultaneous LIF signal detection in three distinct spectral bands. However, in order to reduce experimental complexity, measurements were performed using a single camera only. The use of a single camera required the limitation on an ensemble-average-based analysis. The low repetition rate of the cell furthermore limited the statistics to a small number of LIF images acquired for the various conditions resulting in a relative uncertainty of the LIF signal ratio due to the shot-to-shot fluctuations of 13% which contributed to significantly increase the random error resulting to a low degree of precision for the measurement technique. The precision could be improved by increasing the sample number of LIF images acquired at each condition and – mainly – by using simultaneous data acquisition with three cameras to allow for single-shot imaging of the LIF signal ratios. In this case, the precision would mainly depend on the quality of the post-processing, in particular image superposition, flat field correction, corrections for difference in sensitivity between each of the cameras and the calibration curves as well as the signal-to-noise ratios of the individual images. The use of three cameras would significantly improve LIF ratio measurement precision from 20% down to 5%.

Although the current study was performed with a single camera only, the results acquired were useful to compare with model predictions of the LIF signal ratio extrapolated at high O_2 partial pressures typical of IC engine conditions (40–50 bar and 600–700 K). These models [25,72,85, 87,88] were then used to investigate the O_2 partial pressure ranges that can be measured with the two-tracer LIF technique. Based on this investigation, the two-tracer LIF technique reveals potential for measuring O_2 mole fractions in a wide range (0–0.21) at atmospheric pressure conditions but the achievable O_2 mole fractions were limited at higher pressures typical to IC engine conditions.

6 Conclusions and outlook

For the further development of IC engine technology, experimental characterization of the fuel/air mixture in the combustion chamber is required for a better understanding of the mixing and combustion, and to validate the computational models. The present work aimed at developing a non-intrusive laser diagnostic technique for simultaneous measurements of fuel concentration, temperature and O_2 concentration in conditions representative for IC engines. In order to enable measurements applicable for validating computational models, high spatial resolution and low measurement uncertainty were targeted.

The technique developed was based on two-tracer LIF with single-wavelength laser excitation. One tracer with high sensitivity to temperature was used to measure temperature with ideally a low influence of O_2 partial pressure on the measurement. A second tracer with a different O_2-sensitivity compared to the first tracer was used to measure the O_2 partial pressure. Two aromatics (toluene and naphthalene) were selected. An aromatic pair was preferred to aromatic/ketone pairs because of the low photophysical interaction between the two tracers. The spectral properties of toluene and naphthalene were analyzed for various temperatures, pressures and O_2 partial pressures to obtain information on the photophysical properties of the fluorescence of those tracers. The mixture was also characterized to verify the low level of photophysical interaction between the two selected tracers. An important part of the development aimed at characterizing and optimizing the measurement precision and accuracy. The sources of measurement uncertainties were analyzed in detail, and a specific strategy was developed to determine and optimize the precision and the accuracy. The methodology was first developed for single-tracer LIF temperature measurements applied to a Diesel jet configuration under engine type conditions. This methodology was then used to evaluate the potential of tracer-LIF techniques for simultaneous measurements of fuel concentration, temperature and O_2 partial pressure at conditions representative of IC engines (high temperatures, high pressures and high in-homogeneities in temperature and species concentrations).

The main outcomes of this work are:

- The investigation of the spectral properties of a mixture of toluene and naphthalene. These two tracers can be used for a two-tracer LIF technique. Both tracers can be excited at the same wavelength of 266 nm and the LIF emission of both tracers can be spectrally separated. The photophysical interaction between both tracers can be neglected in the presence of O_2 molecules.

- The determination of the calibration curves for temperature and O_2 partial pressure measurements from photophysical data obtained at various temperatures (370–830 K), pressures (1–10 bar) and O_2 partial pressures (0–2.1 bar).

- The investigation of a single-tracer LIF technique (using toluene) under high pressure and high temperature conditions which enabled the development of a quantitative methodology to evaluate and optimize measurement uncertainty of tracer-LIF requiring LIF-ratio calculations.

- The application of the toluene-LIF technique in a high-temperature and high-pressure cell to measure unburned gas temperature in an evaporating Diesel jet using single-wavelength excitation at 248 nm and two-color detection. Under these conditions, the measurement precision of the technique was evaluated in the 20–40 K range.

- The development of a methodology to characterize and evaluate the random and systematic errors. Some optimization of the post-processing, the experiment and the calibration procedure could minimize these random and systematic errors. This approach can be extended to tracer-LIF techniques in general requiring LIF-ratio calculations.

- The evaluation of the measurement accuracy by comparing the temperature measured by the two-color LIF technique with a known ambient/bath gas temperature measurement. A straightforward comparison was possible at low temperature (453 K). However, at higher temperatures, only indirect comparison was possible between the jet temperatures derived from the two-color LIF technique with those derived from a single-color LIF measurement using an adiabatic mixing model.

- The investigation of a two-tracer three-color-LIF technique (using toluene and naphthalene) under high pressure and high temperature conditions to evaluate the experimental methodology and quantify the effects of temperature and O_2 partial pressure on toluene- and naphthalene-LIF signals. This study was performed with a simplified experimental configuration based on a single camera for subsequent detection of the images at three distinct spectral ranges and an ensemble-averaged analysis of the LIF images. This approach generated difficulties due to high shot-to-shot fluctuations of average quantities leading to an increase of the measurement uncertainty, especially for small samples. Ideally, three cameras would be required for simultaneous LIF signal detection in three distinct spectral bands.

- However, despite these limitations, the experimental configuration was found suitable to perform an initial evaluation of the methodology and analysis of the precision of the two-tracer three-color LIF technique to measure temperature and O_2 partial pressure measurements. It was possible to investigate the O_2-sensitivity of the technique at high temperature (600–700 K) and high O_2 partial pressure (0–8 bar O_2 partial pressure) typical of IC engine conditions. The two-tracer LIF technique revealed potential for measuring O_2 mole fractions in a wide range (0–0.21) at atmospheric pressure conditions but the achievable O_2 mole fractions is limited at higher pressures typical for IC engine conditions. Even at atmospheric conditions, the use of three cameras is still required to achieve reasonable measurement precision.

Based on these results, the following perspectives are emerging:

- Toluene two-color LIF thermometry based on the red-shift of the fluorescence spectra with increasing temperature at 248 nm was investigated in the present work at high-temperature high-pressure in nitrogen to optimize various aspects of the technique and to evaluate the measurement accuracy and precision. Due to the decrease of the toluene-LIF signal with increasing temperature, the toluene two-color LIF thermometry has limitations at temperatures above 700 K. The laser fluence guaranteeing linear response of the toluene-LIF signal on fluence at 450 K was also used for higher temperatures. At these temperatures, however, the saturation limit is higher. Therefore, it would be possible to perform measurements at higher temperature by improving the signal-to-noise ratio trough an increase of the laser fluence. A particular linearity check would be required for different temperature ranges to allow the application of the toluene two-color LIF technique with different laser fluence depending on the temperature range targeting. In addition, toluene-LIF is quenched by O_2 and the subsequent reduction of the toluene-LIF signal in the presence of O_2 increases the measurement uncertainty due to lower signal-to-noise ratios. The reduction of the signal-to-noise ratio in the presence of O_2 is expected to be limited for high partial pressure (above 0.5 bar O_2 partial pressure, cf. Chapter 5). Therefore, the two-color LIF technique could still have potential in the presence of O_2 with a careful optimization of the laser fluence since the saturation level is obtained at higher laser fluence in the presence of O_2 and the laser fluence can be increased in the presence of O_2 compared to N_2.

- The toluene two-color LIF thermometry could also be applied with a laser excitation wavelength of 266 nm instead of 248 nm. The performance of the toluene-LIF technique is expected to be similar for the two wavelengths in N_2. However, in the presence of O_2, it is preferable to use 248 nm laser excitation rather than 266 nm since O_2-quenching on the toluene LIF signal is minimized at 248 nm. The two-color LIF thermometry based on the red-shift of the fluorescence spectra with increasing temperature could be investigated at high-temperature high-pressure for naphthalene. The fluorescence spectra for naphthalene were measured with 266 nm laser excitation, it might be interesting to study the photophysical behavior of naphthalene with 248 nm laser excitation.

- The two-tracer three-color LIF technique using toluene and naphthalene with 266 nm laser excitation showed strong limitations for measuring O_2 concentration under the high O_2 partial pressures conditions occurring in the IC engines. This technique is more suitable for lower O_2 partial pressure relevant for atmospheric conditions. For IC-engine applications, another pair of tracers should be found. The use of two aromatics seemed attractive because of reduced photophysical interactions between the two tracers. The toluene- and naphthalene-LIF signals are both quenched by O_2 but with an O_2-sensitivity difference which can be exploited to

measure O_2 concentration only for low O_2 partial pressure. Additional experiments on other aromatics should be performed at high O_2 partial pressures to investigate the reduction of the O_2-quenching on the LIF signal at high O_2 partial pressure relevant for IC engines. If the behavior of the toluene and naphthalene are confirmed for other aromatics, the application of a two-tracer LIF technique to measure O_2 concentration should not use two aromatics. The use of one aromatic and one ketone should be investigated in more details at high O_2 partial pressure (up to 10 bar O_2 partial pressure) for defining the potential of a two-tracer LIF technique for measuring absolute O_2 partial pressure. In addition, the photophysical interaction between the two tracers should be investigated to quantify the impact on the measurements uncertainties of the two-tracer LIF technique. In this case of one aromatic, one ketone, the use of laser excitation at two wavelengths (required for the temperature measurement with a ketone) should be investigated into detail to define the strategy for simultaneous measurement of fuel concentration, temperature and O_2 concentration.

- An *a priori* random error determination methodology was developed to allow the determination of the actual random error directly related to the measurement configuration using the toluene two-color LIF thermometry. This methodology was carried out in the same configuration as the actual measurement and therefore took into account in particular uncertainties of the image superposition and the effects of high-temperature gradients. In addition, determining this *a priori* error also allowed an improved identification of the different error sources and enabled these error sources to be minimized in terms of their influence on the total error. This quantitative methodology to evaluate and optimize measurement uncertainty can also be applied to other tracer-LIF requiring LIF-ratio calculations.

References

1. M. G. Allen, “Diode laser absorption sensors for gas-dynamic and combustion flows”, Meas. Sci. Techno. 9 (1998) 545-562.

2. R. M. Mihalcea, D. S. Baer, R. K. Hanson, “Advanced diode laser absorption sensor for in situ combustion measurements of CO_2, H_2O, and gas temperature”, Proc. Combust. Inst. 27 (1998) 95-101.

3. D. S. Baer, V. Nagali, E. R. Furlong, R. K. Hanson, “Scanned- and fixed-wavelength absorption diagnostics for combustion measurements using multiplexed diode lasers,” AIAA Journal 34 (1996) 489-493.

4. S. T. Sanders, J. A. Baldwin, T. P. Jenkins, D. S. Baer, R. K. Hanson, “Diode-laser sensor for monitoring multiple combustion parameters in pulse detonation engines,” Proc. Combust. Inst. 28 (2000) 587-594.

5. X. Zou, J. B. Jeffries, R. K. Hanson, G. Li, E. J. Gutmark, “Wavelength-scanned tunable diode laser temperature measurements in a model gas turbine combustor,” AIAA Journal 45 (2007) 420-425.

6. S. T. Sandaers, T. Kim, J. B. Ghandhi, “Gas temperature measurements during ignition in an HCCI”, SAE Technical Paper Series 2003-01-0744 (2003).

7. D. W. Mattison, J. B. Jeffries, R. K. Hanson, R. R. Steeper, S. D. Zilwa, J. E. Dec, M, Sjöberg, W. Hwang, “In-cylinder gas temperature and water concentration measurements in HCCI engines using a multiplexed-wavelength diode-laser system: Sensor development and initial demonstration”, Proc. Combust. Inst. 31 (2007) 791-798.

8. A. E. Klingbeil, J. M. Porter, J. B. Jeffries, R. K. Hanson, “Two-wavelength mid-IR absorption diagnostic for simultaneous measurements of temperature and hydrocarbon fuel concentration”, Proc. Combust. Inst. 32 (2009) 821-829.

9. J. B. Jeffries, J. M. Porter, S. H. Pyun, R. K. Hanson, K. R. Sholes, K. Shouji, T. Chaya, “An in-cylinder laser absorption sensor for crank-angle-resolved measurements of gasoline concentration and temperature”, SAE Technical Paper Series 2010-01-2251 (2010).

10. A. C. Eckbreth, “Laser diagnostics for combustion temperature and species”, Gordon and Breach (1996).

11. C. A. Idicheria, L. M. Picket, “Quantitative mixing measurements in a vaporizing Diesel spray by Rayleigh imaging”, SAE Technical Paper Series 2007-01-0647 (2007).

12. J. Zetterberg, Z. S. Li, S. Afzelius, M. Aldén, “Two-dimensional temperature measurement in flames using filtered Rayleigh scattering at 254 nm”, Proc. European Comb. Meeting (2003).

13. C. Epsey, J. Dec, “Planar laser Rayleigh scattering for quantitative vapor-fuel imaging in a diesel jet”, Combust. Flame 109(1997) 65-86.

14. C. A. Idicheria, L. M. Picket, “Effect of EGR on Diesel pre-mixed-burn equivalence ratio”, Proc. Combust. Inst. 31 (2007) 2931-2938.

15. L. M. Picket, J. Manin, C. L. Genzale, D. L. Siebers, M. P. B. Musculus, C. A. Idicheria, “Relationship between Diesel fuel spray vapor penetration/dispersion and local fuel mixture fraction”, SAE Technical Paper Series 2011-01-0686 (2011).

16. A. Adam, P. Leick, G. Bittlinger, C. Schulz, “Visualization of the evaporation of a Diesel spray using combined Mie and Rayleigh scattering techniques”, Exp. Fluids 47 (2009) 439-449..

17. L. P. Lucht, M. Maris, “CARS measurements of temperature profiles near a wall in an internal combustion engine”, SAE Technical Paper Series 870459 (1987).

18. R. P. Lucht, R. E. Teets, R. M. Green, R. E. Palmer, C. R. Ferguson, “Unburned gas temperatures in an internal combustion engine. I: CARS temperature measurements”, Combust. Sci. Technol. 55 (1987) 41-61.

19. P. E. Bengtsson, L. Martinsson, M. Aldén, B. Johansson, B. Lassesson, K. Marforio, G. Lundholm, “Dual-broadband rotational CARS measurements in an IC engine”, Proc. Combust. Inst. 25 (1994) 1735-1742.

20. J. Bood, P. E. Bengtsson, F. Mauss, K. Burgdorf, I. Denbratt, “Knock in spark-ignition engines: end-gas temperature measurements using rotational CARS and detailed kinetic calculations of the auto ignition process” SAE Technical Paper Series 971669 (1997).

21. I. Choi, K. M. Chun, C.-W. Park, J. W. Hahn, “End-gas temperature measurements in a DOHC spark-ignition engine using CARS”, SAE Technical Paper Series 2000-01-0237 (2000).

22. P. Ewart, R. B. Williams, E. P. Lim, C. R. Stone, “Comparison of in-cylinder coherent anti-Stockes-Raman scattering temperature measurements with predictions from an engine simulation”, Int. J. Engine Res. 2 (2001) 149-162.

23. C. Brackmann, J. Bood, M. Afzelius, P.-E. Bengtsson, “Thermometry in internal combustion engines via Dual-broadband rotational CARS thermometry”, Meas. Sci. Technol. 15 (2004) 13-25.

24. F. Beyrau, A. Bräuer, T. Seeger, A. Leipertz, “Determination of the gas-phase temperature in the vaporizing spray of a GDI-injector using pure rotational CARS”, SAE Technical Paper Series 2004-01-1350 (2004).

25. W. Koban, “Photophysical characterization of toluene and 3-pentanone for quantitative imaging of fuel/air ratio and temperature in combustion systems,” PhD thesis, University of Heidelberg, Germany (2005).

26. C. Schulz, V. Sick, “Tracer-LIF diagnostics: quantitative measurement of fuel concentration, temperature and fuel/air ratio in practical combustion systems”, Prog. Energy Combust. Sci. 31 (2005) 75-121.

27. A. Lozano, B. Yip, R. K. Hanson, “Acetone: a tracer for concentration measurements in gaseous flows by planar laser-induced fluorescence”, Exp. Fluids 13 (1992) 369-376.

28. F. Grossmann, P. B. Monkhouse, M. Ridder, V. Sick, J. Wolfrum, “Temperature and pressure dependences of the laser-induced fluorescence of gas-phase acetone and 3-pentanone,” Appl. Phys. B 62 (1996) 249-253.

29. M. C. Thurber, F. Grisch, B. J. Kirby, M. Votsmeier, R. K. Hanson, “Measurements and modelling of acetone laser-induced fluorescence with implications for temperature-imaging diagnostics,” Appl. Opt. 37 (1998) 4963-4978.

30. M. C. Thurber, R. K. Hanson, “Pressure and composition dependence of acetone laser induced fluorescence with excitation at 248, 266, and 308 nm,” Appl. Phys. B 69 (1999) 229-240.

31. N. Wermuth, V. Sick, “Absorption and fluorescence data of acetone, 3-pentanone, biacetyl, and toluene at engine-specific combinations of temperature and pressure”, SAE 2005-01-2090 (2005).

32. A. Brauer, F. Beyrau, A. Leipertz, “Laser-induced fluorescence of ketones at elevated temperatures for pressures up to 20 bars by using a 248 nm excitation laser wavelength: experiments and models improvements”, Appl. Opt. 45 (2006) 4982-4989.

33. J. D. Koch, J. Gronki, R. K. Hanson, “Measurements of near-UV absorption spectra of acetone and 3-pentanone at high temperatures”, J. Quant. Radiat. Transf. 109 (2008) 2037-2044.

34. M. Richter, B. Axelsson, K. Nyholm, M. Aldffen, “Real-time calibration of planar laser-induced fluorescence air-fuel ratio measurements in combustion environments using in situ Raman scattering”, Proc. Combust. Inst. 27 (1998) 51-57.

35. M.C. Thurber, F. Grisch, R.K. Hanson, “Temperature imaging with single- and dual-wavelength acetone planar laser-induced fluorescence”, Opt. Lett. 22 (1997) 251-253.

36. M. C. Thurber, R. K. Hanson, “Simultaneous imaging of temperature and mole fraction using acetone planar laser-induced fluorescence”, Exp. Fluids 30 (2001) 93-101.

37. M. C. Thurber, B. J. Kirby, R. K. Hanson, “Instantaneous imaging of temperature and mixture fraction with dual-wavelength acetone PLIF”, AIAA 98-0397 (1998).

38. A. Hultqvist, M. Christensen, B. Johansson, M. Richter, J. Nygren, J. Hult, M. Aldén, “The HCCI combustion process in a single cycle-high-speed fuel tracer LIF and chemiluminscence imaging”, SAE Technical Paper Series 2002-01-0424 (2002).

39. M. Löffler, B. U. Melcher, A. Braeuer, F. Beyrau, A. Leipertz, “Behavior of the acetone laser-induced fluorescence under engine relevant conditions for the simultaneous visualization of temperature and concentration fields”, SAE Technical Paper Series 2007-01-0642 (2007).

40. H. Seyfried, J. Olofsson, J. Sjöholm, M. Richter, M. Aldén, A. Vressner, A. Hultqvist, B. Johansson, “High-speed PLIF imaging for investigation of turbulence effects on heat release rates in HCCI combustion”, SAE Technical Paper Series 2007-01-0213 (2007).

41. M. Löffler, K. Kröckel, P. Koch, F. Beyrau, A. Leipertz, S. Grasreiner, A. Heinisch, “Simultaneous quantitative measurements of temperature and residual gas fields inside a fired SI-engine using acetone laser-induced fluorescence”, SAE Technical Paper Series 2009-01-0656 (2009).

42. J. Trost, M. Löffler, L. Zigan, A. Leipertz, “Simultaneous quantitative acetone-PLIF measurements for determination of temperature and gas composition fields in an IC-engine”, Physics Procedia 5 (2010) 689-696.

43. J.D. Koch, R.K. Hanson, “Temperature and excitation wavelength dependencies of 3-pentanone absorption and fluorescence for PLIF applications”, Appl. Phys. B 76 (2003) 319-324.

44. W. Koban, J. D. Koch, V. Sick, N. Wermuth, R. K. Hanson, C. Schulz, “Predicting LIF signal strength for toluene and 3-pentanone under engine-related temperature and pressure conditions”, Proc. Combust. Inst. 30 (2005) 1545-1553.

45. V. Modica, C. Morin, P. Guibert, “3-pentanone LIF at elevated temperatures and pressures: measurements and modelling”, Appl. Phys. B 87 (2007) 193-204.

46. H. Neij, B. Johansson, M. Aldén, “Development and demonstration of 2D-LIF for studies of mixture preparation in SI engines”, Combust. Flame 99 (1994) 449-457.

47. S. Einecke, C. Schulz, “Two-dimensional temperature measurements in an SI engine using two-line tracer LIF”, SAE Technical Paper Series 982468 (1998).

48. S. Einecke, C. Schulz, V. Sick, “Measurement of temperature, fuel concentration and equivalence ratio fields using tracer LIF in IC engine combustion”, Appl. Phys. B 71 (2000) 717-723.

49. D. A. Rothamer, J. A. Snyder, R. K. Hanson, R. R. Steeper, “Two-wavelength PLIF diagnostics for temperature and composition”, SAE Technical Paper Series 2008-01-1067 (2008).

50. D. A. Rothamer, J. A. Snyder, R. K. Hanson, R. R. Steeper, “Optimization of a tracer-based PLIF diagnostic for simultaneous imaging of EGR and temperature in IC engines”, Appl. Phys. B 99 (2010) 371-384.

51. R. P. Fitzgerald, R. R. Steeper, “Dual-wavelength PLIF measurements of temperature and composition in an optical HCCI engine with negative valve overlap”, SAE Technical Paper Series 2009-01-0661 (2009).

52. R. E. Herold, J. B. Ghandhi, “Investigation of bulk in-cylinder stratification with split intake runners”, SAE Technical Paper Series 2007-01-4044 (2007).

53. R. P. Fitzgerald, R. R. Steeper, J. Snyder, R. Hessel, “Determination of cycle temperatures and residual gas fraction for HCCI negative valve overlap operation”, SAE Technical Paper Series 2010-01-0343 (2010).

54. J. Snyder, N. Dronniou, J. Dec, R. Hanson, “PLIF measurements of thermal stratification in an HCCI engine under fired operation”, SAE Technical Paper Series 2011-01-1291 (2011).

55. D. A. Rothamer, J. A. Snyder, R. K. Hanson, R. R. Steeper, R. P. Fitzgerald, “Simultaneous imaging of exhaust gas residuals and temperature during HCCI combustion”, Proc. Combust. Inst. 32 (2009) 2869-2876.

56. S. Busch, C. Disch, H. Kubach, U. Spicher, “Optical investigations of the vaporization behaviours of isooctane and an optical, non-fluorescing multicomponent fuel in a spark ignition direct injection engine”, SAE Technical Paper Series 2010-01-2271 (2010).

57. H. Fujimoto, “Distribution of vapor concentration of fuel mixed with volatility component and low volatility component”, SAE Technical Paper Series 2010-01-2274 (2010).

58. P. Guibert, V. Modica, C. Morin, “Influence of pressure, temperature and gas composition on biacetyl laser-induced fluorescence”, Exp. Fluids 40 (2006) 245-256.

59. J. D. Smith, V. Sick, “Quantitative, dynamic fuel distribution measurements in combustion-related devices using laser-induced fluorescence imaging of biacetyl in isooctane”, Proc. Combust. Inst. 31 (2007) 747-755.

60. B. Peterson, V. Sick, “Simultaneous flow field and fuel concentration imaging at 4.8 kHz in an operating engine”, Appl. Phys. B. 97 (2009) 887-895.

61. W. Koban, J.D. Koch, R.K. Hanson, C. Schulz, “Absorption and fluorescence of toluene vapor at elevated temperatures”, Phys. Chem. Chem. Phys. 6 (2004) 2940-2945.

62. M. Luong, W. Koban, C. Schulz, “Novel strategies for imaging temperature distribution using toluene LIF”, J. of Physics: Conf. Series 45 (2006) 133-139.

63. F. Zimmermann, W. Koban, C. Schulz, “Optical diagnostics using laser-induced fluorescence (LIF) of toluene”, in Laser Applications to Chemical Security and Environment Analysis (2006), Nevada, USA.

64. M. Luong, R. Zhang, C. Schulz, V. Sick, “Toluene laser-induced fluorescence for in-cylinder temperature imaging in internal combustion engines”, Appl. Phys. B 91 (2008) 669-675.

65. R. Devillers, G. Bruneaux, C. Schulz, “Investigation of toluene LIF at high pressure and high temperature in an optical engine”, Appl. Phys. B 96 (2009) 735-739.

66. J. E. Dec, W. Hwang, “Characterizing the development of thermal stratification in an HCCI engine using planar-imaging thermometry”, SAE Technical Paper Series 2009-01-0650 (2009).

67. N. Dronniou, J. Dec, “Investigating the Development of thermal stratification from the near-wall regions to the bulk-gas in an HCCI engine with planar imaging thermometry”, Int. J. Engines 5 (2012) 1046-1074.

68. C. Strozzi, J. Sotton, A. Mura, M. Bellenoue, “Characterization of a two-dimensional temperature field within a rapid compression machine using a toluene planar laser-induced fluorescence imaging technique”, Meas. Sci. Technol. 20 (2009) 1-13.

69. J. Redoux, D. Puerchberty, F. Dionnet, “Study of mixture inhomogeneities and combustion development in an S.I. engine using a new approach of laser induced fluorescence (FARLIF)”, SAE Technical Paper Series 941988 (1996).

70. J. Sacadura, L. Robin, F. Dionnet, D. Gervais, P. Gastaldi, A. Ahmed, “Experimental investigation of an optical direct injection s.i. engine using fuel-air ratio laser induced fluorescence”, SAE Technical Paper Series 2000-01-1794 (2000).

71. W. Koban, C. Schulz, “Toluene laser-induced fluorescence (LIF) under engine-related pressures, temperatures and oxygen mole fractions”, SAE Technical Paper Series 2005-01-2091 (2005).

72. W. Koban, J. D. Koch, R. K. Hanson, C. Schulz, “Oxygen quenching of toluene fluorescence at elevated temperatures”, Appl. Phys. B 80 (2005) 777-784.

73. W. Koban, J. D. Koch, R. K. Hanson, C. Schulz, “Toluene LIF at elevated temperatures: implications for fuel-air ratio measurements”, Appl. Phys. B 80 (2005) 147-150.

74. J. Scholz, M. Röhl, T. Wiersbinski and V. Beushausen, “Verification and application of fuel-air-ratio-LIF”, in 13th Int. Symp. on Applications of Laser Techniques to Fluid Mechanics (2006), Lisbon, Portugal.

75. M. Orain, P. Baranger, B. Rossow, F. Grisch, “Fluorescence spectroscopy of 1,2,4-trimethylbenzene at high temperatures and pressures: application to temperature measurements”, Appl. Phys. B 100 (2010) 945-952.

76. S. Kaiser, D. C. Kyritsis, P. Dobrowski, M. B. Long, A. Gomez, “The electrospray and combustion at the mesoscale”, J. Mass Spectrom. Soc. Jpn 51 (2003) 42-48.

77. S. A. Kaiser, M. B. Long, “Quantitative planar laser-induced fluorescence of naphthalene as fuel tracers”, Proc. Combust. Inst. 30 (2005) 1555-1563.

78. M. Orain, P. Baranger, B. Rossow, F. Grisch, “Fluorescence spectroscopy of naphthalene at high temperatures and pressures: implications for fuel-concentration measurements”, Appl. Phys. B 102 (2011) 163-172.

79. M. Kühni, C. Morin, P. Guibert, “Fluoranthene laser-induced fluorescence at elevated temperatures and pressures: implications for temperature-imaging diagnostics”, Appl. Phys. B 102 (2011) 659-671.

80. W. Koban, J. Schorr, C. Schulz, “Oxygen distribution imaging with a novel two-tracer laser-induced fluorescence technique”, Appl. Phys. B 74 (2002) 111-114.

81. D. Frieden, V. Sick, J. Gronki, C. Schulz, “Quantitative oxygen imaging in an engine”, Appl. Phys. B 75 (2002) 137-141.

82. D. Frieden, V. Sick, “A two-tracer LIF strategy for quantitative oxygen imaging in engines applied to study the influence of skip-firing on in-cylinder oxygen contents of an SIDI engine”, SAE Technical paper 2003-01-1114 (2003).

83. C. Ledier, M. Orain, F. Grisch, J. Kashdan, G. Bruneaux, “Vapour concentration measurements in biofuel sprays using innovative planar laser-induced fluorescence strategies”, ILASS, 24th European Conference on Liquid Atomization and Spray Systems (2011), Estoril, Portugal.

84. B. Rossow, “Photophysical processes of organic fluorescence molecules and kerosene – applications to combustion engines”, PhD thesis, University of Paris-Sud 11, France (2011).

85. S. Faust, T. Dreier, C. Schulz, “Temperature and bath gas composition dependence of effective fluorescence lifetimes of toluene excited at 266 nm”, Chem. Phys. 383 (2011) 6-11.

86. F. Ossler, T. Metz, M. Aldén, “Picosecond laser-induced fluorescence from gas-phase polycyclic aromatic hydrocarbons at elevated temperatures”, Appl. Phys. B 172 (2011) 465-478.

87. S. Faust, G. Tea, T. Dreier, C. Schulz, “Temperature, pressure, and bath gas composition dependence of fluorescence spectra and fluorescence lifetimes of toluene and naphthalene”, Appl. Phys. B 110 (2013) 81-93.

88. S. Faust, “Characterisation of organic fuel tracers for laser-based quantitative diagnostics of fuel concentration, temperature, and equivalence ratio in practical combustion processes”, PhD thesis, University of Duisburg-Essen, Germany (2013).

89. G. Tea, G. Bruneaux, J. Kashdan, C. Schulz, “Unburned gas temperature measurements in a surrogate Diesel jet via two-color toluene imaging”, Proc. Combust. Inst. 33 (2011) 783-790.

90. D. Verhoeven, J. L. Vanhemelryck and T. Baritaud, “Macroscopic and ignition characteristics of high-pressure sprays of single-components fuels”, SAE Technical Paper Series 981069 (1998).

91. D. Siebers, “Ignition Delay Characteristics of Alternative Diesel Fuels: Implications on Cetane Number”, SAE Technical Paper Series 852102 (1985).

92. R. Devillers, “Développement et exploitation de techniques de diagnostic optique de mesure de température pour la compréhension des phénomènes de combustion dans les moteurs thermiques”, PhD Thesis, EM2C Ecole Centrale Paris, France (2008).

93. G. Bruneaux, “Mixing Process in High Pressure Diesel Jets by Normalized Laser Induced Exciplex Fluorescence. Part I: Free Jet”, SAE Trans. 114 (2005) 1444-1461.